Detailed Analysis of Thermochemistry Modeling for Hypersonic Air Flows

by

Michael E. Holloway

A dissertation submitted in partial fulfillment
of the requirements for the degree of
Doctor of Philosophy
(Aerospace Engineering)
in the University of Michigan
2021

Doctoral Committee:

Associate Professor Krzysztof Fidkowski, Chair
Adjunct Professor Iain D. Boyd
Associate Professor Mirko Gamba
Associate Professor Eric Johnsen

"When all else fails, give up and go to the library."
Stephen King, *11/22/63*

Michael E. Holloway
mhollo@umich.edu
ORCID iD: 0000-0001-6767-4374

For Brooke

ACKNOWLEDGEMENTS

The following dissertation would not have been possible without the instruction, support, and friendship of several individuals. I am very grateful for you.

First, I would like to thank my advisor Professor Iain Boyd, who extended his wealth of knowledge, expertise, and patience to me. Under his guidance the last five years, I have learned much about the world of hypersonics. I would also like to thank my other committee members, Professors Krzysztof Fidkowski, Mirko Gamba, and Eric Johnsen for offering their valuable time to serve on my committee. I would also like to thank Professor Fidkowski for valuable conversations related to this thesis and for assuming the duties of Chair. Additionally, I would like to thank Drs. Kyle Hanquist and Ross Chaudhry for offering their valuable assistance and contributions to this thesis.

There are also numerous educators outside of Michigan that played a valuable role in shaping me into who I am today. I could not possibly list them all, but some of the most influential were Mrs. Kathy McCormack and Mr. John Lennon at Signal Mountain High School and Professors Stephanie TerMaath, Kivanc Ekici, and Dr. Robert Bond at the University of Tennessee. Each challenged me and encouraged me further than I could have imagined. They helped me realize that pursuing my dreams was possible.

I thank my NGPDL labmates and other friends, both in Ann Arbor and elsewhere. Your friendship and our intramural teams made this time more enjoyable. I also thank those in the Aerospace department for their willingness to study with me. I

will cherish these memories forever. Additionally, I would like to thank those in and around the Pinckney Community. I could not think of a better group to travel and watch softball with, your hospitality is treasured. I also thank my friends and family from GradCru and Grace Bible Church. Your wisdom and encouragement filled my time at Michigan with joy.

Finally, I would like to recognize my family for their constant support and encouragement. Most importantly, I thank my wife, Brooke. She was always supportive, even on the numerous occasions when I was absent both physically and mentally. I love you.

This research was supported in part through computational resources and services provided by Advanced Research Computing at the University of Michigan, Ann Arbor. Funding was provided through the U.S. Air Force Office of Scientific Research Grants FA9550-16-1-0291 and FA9550-21-1-0075.

TABLE OF CONTENTS

LIST OF FIGURES

FIGURE

LIST OF TABLES

TABLE

LIST OF ABBREVIATIONS

2T two-temperature

AFRL Air Force Research Laboratory's

CalTech the California Institute of Technology

DARPA Defense Advanced Research Projects Agency's

CFD Computational Fluid Dynamics

CUBRC the Calspan-University of Buffalo Research Center

HET Hypervelocity Expansion Tube

HTV-2 Hypersonic Technology Vehicle 2

LeMANS "Le" Michigan Aerothermodynamic Navier-Stokes Solver

MMT Modified Marrone-Treanor

PCE polynomial chaos expansion

PESs potential energy surfaces

QCT quasiclassical trajectory

QoI quantity of interest

RE radiative equilibrium

RMS root mean square

STS State-to-State

VDF velocity distribution function

ABSTRACT

Hypersonic vehicles operate at speeds in excess of Mach 5, producing extreme temperatures and nonequilibrium flow phenomena. A principle challenge associated with designing hypersonic platforms lies in the modeling of the nonequilibrium environment in which they will operate. The overall goal of this thesis is to perform a detailed investigation into the thermochemistry modeling of hypersonic air flows and is broken into two main sections.

The first section provides an assessment of different assumptions for thermochemistry modeling on hypersonic air flows. A computational analysis is used to study flows over a double-cone using three different thermochemical approaches: nonequilibrium flow, equilibrium flow, and frozen flow for air at several different freestream conditions. The thermochemical model effects on the flow field and surface properties are specific areas of interest. The resulting aerothermodynamic loads are compared to experiments performed in the CUBRC LENS-I and LENS-XX facilities and indicates that thermochemistry modeling plays an important role in determining surface properties. The results indicate that the specific thermochemistry model used to describe hypersonic flow over a double-cone plays an important role in determining surface properties for both CUBRC facilities, especially at high enthalpies. A comparison of Park and Modified Marrone-Treanor thermochemistry models is also made and conclude that both models produce similar surface properties, a result of the freestream density, and fail to reproduce experimental results. Careful analysis concludes that consistent over and under prediction of pressure drag and heat load indicates there is

some unknown fundamental difference between the actual experiments and the simulations, thus limiting the usefulness of these double-cone experiments for validation of thermochemistry models.

The second section focuses on understanding the uncertainties between computational simulations and experiments by conducting a sensitivity analysis on the thermochemical kinetics of hypersonic flow over a cylinder. A computational analysis is used to model Mach 5 and Mach 7 flows over a cylinder, where freestream properties are representative of experiments to be conducted in the Hypervelocity Expansion Tube at the California Institute of Technology. The sensitivity analysis is conducted using the polynomial chaos expansion method and Sobol indices are used to determine which thermochemical nonequilibrium phenomena most affect various quantities of interest. The results show that the O_2-N_2 and O_2-O reactions dominate surface pressure, surface heat transfer, drag, heating rate, and rotational temperature, while the first two Zeldovich reactions dominate the surface number density of NO. The O_2-O_2 reaction was found to be less important than other reactions. Surface pressure and drag are also shown to be relatively insensitive overall. The results also indicate flow separation and recirculation near the trailing edge of the cylinder. These findings will help diagnostic developments to lower discrepancies between computation and experiments, and indicate that the Hypervelocity Expansion Tube experiments should be successful for the future evaluation of thermochemistry modeling.

CHAPTER 1

Introduction

"The man in black fled across the desert, and the gunslinger followed."

Stephen King, *The Gunslinger*

1.1 Background

Hypersonic flight took on serious international interest in the late 1940's after the end of World War II. In 1949 the first manufactured object reached hypersonic velocities of Mach 6.7 at a facility in White Sands, New Mexico. However, this vehicle burned up during reentry due to extreme heat loads. Studies continued during the cold war with nations sending humans to pilot hypersonic vehicles, and perhaps climaxed during the Apollo program with man's landing, and safely returning, trip to the moon. These initial hypersonic applications were largely blunt-nosed, slender-bodied rockets, or in the case of the Mercury, Gemini, and Apollo programs, blunt capsules. Hypersonic flight vehicles have successfully flown for more than 72 years, with Apollo reentry reaching Mach 35. Much of this success is credited to conservative designs, due to the lack of computational resources and knowledge, and enormous

funding allowing for numerous and expensive testing. A wide spectrum of hypersonic test facility categories is shown in Fig. 1.1 where the ranges of velocities and test time, assuming air as the test gas, are displayed. However, with the improvement of computational resources, over time focus began shifting to hypersonic approaches and applications that can reduce cost [1].

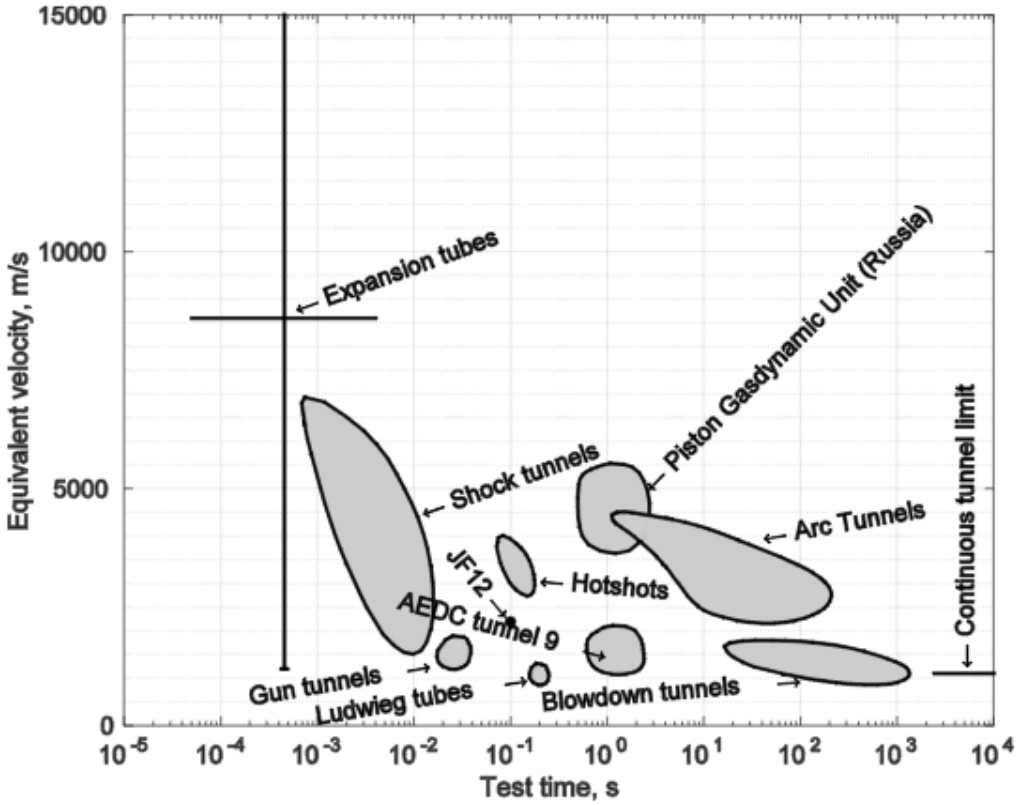

Figure 1.1: Hypersonic test facility categories assuming air as the test gas [1].

Many experiments on hypersonics were carried out between the late 1940's and today. In the late 1950's and 1960's shock tube studies were conducted to measure the rate of oxygen and nitrogen dissociation [2–4]. The shock tube produces a strong shock that travels down stream and over some measurement system. These experiments can only measure on the order of milliseconds, shown by Fig. 1.1. These

experiments still inform popular models today. The estimated uncertainty in these experiments was about 30%, mostly due to the measurement of the shock speed. The disregard of thermal nonequilibrium also produced errors in the measurements. These assumptions are now known to significantly influence quantities of interest.

Continuing the investigation into hypersonics, Chul Park interpreted the shock tube data using a two-temperature (2T) model in the 1980's and 1990's [5–10]. The overall objective of interpreting the data was to account for the effects of vibrational energy. Park was eventually able to propose a chemical kinetics model after several shock tube experiments were simulated so rates could be determined. This model is known today as Park's 2T model. The Park 2T model is one of the most popular utilized tools for researchers today and is discussed later in Chapter 2.

Recent advances in computational hypersonics includes the introduction of the quasiclassical trajectory (QCT) method [11–13]. This method was constructed by the production of several potential energy surfaces (PESs), which describes the force on each atom during a molecular interaction, allowing the time-evolution of a system to be simulated using the classical equations of motion. Such a method allows for detailed information about dissociation and relaxation. However, QCT is computationally expensive when compared to Park's 2T model, leaving computationalist to wonder if the method is worth the extra expense or if Park's 2T approach is "good enough" for their investigation. This dissertation aims to help answer that question.

The past several years has also seen a significant growth in international interest for hypersonic flight. The United States Department of Defense has recently made hypersonics one of its highest technical priorities, and as a result there has never been

more activity on hypersonics than there is today in the United States [14]. Other nations around the world are also funding military and civilian programs involving hypersonic flight [15], leaving citizens to wonder if the United States is moving quickly enough to respond [16]. A few United States examples of hypersonic flight include the Space Shuttle program, the Defense Advanced Research Projects Agency's (DARPA) Hypersonic Technology Vehicle 2 (HTV-2) program shown in Fig. 1.2 [17], and the Air Force Research Laboratory's (AFRL) HIFiRE program shown in Fig. 1.3 [18]. The United States also recently launched American astronauts from United States soil for the first time in nearly a decade [19] and like the Space Shuttle before it, the redesigned capsule reenters at hypersonic velocities. Several examples of international hypersonic programs can be found in Ref. [20].

Figure 1.2: An illustration of DARPA'S HTV-2 [17].

Figure 1.3: Launch of AFRL's HIFiRE hypersonic test vehicle [18].

One important test facility in the advancement of hypersonic research is the Calspan-University of Buffalo Research Center (CUBRC). CUBRC was founded in 1983 as an independent non-profit research and development company. CUBRC's facilities, however, date back to the 1950's where it made contributions to NASA's Gemini and Apollo capsules as well as the Space Shuttle. More recently, CUBRC has worked in the area of hypersonics by completing their LENS-I high energy shock tunnel which can operate up to 12,000 ft/sec. This tunnel served many United States Department of Defense and NASA projects, such as the X-43 Scramjet.

A major contribution to hypersonic experiments was the LENS-I experiments of the double-cone. In 2001, a set of these experiments were conducted by Harvey et al. [21] and they have been widely used for code validation the last two decades. The double-cone experiments agreed with numerical simulations for high enthalpy nitrogen flows [22], however there were large discrepancies when dealing with air and oxygen [23]. Further investigation found that the double-cone flow field was sensitive to the nonequilibrium effects [24]. Further studies by Druguet et al. [25] eventually led researches to believe that the previously conducted high enthalpy double-cone experiments suffered from nonequilibrium in the freestream and reflected shock tunnel, thus impacting surface properties [26]. It was determined that new hypersonic experiments should be conducted in a facility free of a freestream in nonequilibrium, thus new double-cone experiments were conducted in the newer LENS-XX shock tunnel in 2013 [27]. The LENS-XX shock tunnel can produce freestream conditions up to 35,000 ft/sec to simulate re-entry into Earth and other planetary atmospheres. It was believed that the freestream would be better characterized in this facility, thus low-

ering discrepancies between numerical simulations and experimental measurements. CUBRC is discussed further in Chapters 3 and 4.

1.1.1 Hypersonic Flight

Hypersonic flight refers to the flight regime where ideal gas assumptions begin to break down. This means that chemical reactions and activation of the vibrational energy modes are beginning to take place in the flow and nonequilibrium effects begin to occur and dominate the flow physics. This phenomenon is generally understood to take place at speeds above Mach 5.

A principal challenge associated with designing these hypersonic platforms lies in the modeling of the nonequilibrium flow environment in which they will operate. Nonequilibrium flow can be characterized in two categories, thermal and chemical nonequilibrium. Thermal nonequilibrium occurs behind shock waves where the gas is suddenly heated and the internal energy modes, characterized by a temperature, are in nonequilibrium. This is due to the difference in time scales it takes different internal energy modes, such as the various translational, rotational, vibrational, and electronic modes, to equilibrate. Chemical nonequilibrium refers to the population distribution of individual species in multi-species mixtures. The flow is in chemical equilibrium when the population distribution of species is unchanging. With a 50% difference in vibrational energy spacing between nitrogen and oxygen, and an almost 100% difference in chemical bond strength, the accuracy of these nonequilibrium flow models become very important in sustained hypersonic flight conditions where oxygen

is not entirely dissociated. This phenomenon occurs at flight conditions between about Mach 5 and Mach 10.

Atomic oxygen is also highly reactive with the vehicle surface material. This surface thermochemistry involves surface-fluid interactions due to the intense heating a flow experiences during hypersonic conditions. In a nonequilibrium flow, air species upstream of the surface have not fully equilibrated by the time they reach the wall. This allows these air species to interact with the generally cooler wall and impart some of their energy into the wall, initializing catalytic reactions between the gas-phase molecules and atomic species bound to the surface. These chemical reaction can significantly affect surface properties and release atoms of the surface material into the gas-phase, which can alter the chemical pathways associated with plasma formation [28]. The degree to which surface properties are effected depend on the composition and behavior of the surface material and the characterization of chemical reactions in the flow.

Additionally, hypersonic flight vehicles approaching velocities near or in excess of Mach 10, like those produced by the Space Shuttle during reentry, produce an intense heating of the gas that generates a layer of plasma around the vehicle [29]. This generation of plasma is known to hinder characteristics of the flight vehicle, such as surface ablation and the transmission of radio-waves, and can lead to a total loss of communication between the flight vehicle and the satellites and ground stations that are tracking it [30, 31]. For reentry vehicles like the Space Shuttle, this blackout of communication occurs during a relatively short time frame. However, the phenomena becomes more of a challenge when dealing with sustained hypersonic flight vehicles

where the mission may spend a considerable amount of time within the blackout regime, potentially affecting guidance, tracking, radar identification, electronic countermeasures, and abort functionality [30].

A predominant characteristic of sustained hypersonic flight is the aerothermochemistry. Aerothermochemistry is a scientific term for the study of gases taking into account the effects of motion, heat, and chemical changes. Understanding the aerothermochemistry of sustained hypersonic flight has been the focus of a large body of research over the course of the last several years. Some recent examples of these studies include developing numerical methods for molecular dissociation and relaxation, nonequilibrium flows, fluid-surface interactions, and others [32–35]. Despite extensive research the past decade, there are still discrepancies when dealing with aerothermochemistry, shown by differences between Computational Fluid Dynamics (CFD) and experimental measurements in Refs. [36–38]. Due to the extreme challenge of replicating the high-enthalpy freestream conditions associated with hypersonic flows in ground test facilities, the advancement of the state-of-the-art in this area will rely heavily on computational simulations.

There is still a great deal of uncertainty regarding the range of applicability of the underlying thermochemical models governing the physics of these nonequilibrium flows. The need for improved computational understanding of hypersonic flight is demonstrated by the DARPA HTV-2 project. The overall goal of the project was to provide the United States the capability to reach any target in the world with an unmanned flight vehicle in one hour or less. Obviously, this requires a flight vehicle that will spend a considerable amount of time in the hypersonic flight regime.

During a 2011 test flight, HTV-2 was able to fly for about three minutes before its safety system aborted the mission and crashed into the Pacific Ocean. The ensuing investigation found that the vehicle had endured flight loads larger than what was predicted, causing fatal damage to the surface and termination of flight. The outcome of the demonstration indicates the need for an improved understanding of the thermochemical models governing the physics of hypersonic flow. Therefore, this dissertation aims to, first, identify hypersonic flow conditions that are good test cases for assessment of detailed thermochemistry modeling. Second, the current work aims to lower discrepancies when dealing with hypersonic flows and thermochemistry models by collaborating with experimentalists in identifying key reactions that influence quantities of interest.

1.2 Motivation and Scope

One of the most important aspects of hypersonic aerothermodynamics is how the thermochemistry affects the surface properties. Flow with extreme temperatures of several thousand Kelvin is produced around hypersonic vehicles. These extreme temperatures lead to complex physical processes such as activation of internal energy modes and chemical reactions. These processes along with the shock wave interaction with the boundary-layer significantly affect the aerothermodynamic properties of the gas, such as pressure and temperature. Therefore, it is important that these interactions can be predicted with physical accuracy and numerical efficiency.

The overall motivation of this dissertation is to develop a better understanding of

the aerothermochemistry that accompanies hypersonic flight to help enable vehicles to fly faster, longer, and at different freestream conditions. This is accomplished by utilizing CFD and other computational tools to analyze the effects of thermochemistry modeling for hypersonic relevant air flows that would otherwise be too expensive or complicated to replicate in a laboratory setting.

This dissertation focuses on the external aerothermodynamics. Specifically, the current works aims to study 5-species air modeled as a laminar flow. Though the transition to turbulence is important, the presented flow scenarios are understood to be laminar. The laminar model also allows for an in-depth analysis of hypersonic reacting flows at low computational cost. The 5-species air model involves: (1) molecular nitrogen, N_2, (2) molecular oxygen, O_2, (3) atomic nitrogen, N, (4) atomic oxygen, O, and (5) nitric oxide, NO. Hypersonic air species can also be ionized and the flow can contain free electrons, making an 11-species air model relevant. However, the current work focuses on hypersonic conditions where temperatures are not high enough to ionize the flow. Therefore, the 5-species air model allows for a sufficient study of the aerothermodynamics at low computational expense.

A recurring strategy in this dissertation involves the alteration of the thermochemical kinetics that is associated with the modeling of hypersonic flows. This approach allows computationalists to compare modeling assumptions side-by-side to help determine the impact of those assumptions. For example, the thermochemical kinetics model can be altered such that chemical reactions do not take place in the flow. This is identical to the perfect gas model. CFD simulations with chemistry turned on and turned off can be compared against each other to help determine the significance

of the thermochemistry model. Particular reactions are also studied individually to help determine how they influence a particular hypersonic flow. This requires the incorporation of multiple computational tools, which accounts for a major portion of the presented work. Additionally, this work provides insight into the usefulness of past and current hypersonic experiments for validation of thermochemistry models by comparing different models to each other and to experimental measurements.

A significant portion of this work is also motivated by the collaboration between experimentalists and computationalists. Creating hypersonic experiments and computational simulations is a difficult task that often leads to multiple inconsistencies between the two groups, like those discussed in Section 1.1. However, when the two groups work together it can help create ideal experiments that are relevant to real-life flight vehicles, that can be reproduced by computational simulations, and that produce high-quality data which can be used to validate new thermochemistry models. Hypersonic facilities are crucial in the development to any real-world vehicle. Computational simulation of the hypersonic facilities themselves help aid in the characterization and development, which can lower inconsistencies by providing data that can be used to improve diagnostics.

1.3 Dissertation Outline

This dissertation is divided into six chapters. The first chapter presented a brief background and motivation for the current work. More importantly, it underlines the main objective of this dissertation which is to gain a better understanding of

the aerothermochemistry that accompanies hypersonic flight. The second chapter provides a discussion on thermodynamics and equilibrium. Additionally, Chapter 2 provides an in-depth description on the numerical modeling and simulation of hypersonic gas dynamics and the numerical methods utilized in this dissertation.

The major results of this dissertation are provided in Chapters 3-5. Chapter 3 investigates the effects of thermochemistry modeling for hypersonic flow with freestream conditions in a nonequilibrium state. Chapter 3 lays a foundation for Chapter 4 where the effects of thermochemistry modeling for hypersonic flow is also investigated, but the freestream has now been measured in what is believed to be a better characterized facility. Chapter 4 also compares the effect of a newly implemented thermochemistry model against Park's 2T model. Chapters 3 and 4 provide a foundation for the motivation of Chapter 5 where a sensitivity analysis on the thermochemical kinetics is examined to help better understand inconsistencies between CFD and experiments, which required collaboration between the two groups. Chapter 5 also required the coupling of different numerical tools, which accounted for a major portion of the current effort.

This dissertation ends with Chapter 6, which includes an in-depth discussion on conclusions based on trends observed in Chapters 3-5. It also provides an overview of specific research contributions, recommendations for future work, and a list of publications by the author.

CHAPTER 2

Numerical Modeling and Simulation of Hypersonic Gas Dynamics

A principal challenge associated with designing hypersonic platforms lies in the modeling of the nonequilibrium flow environment in which they will operate. Consequently, this requires a fundamental understanding of thermodynamics and equilibrium and is discussed below.

This chapter begins by briefly discussing the underlying physics associated with nonequilibrium flow phenomena typically found in hypersonic flow environments. Next, a description of the CFD used to simulate hypersonic flow fields is provided. The chapter ends with a brief overview of the toolkit used to conduct the sensitivity analysis on the chemistry model.

2.1 Thermodynamic Equilibrium

The physics for any gas species governed by the ideal gas law accounts for several different energy modes. The gas particles interact with each other through collisions, thus transferring energy between particles and different internal energy modes. The energy levels of each mode can be quantized. A brief overview of energy modes for diatomic molecules is discussed in the following paragraphs.

The translational energy mode describes the kinetic energy of a particle. Each particle's translational energy is due to its kinetic motion and can be defined classically by simply $\epsilon_{tr} = \frac{1}{2}mv^2$. Therefore, the translational energy mode is also related to the velocity distribution function (VDF). The VDF can simply be defined as the probability function of finding a particle at a particular velocity. There are three degrees of freedom in three dimensional space. Translational energy levels are usually treated as a continuum due to the extremely small spacing between energy levels ($\approx 10^{-38}$ J) [39].

The rotational energy mode describes a particle's energy due to rotation. The rotation is often described by the rigid-rotor model [39]. For diatomic molecules, there are two degrees of freedom. The rotational energy is quantized, however, due to the small spacing between energy levels, a classical treatment is typically utilized. Monatomic gas particles do not have a rotational mode.

The vibrational energy mode describes a particle's energy due to oscillations in molecules. The energy levels are quantized and unlike the rotational and translational modes, the spacing is relatively large. It is likely that the vibrational mode is never

fully activated due to molecular dissociation at high vibrational levels. Monatomic gas particles do not have a vibrational mode.

Bound electrons also contribute to the internal energy of a particle. The electrons bound to an atom or molecule can occupy different energy levels, and these levels have very large spacing. In general, the ground state is the most heavily populated. However, other excited levels are important for understanding radiation.

Lastly, free electrons also contribute to the internal energy of a gas and they describe electrons that are not bound to a particle. These electrons have their own translational mode, small mass, and high velocities. The energy of free electrons is treated as continuum. The free electron mode is not considered in this dissertation due to their absence in the emphasized 5-species gas model (N_2, N, O_2, O, and NO).

Additionally, it is important to understand the time it takes for spatial changes to occur in the flow properties. This is usually described by some characteristic flow time τ. The degree of nonequilibrium can be determined by comparing different time scales. Another important parameter for understanding the degree of nonequilibrium are the length scales. Typically, this is determined by the Knudsen number, shown in Eq. 2.1 where λ is the mean-free-path and L is a characteristic length scale. Equation 2.1 is useful in determining the flow regime. When $K_n < 0.01$, the flow regime is in continuum and when $K_n > 10$ the regime is defined as free molecular flow. The presented work considers flows that are in the continuum regime.

$$K_n = \frac{\lambda}{L} \tag{2.1}$$

The temperature can describe the distribution of energy in thermal equilibrium. In this approach, thermal equilibrium is expressed as:

$$T_{\mathrm{tr}} = T_{\mathrm{r}} = T_{\mathrm{vib}} = T_e \tag{2.2}$$

For gases in thermal nonequilibrium, a multi-temperature approach is needed. One of the most popular examples of this is the 2T model [9]:

$$T_{\mathrm{tr}} = T_{\mathrm{r}}, \quad T_{\mathrm{vib}} = T_e, \quad T_{\mathrm{tr}} \neq T_{\mathrm{vib}} \tag{2.3}$$

The previous paragraphs explain the relation between particles and the energy distribution between them. Specifically, when the internal energy of a gas was distributed equally between modes, and between species for multi-species mixtures, the gas was in thermal equilibrium. Additionally, an understanding of chemical equilibrium is important to grasp hypersonic flow physics.

Chemical equilibrium refers to the population distribution of individual species in a multi-species mixture. The flow is in chemical equilibrium when the population distribution of species is unchanging and the values are determined by statistical mechanics. When the gas is in both chemical equilibrium and thermal equilibrium, this work simply describes the flow as in a state of equilibrium.

2.2 LeMANS: Hypersonic Flow Solver

The numerical simulations presented in this study are partially performed using the CFD code "Le" Michigan Aerothermodynamic Navier-Stokes Solver (LeMANS), which was developed at the University of Michigan to simulate hypersonic reacting flows. LeMANS has been benchmarked by NASA hypersonic CFD codes DPLR and LAURA and verified and validated for a wide range of hypersonic conditions, such as Apollo, Fire II, and RAM-C [40, 41]. A complete overview of LeMANS can be found in Ref. [42].

LeMANS is a multi-dimensional, parallel code that solves the Navier-Stokes equation with second-order spatial accuracy on structured and unstructured computational grids. Both the Park [9] and Modified Marrone-Treanor (MMT) [43] 2T models are implemented in LeMANS. Each model is discussed in detail below. LeMANS includes thermochemical nonequilibrium effects and the flow is modeled assuming that the continuum approximation is valid. LeMANS couples the Navier-Stokes equations with thermodynamic and transport property models [40]. LeMANS solves the flow field by integrating differential equations spatially and temporally. The finite volume method is implemented to integrate spatially. A modified Steger-Warming flux vector splitting scheme [44] is implemented to calculate the flux of inviscid components across cell faces and a central scheme is used for the viscous fluxes [40]. The code is parallelized using the OpenMPI software library and mesh partitioning is performed with the METIS software library [45]. A detailed discussion on LeMANS is provided below.

2.2.1 Navier-Stokes Equations

The Navier-Stokes equations are a set of partial differential equations used to describe the physics of fluid motion that express the conservation of mass, momentum, and energy. LeMANS solves the compressible Navier-Stokes equations that account for any number of fluid species as well as thermal and chemical nonequilibrium. The compressible Navier-Stokes equations are shown in Eq. 2.4 – 2.8. The inviscid and viscous fluxes are split into vectors $\mathbf{F}$ and $\mathbf{F_v}$, with conserved variables $\mathbf{Q}$ and source terms $\mathbf{S_{cv}}$.

$$\frac{\partial \mathbf{Q}}{\partial t} + \nabla \cdot (\mathbf{F} - \mathbf{F_v}) = \mathbf{S_{cv}} \tag{2.4}$$

$$\mathbf{Q} = \begin{Bmatrix} \rho_1 \\ \vdots \\ \rho_{ns} \\ \rho u_i \\ \rho u_j \\ E \\ E_{ve} \end{Bmatrix} \tag{2.5}$$

$$\mathbf{F_i} = \begin{Bmatrix} \rho_1 u_i \\ \vdots \\ \rho_{ns} u_i \\ \rho u_i^2 + p \\ \rho u_i u_j \\ (E+p)u_i \\ E_{ve} u_i \end{Bmatrix} \tag{2.6}$$

$$\mathbf{F_{v,i}} = \begin{Bmatrix} -J_{i,1} \\ \vdots \\ -J_{i,ns} \\ \tau_{ii} \\ \tau_{ij} \\ \tau_{ii} u_i + \tau_{ij} u_j - (q_{tr,i} + q_{ve,i}) - \sum_s (J_{i,s} h_s) \\ -q_{ve,i} - \sum_s (J_{i,s} e_v e, s) \end{Bmatrix} \tag{2.7}$$

$$\mathbf{S_{cv}} = \begin{Bmatrix} \dot{\omega}_1 \\ \vdots \\ \dot{\omega}_{ns} \\ 0 \\ 0 \\ 0 \\ \dot{\omega}_{ve} \end{Bmatrix} \tag{2.8}$$

2.2.2 Thermodynamic and Transport Properties

Thermodynamic and transport properties also need to be taken into consideration to understand the CFD code. The species mass diffusion fluxes are modeled using a modified version of Fick's law:

$$J_i = -\rho D_i \nabla Y_i + Y_i \sum_{k=1}^{ns} J_k \tag{2.9}$$

The viscous stresses are modeled by assuming the flow is Newtonian and applying Stoke's hypothesis:

$$\tau_{ij} = \mu \left(\frac{\partial u_i}{\partial x_i} + \frac{\partial u_i}{\partial x_j} \right) + \delta_{ij} \lambda \nabla \bar{u} \tag{2.10}$$

$$\lambda = -\frac{2}{3}\mu \tag{2.11}$$

Heat fluxes are modeled according to Fourier's law for the translational-rotational and vibrational-electronic energy modes:

$$q_{tr} = -\kappa_{tr} \nabla T_{tr} \tag{2.12}$$

$$q_{ve} = -\kappa_{ve} \nabla T_{ve} \tag{2.13}$$

Species thermodynamic data for LeMANS is determined from NASA-9 polynomial fits [46]. The polynomials for the curve fit provides normalized enthalpy and entropy for each species:

$$\frac{h^0}{RT_{\text{tr}}} = -a_0\frac{1}{T_{\text{tr}}^2} + a_1\frac{\ln T_{\text{tr}}}{T_{\text{tr}}} + a_2 + a_3\frac{T_{\text{tr}}}{2} + a_4\frac{T_{\text{tr}}^2}{3} + a_5\frac{T_{\text{tr}}^3}{4} + a_6\frac{T_{\text{tr}}^4}{5} + a_7\frac{1}{T_{\text{tr}}} \tag{2.14}$$

$$\frac{s^0}{R} = -\frac{a_0}{2}\frac{1}{T_{\text{tr}}^2} - a_1\frac{1}{T_{\text{tr}}} + a_2\ln T_{\text{tr}} + a_3 T_{\text{tr}} + a_4\frac{T_{\text{tr}}^2}{2} + a_5\frac{T_{\text{tr}}^3}{3} + a_6\frac{Ttr^4}{4} + a_7 \tag{2.15}$$

The species diffusion, viscosity, and thermal conductivity transport properties are calculated using Wilke's mixing rule with Blottner's curve fits for viscosity and Eucken's relation for thermal conductivity [47–49].

2.2.3 Nonequilibrium Modeling: Park Two-Temperature

LeMANS is equipped with Park's 2T model to analyze thermal nonequilibrium [9]. Park's 2T model is the most popular two-temperature model for air. Some of the most popular CFD codes designed for hypersonic reacting flows, such as LeMANS, US3D, DPLR, and LAURA [42, 50–52], implement it. LeMANS assumes that the rotational temperature, T_r, can be represented by T_{tr} and that the vibrational and electronic energy modes can be represented by T_{vib}.

$$T_{\text{tr}} = T_{\text{r}} \tag{2.16}$$

$$T_{\text{vib}} = T_e \tag{2.17}$$

LeMANS utilizes the Landau-Teller equation, Eq. 2.18, to model vibrational relaxation. The relaxation times for gas species are calculated by the standard Millikan-White expression in Eq. 2.19 with the high temperature correction of Park, where a and b are determined from experimental measurements [9, 53]. The vibrational relaxation time is then used in Eq. 2.18 as a source term in Eq. 2.8.

$$\dot{\omega}_{t-v} = \sum_s \rho_s \frac{e^*_{v,s} - e_{v,s}}{\tau_s} \tag{2.18}$$

$$\tau_s = \frac{1}{P_{atm}} \exp\Big[a(T^{-\frac{1}{3}} - b) - 18.42\Big] \tag{2.19}$$

Chemistry is modeled using rate coefficients expressed in modified Arrhenius form, as shown in Eq. 2.20, where C and η are defined by the chemical kinetics model. Increasing C increases the rate of the particular reaction pushing it closer to equilibrium. Decreasing C will slow the reaction leaving the gas in a chemically frozen state. Some reactions are controlled by a combination of T_{tr} and T_{vib}, $T_a = \sqrt{T_{tr}T_{vib}}$.

$$K = CT^{\eta} \exp\left(-\frac{\theta_d}{T_a}\right) \tag{2.20}$$

In the computational analyses, the *nonequilibrium* case uses standard rates in the chemistry and the vibrational-translational energy transfer equations. For the purposes of this dissertation, the nonequilibrium case is the standard Park model. The *equilibrium* case increases the leading coefficient C in Eq. 2.20 by six orders of magnitude and assumes vibrational equilibrium, $T_{vib} = T_{tr}$. The *frozen* flow case decreases

the leading coefficient by six orders of magnitude and the vibrational relaxation time is increased by six orders of magnitude.

The vibrational energy change per dissociation is equal to the average vibrational energy of the gas, which is the standard treatment for the Park model [54]. Recombination rates are computed using the forward reaction rate evaluated at T_{tr} and equilibrium constants from Park [8, pp. 35–41]:

$$k_b(T) = \frac{k_f(T)}{K_c(T)} \tag{2.21}$$

2.2.4 Nonequilibrium Modeling: Modified Marrone-Treanor

The MMT chemical kinetics model has also been implemented into LeMANS. MMT has been developed recently by Chaudhry et al. [43, 55, 56] using high-quality quantum chemistry data. A brief summary of the development, form, and implementation of MMT is described below.

QCT simulations for N_2 + N_2, N_2 + N, N_2 + O_2, O_2 + O_2, and O_2 + O, using high-quality *ab-initio* PESs, were analyzed in aggregate by Chaudhry et al. [55]. These QCT calculations were sampled from Boltzmann distributions described by T_{tr} and T_{v}, and were intended to construct reduced-order models for CFD. The classic Marrone-Treanor preferential dissociation model [57] was found to almost match the reaction rates and vibrational energy changes per dissociation, except that it neglects the effect that rotational energy has on dissociation. A modification was proposed, called MMT, that was found to accurately fit the data and be consistent with the

dominant mechanisms of dissociation. The forward reaction rate for this Boltzmann-based model is defined as,

$$k_{f,\mathrm{Boltz}}\left(T_{\mathrm{tr}}, T_{\mathrm{vib}}\right) = k_{\mathrm{arr}}\left(T_{\mathrm{tr}}\right)\ Z\left(T_{\mathrm{tr}}, T_{\mathrm{vib}}\right) \tag{2.22}$$

$$k_{\mathrm{arr}}\left(T_{\mathrm{tr}}\right) = C T_{\mathrm{tr}}^{n} \exp\left(-\frac{T_{\mathrm{D}}}{T_{\mathrm{tr}}}\right) \tag{2.23}$$

$$\mathrm{Z}\left(T_{\mathrm{tr}}, T_{\mathrm{vib}}\right) = \frac{\mathrm{Q}\left(T_{\mathrm{tr}}\right)\ \mathrm{Q}\left(T_{\mathrm{F}}\right)}{\mathrm{Q}\left(T_{\mathrm{vib}}\right)\ \mathrm{Q}\left(-U\right)} \tag{2.24}$$

in which k_{arr} is the modified Arrhenius reaction rate, defined only in terms of T_{tr}, and Z is the nonequilibrium correction factor. Q is the approximate vibrational partition function, and T_{F} and U are pseudotemperatures, defined as,

$$\mathrm{Q}\left(T\right) = \frac{1 - \exp\left(-T_{\mathrm{D}}/T\right)}{1 - \exp\left(-\theta_{\mathrm{v}}/T\right)} \tag{2.25}$$

$$\frac{1}{T_{\mathrm{F}}} = \frac{1}{T_{\mathrm{vib}}} - \frac{1}{T_{\mathrm{tr}}} - \frac{1}{U} \tag{2.26}$$

$$\frac{1}{U} = \frac{a_U}{T_{\mathrm{tr}}} + \frac{1}{U^*} \tag{2.27}$$

The vibrational energy change per dissociation is defined as,

$$-\frac{\left\langle \varepsilon_{\mathrm{vib}} \right\rangle_{\mathrm{d,Boltz}}}{k_{\mathrm{B}}} = \frac{\theta_{\mathrm{v}}}{\exp\left(\theta_{\mathrm{v}}/T_{\mathrm{F}}\right)} - \frac{T_{\mathrm{D}}}{\exp\left(T_{\mathrm{D}}/T_{\mathrm{F}}\right)} \tag{2.28}$$

The model parameters are specific to each dissociating molecule and collision partner, and are shown in Table 2.1.

The previously-described equations were fit to two-temperature Boltzmann QCT data, but non-Boltzmann distributions, especially of vibrational energy, exist and can

Table 2.1: Coefficients for the MMT model; A2 is the dissociating molecule and M is the collision partner.

A_2	M	$C\ [cm^3 s^{-1} K^{-n}]$	n	$T_D\ [1000K]$	$\theta_v\ [K]$	a_U	$U^*\ [1000K]$
N_2	N_2	5.973e-06	-0.7017	117.5	3411	0.3868	254.6
N_2	N	1.327e-06	-0.5625	114.0	3411	0.3668	478.7
N_2	O_2	8.372e-05	-0.9991	116.9	3415	0.3001	210.3
O_2	O_2	6.133e-06	-0.7695	60.54	2280	0.3965	57.34
O_2	O	1.529e-06	-0.6541	60.55	2280	0.3537	237.3
O_2	N_2	3.041e-09	-0.02239	59.38	2263	0.3620	385.5

affect quantities of interest for hypersonic flows (see, for example, Refs. [58–60]). As described by Chaudhry et al. [43], a simple correction factor was found to approximate the effect of non-Boltzmann distributions on quantities of interest for a net-dissociating gas ensemble. Consequently, both the reaction rate and vibrational energy change per dissociation are corrected to account for the effect of non-Boltzmann distributions,

$$k_f = \alpha_k^{\mathrm{NB}}\, k_{f,\mathrm{Boltz}} \tag{2.29}$$

$$\langle \varepsilon_{\mathrm{vib}} \rangle_{\mathrm{d}} = \langle \varepsilon_{\mathrm{vib}} \rangle_{\mathrm{d,Boltz}} + \alpha_{\langle \varepsilon \rangle}^{\mathrm{NB}}\, D_0 \tag{2.30}$$

A simple constant correction factor of 0.5 was used previously [43], tuned only to the dynamics of a net-dissociating gas. However, as the gas approaches chemical equilibrium, or is net-recombining, the quantities of interest do not need correction. Therefore, the following variable correction factor is implemented for the dissociation

rate [56], which is based on the work of Singh and Schwartzentruber [61–63],

$$\alpha_k^{\mathrm{NB}} = \min\left\{\exp\left[\ln(0.5)\left(1 - \frac{[A][A]}{[A_2]\,K_{eq}}\right)\right], 1\right\} \tag{2.31}$$

in which [A] and [A_2] are the concentrations of the dissociated and dissociating species, and K_{eq} is the corresponding equilibrium constant. This correction factor limits to 0.5 when the reaction in question yields mostly dissociation, and 1.0 for chemical equilibrium or net recombination. For the vibrational energy change per dissociation, a simpler constant correction factor is used,

$$\alpha_{\langle\varepsilon\rangle}^{\mathrm{NB}} = 0.1 \tag{2.32}$$

which is based on Chaudhry et al. [43]; a variable correction factor for the vibrational energy change term is being considered but does not appear to have a significant effect.

The backward reaction rate coefficient is evaluated using the equilibrium constant and the forward rate coefficient evaluated using only T_{tr}. Exchange reactions are treated using Park rate coefficients [9]. Other details of the MMT model implementation, including the numerical limiting behavior, implicit time stepping, and treatment of other reactions, are described in the implementation-specific papers [43, 56].

2.3 Dakota: Toolkit for Sensitivity Analysis

The sensitivity analysis in Chapter 5 of this dissertation is performed using Dakota, developed at Sandia National Laboratory. Dakota provides a flexible and extensible interface between simulation codes like LeMANS and iterative analysis methods [64]. Dakota contains algorithms for a wide variety of situations, including sensitivity analysis, that would otherwise be complicated or time consuming to implement into CFD codes like LeMANS itself. For the purposes of this dissertation, Dakota works by reading user specified inputs that it communicates to LeMANS. After a LeMANS simulation is complete, Dakota saves quantities of interest and begins to execute its next run of LeMANS based on user inputs and LeMANS outputs. A diagram of how Dakota is wrapped around LeMANS is shown in Fig. 2.1.

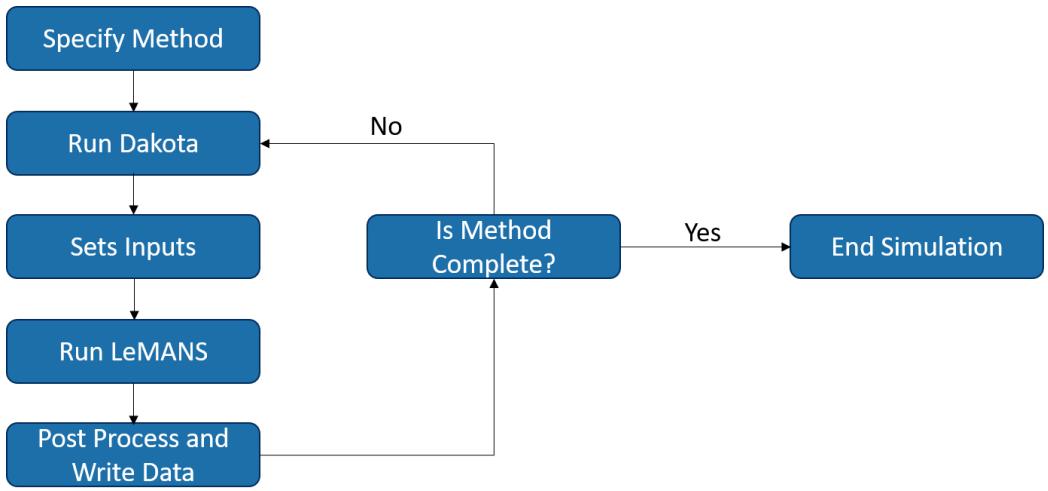

Figure 2.1: Dakota algorithm.

In general, Dakota offers three different strategies to conduct a sensitivity analysis: parameter methods, random-sampling methods, and stochastic expansion methods. The most simple strategy of sensitivity analysis is the parameter method. Parameter

methods simply change the inputs defined by the user for each CFD simulation. The quantities of interest are then saved and the next CFD simulation begins. Parameter methods are computationally inexpensive but leave a lot of responsibility on the user to recognize sensitive inputs. In other words, it can be challenging to find sensitive inputs that effect the quantities of interest. The most common strategy to estimate sensitivity is to randomly sample the sensitive input. Example of these methods include Monte Carlo, quasi-Monte Carlo, and Latin Hypercube Sampling. Random-sampling methods are simple to implement and converge at the same rate, regardless of the number of input variables. However, random-sampling methods converge at low rates and are computationally expensive to run. Lastly, stochastic expansion methods, such as polynomial chaos expansion (PCE) introduced by Wiener [65], use high-order polynomial approximations to generate a mapping between the sensitive input parameters and a quantity of interest (QoI). The convergence rate is much higher for these methods when the quantities of interest are a smooth function of the inputs. However, the scaling between evaluations and number of input parameters is not ideal as it becomes computationally too demanding to reach the convergence domain, as shown by Crestaux et al. [66]. For these situations, sampling methods are more attractive. Examples of PCE applied to hypersonic flow can be found in Refs. [37, 38].

In the current work, Sobol indices are used to measure input-variable sensitivities. Sobol indices are a form of global sensitivity analysis. Sobol indices are calculated by measuring the variance of the QoI across all inputs and then apportioned to each of the input parameters [37]. Therefore, this method of sensitivity analysis is attractive

because it can measure sensitivity across the whole input space, deal with nonlinear responses, and can measure the effect of interactions in non-additive systems. Index values close to 1 indicate that the input dominates the effects of the others. Index values near zero indicate that the QoI is insensitive to the input. For example, consider the relationship between lift and freestream velocity, freestream density, coefficient of lift, and area is unknown. In this example, the inputs are C_l, the coefficient of lift, U, the freestream velocity, and A, the surface area, and L, lift, is the QoI. A sensitivity study on lift would produce a higher Sobol index value for U than for C_l and A, because of the squared term in Eq. 2.33, indicating that the freestream velocity is more important to consider than coefficient of lift or surface area.

$$L = C_l \frac{\rho U^2}{2} A \tag{2.33}$$

As a result of the PCE method providing a mapping between the input parameters and QoI, the Sobol indices can be calculated analytically and automatically by Dakota. Additionally, the current work investigates a low number of inputs. Therefore, the PCE method is utilized to conduct the sensitivity analysis. Sobol indices can also be estimated with random-sampling methods, but they require many more function evaluations and provide only approximate results. In most uses of sensitivity analysis, approximate results are sufficient [37].

Polynomial chaos expansion is a general framework for the approximate representation of random response functions in terms of finite-dimensional series expansions in standardized random variables:

$$R = \sum_{i=0}^{P} \alpha_i \Psi_i(\xi) \tag{2.34}$$

where α_i is a deterministic coefficient, Ψ_i is a multidimensional orthogonal polynomial and ξ is a vector of standardized random variables. The extended method is used as the basis for polynomial expansion, which is the default for Dakota. An important distinguishing feature of the PCE methodology is that the functional relationship between random inputs and outputs is captured, not merely the output statistics as in the case of many nondeterministic methodologies [64].

2.4 Chapter Summary

This chapter lays a foundation that will be referenced throughout this dissertation. Specifically, a brief overview of the underlying physics involved in hypersonic nonequilibrium flows was provided. This included a discussion on thermal and chemical equilibrium. An in depth discussion on the CFD code LeMANS utilized throughout this study was also provided. Generally, LeMANS is a hypersonic Navier-Stokes solver that utilizes models to account for both thermal and chemical nonequilibrium. Finally, an overview of the Dakota toolkit used to conduct the sensitivity analysis on the chemistry model was discussed. Specifically, an explanation of the utilized PCE method and Sobol indices was provided.

CHAPTER 3

Double-Cone Part I: A LENS-I Study

The influence of different assumptions for thermochemistry modeling in hypersonic flow over a double-cone geometry is investigated in the following chapter. A CFD analysis is used to study the double-cone in three different thermochemical cases: nonequilibrium flow, equilibrium flow, and frozen flow for four different mixtures of nitrogen and oxygen. Specific areas of interest include the thermochemistry model effects on the flow field and surface properties.

3.1 Introduction

One of the most important aspects of hypersonic aerothermodynamics is how the thermochemistry affects the surface properties. Flow with extreme temperatures of several thousand Kelvin is produced around hypersonic vehicles. These extreme temperatures lead to complex physical processes such as activation of internal energy modes and chemical reactions. These processes along with the shock wave interaction with the boundary-layer significantly affect the aerothermodynamic properties

of the gas, such as pressure and temperature. Therefore, it is important that these interactions can be predicted with physical accuracy and numerical efficiency.

A simple geometry that creates shock wave boundary layer interaction and includes nonequilibrium effects is the double-cone, shown in Fig. 3.1. The double-cone has been studied extensively throughout the past two decades [36,67–73]. In order to assess the accuracy of nonequilibrium models in predicting aerothermodynamic loads in hypersonic flight, this study specifically focuses on hypersonic shock wave laminar boundary layer interactions. Though the hypersonic shock wave boundary layer interactions in transitional and turbulent flows are important, the laminar boundary layer restriction allows for a straight-forward assessment of the nonequilibrium thermochemistry models without the added complexity and cost of modeling the transitional and turbulent boundary layers [67].

Figure 3.1: Double-cone geometry [27].

In order to determine the sensitivity of the flow and surface properties to ther-

mochemistry modeling, several different double-cone cases are studied. Each case consists of different mixtures of nitrogen and oxygen with different freestream properties.

This chapter will explain the experimental test facility, the numerical approach used, describe each test case condition, examine the resulting flow properties for each thermochemistry model, discuss any differences in surface properties and experimental results, and study the extent of nonequilibrium in each case. The chapter will end with conclusions based on trends observed.

3.2 Experimental Test Facility

A set of widely used double-cone experiments for code validation was conducted at CUBRC facility [74]. CUBRC consists of two facilities that are of importance to this dissertation, the LENS-I facility and the LENS-XX facility. An overview of the complete capabilites of CUBRC is shown in Fig. 3.2. A picture of the LENS-XX expansion tunnel is shown in Fig. 3.3. This chapter will focus on the CUBRC experiments conducted at the LENS-I facility. The double-cone experimental flow field consists of an attached shock at the leading edge of the first cone and a detached shock generated downstream by the second cone. This shock-shock interaction causes a separation in the boundary layer. The separated shock then interacts with the rear shock to form a triple point. The flow field structure is shown in Fig. 3.4. The instrumentation for the double-cone experiments incorporate high-frequency pressure gauges required to accurately follow the flow establishment of the separated interac-

tion region at the junction between the first and second cone in the approximately 1 ms run time [75]. Heating levels were measured with coated thin-film gauges and coaxial thermocouples [27].

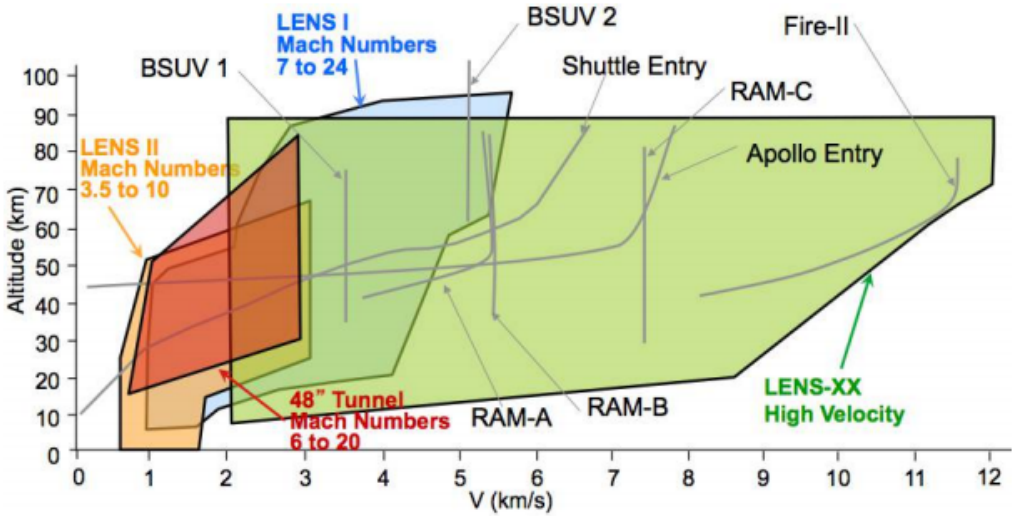

Figure 3.2: Capability Map of CUBRC Facilities to Duplicate Freestream Conditions in Air [76].

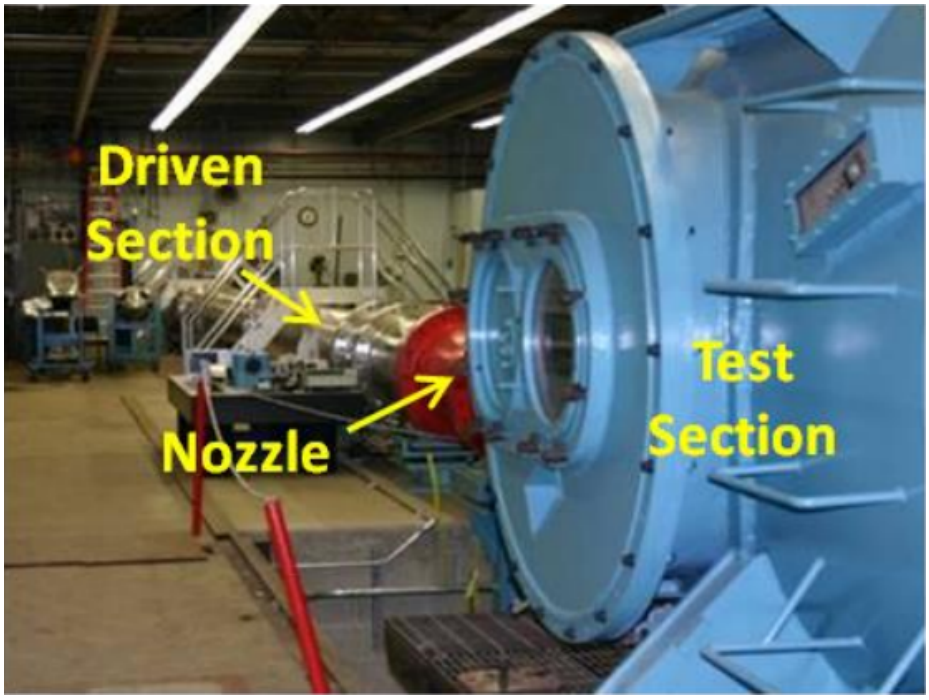

Figure 3.3: LENS-XX Large-Scale Expansion Tunnel at CUBRC [76].

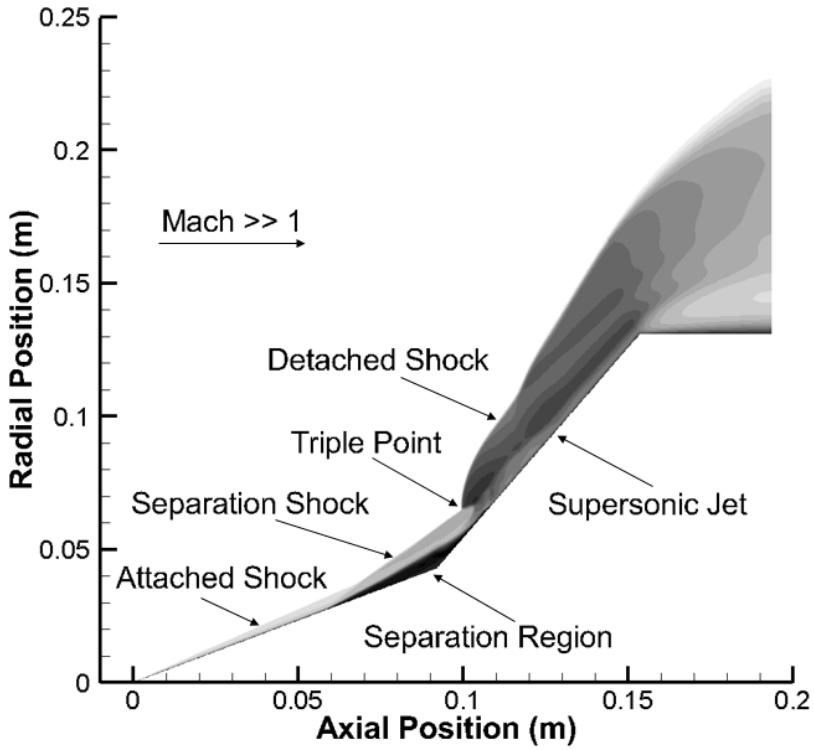

Figure 3.4: Double-cone flow field structure.

3.3 Numerical Approach

The numerical simulations utilized in this chapter are performed using the CFD code LeMANS, which was developed at the University of Michigan to simulate hypersonic reacting flows [40]. A complete overview of LeMANS can be found in Ref. [42] or Chapter 2.2 of this dissertation.

The thermochemical model used in this study utilizes Millikan-White with the high-temperature corrections of Park to model vibrational relaxation time and captures thermochemical nonequilibrium effects by means of Park's 2T model. In the computational analyses, the *nonequilibrium*, *equilibrium*, and *frozen* models discussed in Section 2.2 are utilized. For the purposes of this chapter, the nonequilibrium case is the standard Park model.

In the current chapter, an isothermal or radiative equilibrium (RE) wall condition is employed. The radiative wall condition is accomplished by setting the radiative flux equal to the convective heating crossing the wall to solve for surface temperatures. The wall is also non catalytic.

3.4 Test Case Descriptions

Each double-cone case and the freestream conditions considered in this study are shown in Tables 3.1 and 3.2 [77, 78]. The experiments for each of these cases were conducted at CUBRC's LENS-I facility [74]. Run 90 is studied to determine if thermochemistry modeling is significant for oxygen at low enthalpy. Run 88 is chosen to study the significance of modeling thermochemistry in a high enthalpy oxygen case.

Run 46 is studied to determine if nitrogen is sensitive to thermochemistry models at high enthalpy. A low enthalpy nitrogen case, Run 86, was also studied, but the results did not show sensitivity to thermochemistry and was, therefore, omitted from this dissertation. Run 43 is an air case at high enthalpy. Each case is also chosen for their good agreement between experimental results and past nonequilibrium models; reasonable agreement on the front cone indicates that the data is valid. The geometry specifications of the double-cone are shown in Fig. 3.5 and consists of a 25° first cone and a 55°second cone. The computational grid consists of approximately 320,000 cells with 636 cells along the wall and is shown in Fig. 3.6. The grid convergence study consisted of a coarse grid, approximately 160,000 cells, and a fine grid, approximately 600,000 cells. This is accomplished by multiplying and dividing the number of grid points by two using the meshing software, Pointwise. A root mean square (RMS) study between the surface pressure and surface heat transfer for each grid produced a max percent difference of 1.0% and 1.2%, respectively. The grid is also axisymmetric to save computational cost. Due to the short run time of the experiments, each case is modeled as an isothermal wall to better match the CUBRC results. However, such conditions are not representative of actual flight, so Run 90 is also modeled using the radiative equilibrium wall boundary condition to assess any sensitivity on the surface properties and sensitivity to thermochemistry modeling.

To determine if the isothermal wall model is appropriate, a heat transfer analysis is performed using the material response code MOPAR-MD in Ref. [73]. MOPAR-MD was developed at the University of Michigan and was built upon by several researchers

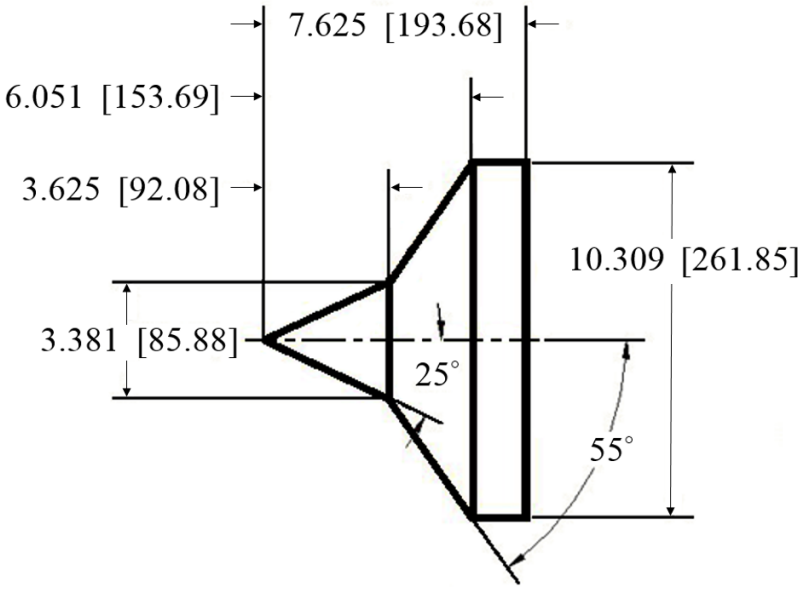

Figure 3.5: Double-cone model (dimensions in inches [mm]).

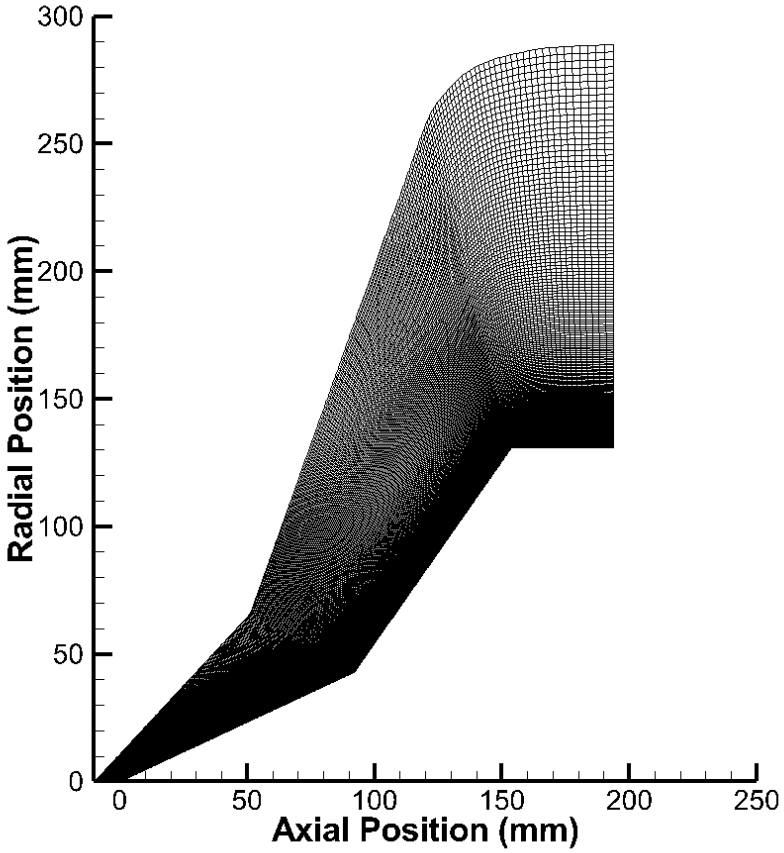

Figure 3.6: Double-cone grid.

Table 3.1: LENS-I double-cone freestream properties [77, 78].

Run:	Mach	h_0 (MJ/kg)	ρ_∞ (g/m^3)	T_∞ (K)	$T_{v\infty}$ (K)	T_{wall} (K)
90*	10.37	3.99	1.8342	190.1	1001	300
88	8.2	8.78	1.0613	569.8	697.6	300
46	11.54	8.4	1.958	281.7	3072	296.3
43	8.87	10.2	2.134	576	576	296.2
*Run 90 is also simulated with the RE wall condition						

Table 3.2: LENS-I double-cone freestream composition in terms of species mass-fractions [77, 78].

Run:	N_2	N	O_2	O	NO
90	0.00	0.00	0.9986	0.0014	0.00
88	0.00	0.00	0.9482	0.0518	0.00
46	0.9984	0.0016	0.00	0.00	0.00
43	0.737	0.00	0.1716	0.0266	0.0648

[79–82]. In this material response code, a first-order implicit time integration scheme is utilized alongside a second-order spatial discretization scheme on an unstructured grid. The energy equations are solved within each time step by means of the Newton-Raphson method. A complete overview of MOPAR can be found in [83]. The analysis is conducted for the approximate experimental run time of 0.2 ms. This analysis indicated almost no increase in surface temperature, much less than 1 K. Therefore, it must be concluded that the isothermal wall model is appropriate for the double-cone experiments analyzed in this study.

3.5 Results

3.5.1 Flowfield Results

Pressure contours from the nonequilibrium and equilibrium solutions for the isothermal wall Run 90 case are shown in Fig. 3.7. Each case demonstrates steady flow results. These pressure contours are representative of the other nonequilibrium and equilibrium Runs. For each Run, as illustrated in Fig. 3.7, the equilibrium cases produce lesser shock angles.

The pressure contours for the frozen flow Run 90 isothermal wall case are shown in Fig. 3.8(a) at 102,000 iterations. This case produces unsteady flow, as shown by the time variation in surface pressure, illustrated in Fig. 3.8(b). This phenomena is not uncommon and is illustrated in Refs. [36, 72, 73]. Each case that produces unsteady flow are cyclical. For the Run 90 frozen simulation, the cyclical nature lasts about every 2,000 iterations, or every 0.5 ms. When compared to the nonequilibrium solution in Fig. 3.7, the frozen case shows larger shock angles. These stronger shock angles are due to molecules holding more thermal energy, thus, increasing the ratio of specific heats. The stronger shocks also produce adverse pressure gradients that lead to earlier points of flow separation.

3.5.2 Surface Properties

The effects that each thermochemistry modeling approach has on the surface of the double-cone, in terms of pressure and heat transfer, are discussed below. The unsteady flow cases use time-averaged results. The experimental results were produced

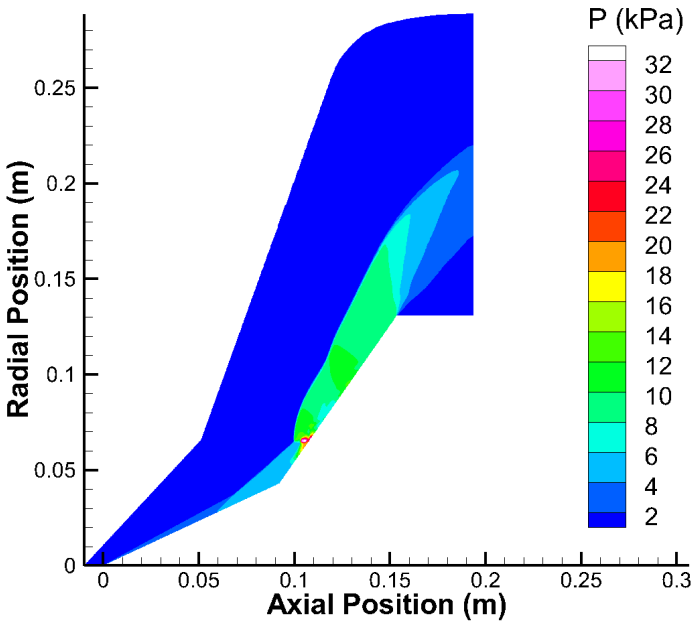

(a) Pressure contours (Run 90 nonequilibrium)

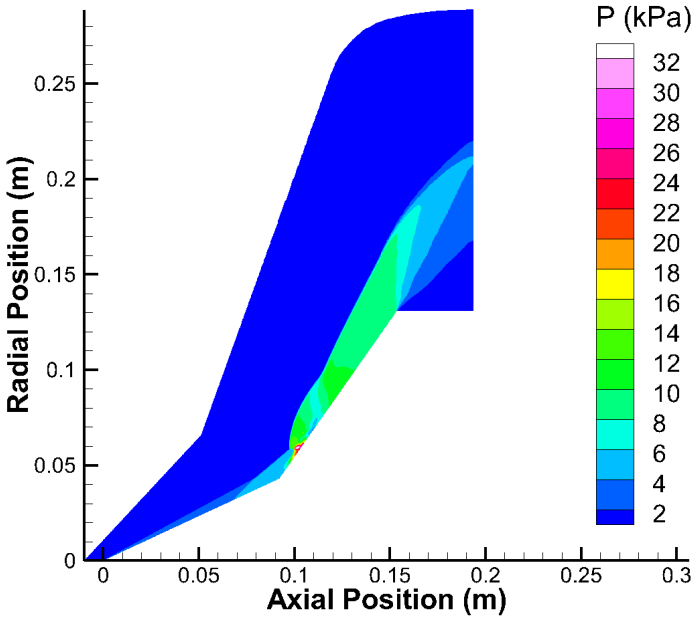

(b) Pressure contours (Run 90 equilibrium)

Figure 3.7: Double-cone nonequilibrium and equilibrium pressure contours.

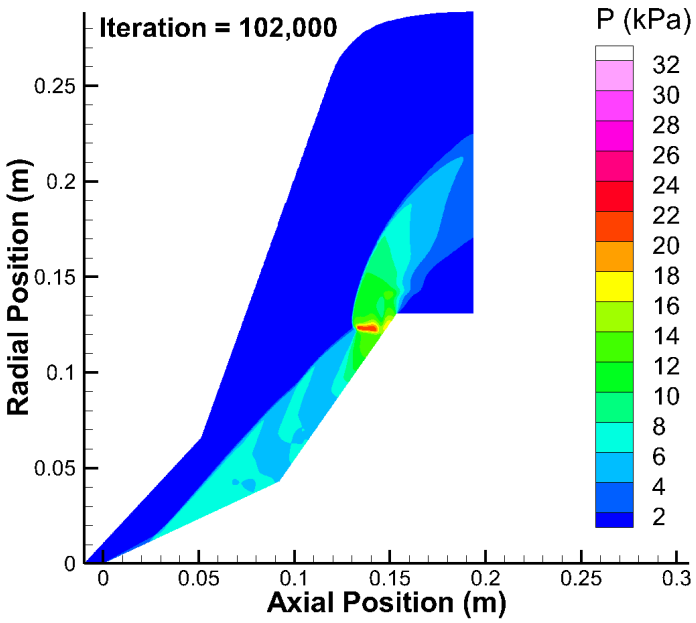

(a) Pressure contours at 102,000 iterations

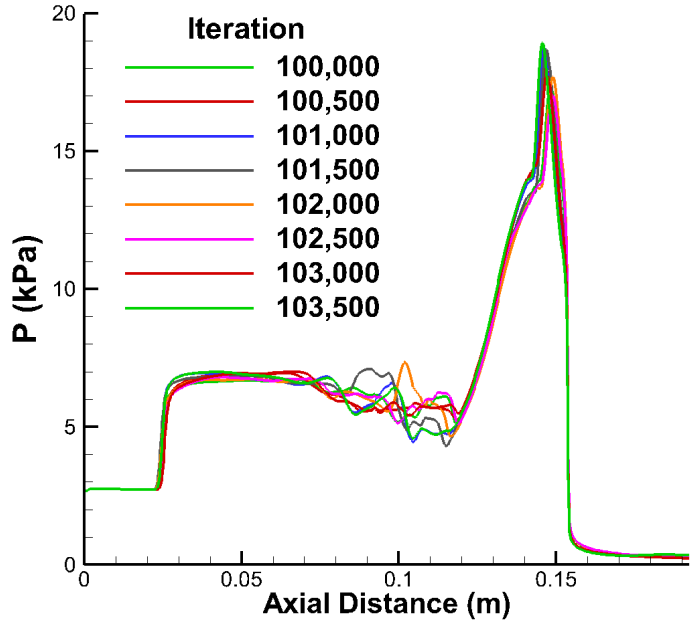

(b) Surface pressure at different time steps

Figure 3.8: Double-cone results for the frozen flow case (Run 90).

at CUBRC [74]. An in-depth evaluation of the resulting drag and heating rate is also discussed.

Each case was, in part, chosen for their agreement with prior CFD analysis. An example of this comparison is shown in Fig. 3.9 for the Run 1 test case [75]. The results in Fig. 3.9 are compared to prior analysis by Nompelis et al [84]. An RMS comparison between the two simulations show a difference of 3.9% in surface pressure and a 2.1% difference in surface heat transfer. Similar levels of agreement are obtained between LeMANS and the solutions of Nompelis et al [77, 78, 84] for all cases considered in this dissertation.

Run 90 is a low enthalpy oxygen case. The surface properties are shown in Fig. 3.10 for the isothermal wall condition and Fig. 3.11 for the RE wall condition. The frozen solution is unsteady for the isothermal wall conditions and steady for the RE wall condition. The results show that there are clear differences between the three thermochemistry approaches. The radiative wall condition also produces differences when thermochemistry modeling is varied. While the radiative wall condition slightly affects surface pressure, it significantly reduced surface heat transfer by as much as 55%. The separation location is also affected. These differences suggest that the specific approach taken to modeling thermochemistry is important for low enthalpy oxygen flows. Further, the use of a cold wall in the experiments has a significant effect on heat transfer in comparison to a more realistic heated wall condition.

Run 88 is a high enthalpy oxygen case. The surface properties are shown in Fig. 3.12. The frozen solution is steady. The nonequilibrium results match the measurements well on the front cone. The results show that the nonequilibrium and

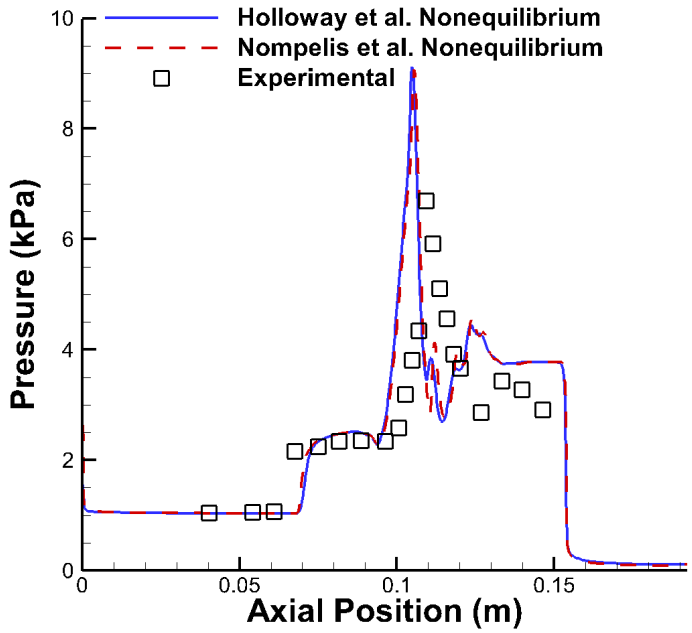

(a) Run 1 surface pressure

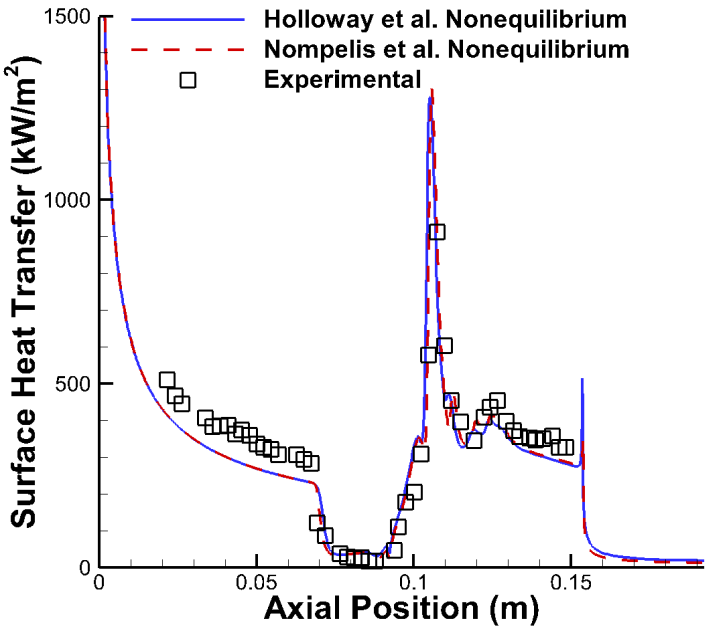

(b) Run 1 surface heat transfer

Figure 3.9: Run 1 comparison with past CFD analysis [84].

equilibrium solutions are similar, however, these two cases are much different than the frozen case simulation. Fig. 3.12(b) also shows that the equilibrium solution best matches the peak heat transfer value. These results suggest that thermochemistry modeling is necessary in a high enthalpy, frozen oxygen flow situation.

Run 46 is a high enthalpy nitrogen case. The surface properties are shown in Fig. 3.13. The nonequilibrium results also show some agreement with the experimental data on the front cone. The thermochemistry models show poor agreement with the experimental results. The frozen case is again unsteady and the results are time-averaged. The results produced by LeMANS show clear differences between the equilibrium, nonequilibrium and frozen cases, and the nonequilibrium case does not agree with the measurements. These results indicate that this high enthalpy nitrogen flow is a particularly good test case for assessment of detailed thermochemistry models.

Run 43 is a high enthalpy air case. The surface properties are shown in Fig. 3.14. The frozen solution is again unsteady and the results are time-averaged. While the equilibrium and nonequilibrium results appear similar, the equilibrium solution shows a higher spike in pressure and heat transfer in the separated flow region. However, these two solutions differ greatly from the frozen case indicating that this high enthalpy air flow is a particularly interesting case for showcasing the assessment of detailed thermochemistry models.

Each double-cone case displays similar physical phenomena, like the trends discussed between Figs. 3.7 and 3.8. Every simulation shows that separation occurs earliest for the frozen simulation and is postponed when the flow is pushed towards

an equilibrium state. This is due to the frozen simulation holding more thermal energy and increasing the shock angle to onset earlier points of flow separation.

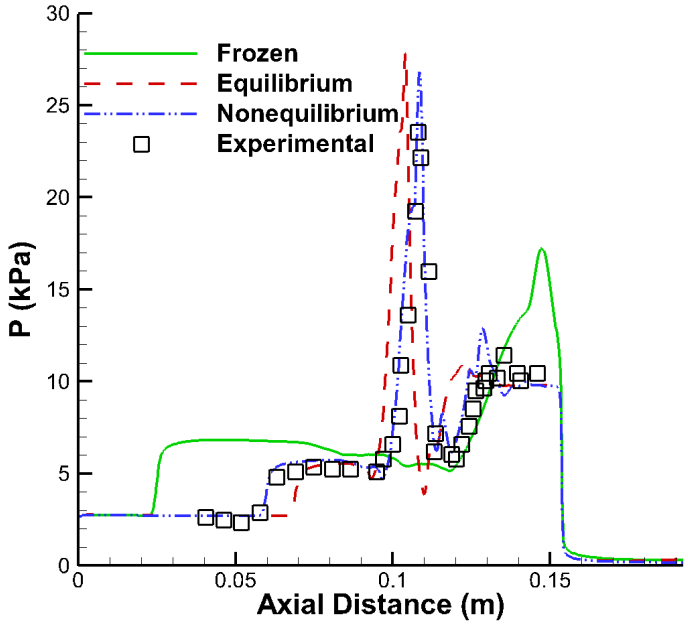

(a) Pressure

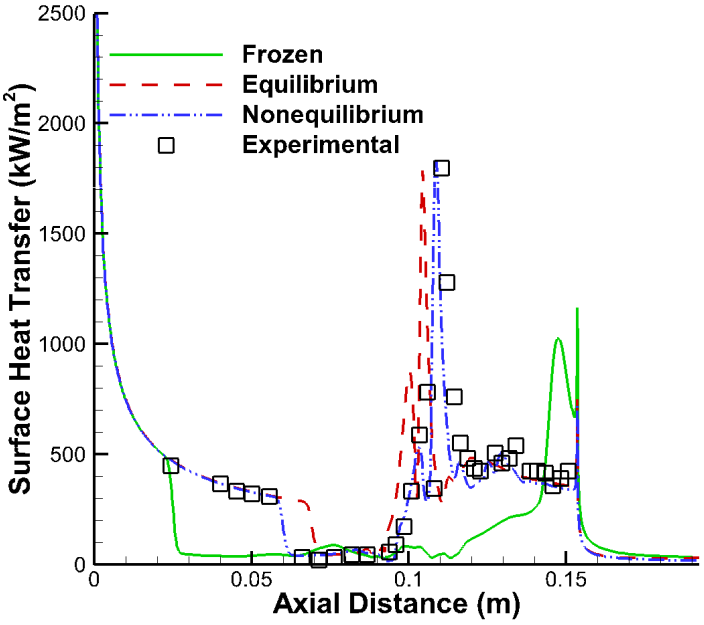

(b) Heat Transfer

Figure 3.10: Run 90 surface properties.

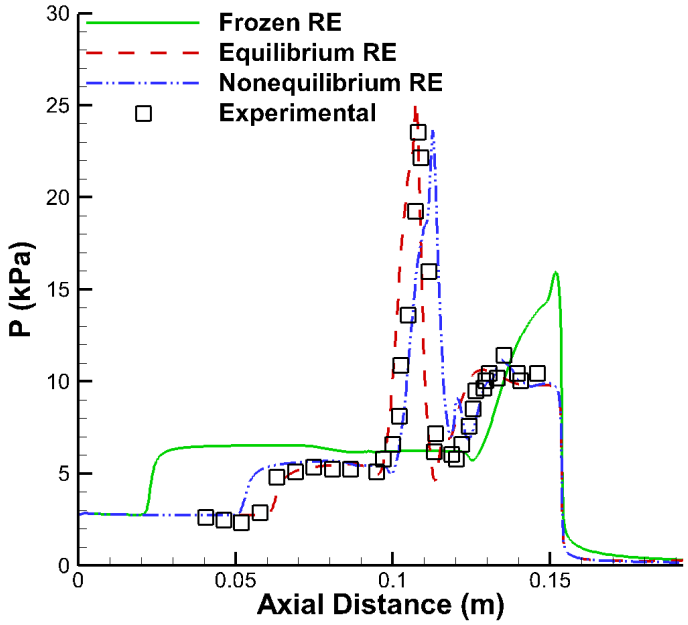

(a) Pressure RE

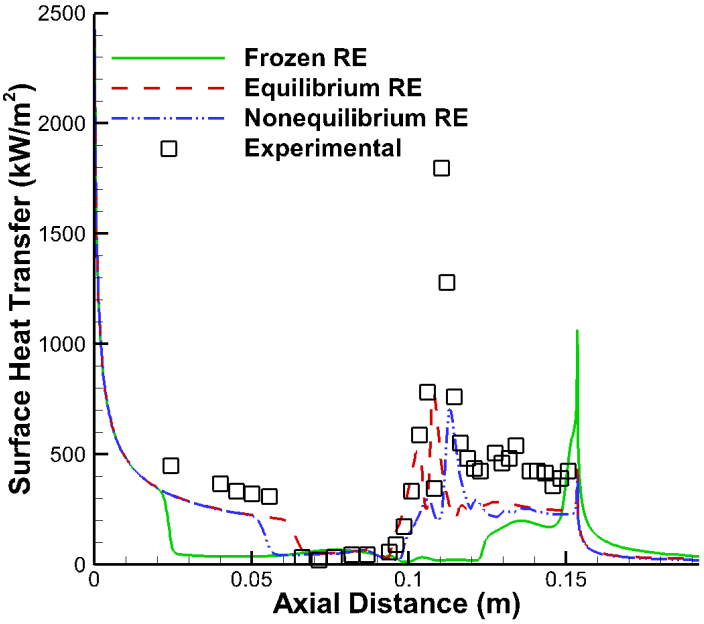

(b) Heat Transfer RE

Figure 3.11: Run 90 surface properties with the RE wall condition.

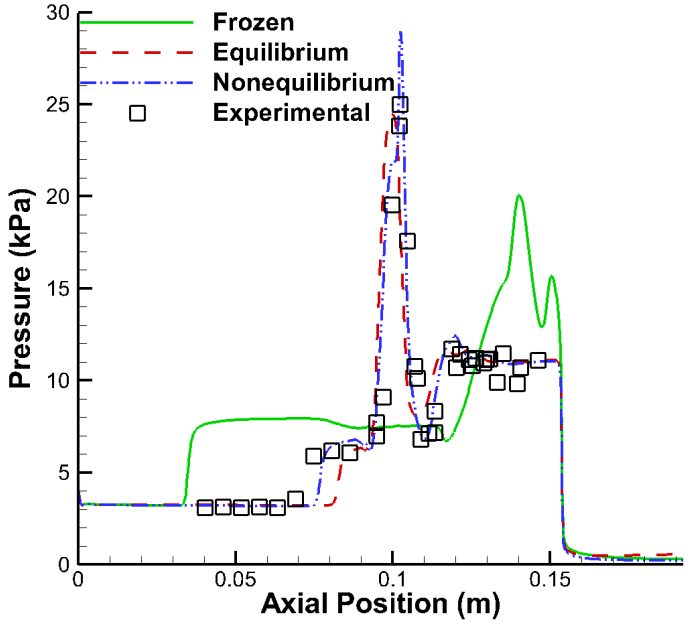

(a) Surface pressure

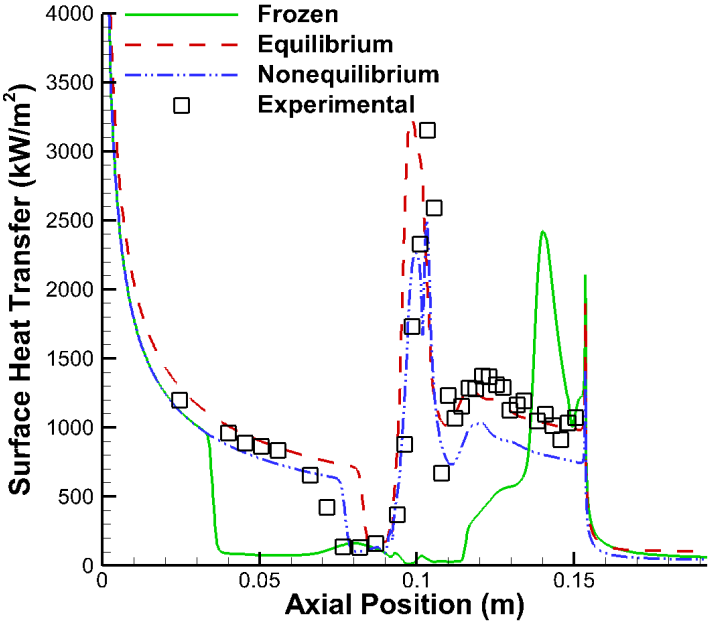

(b) Surface heat transfer

Figure 3.12: Run 88 surface properties.

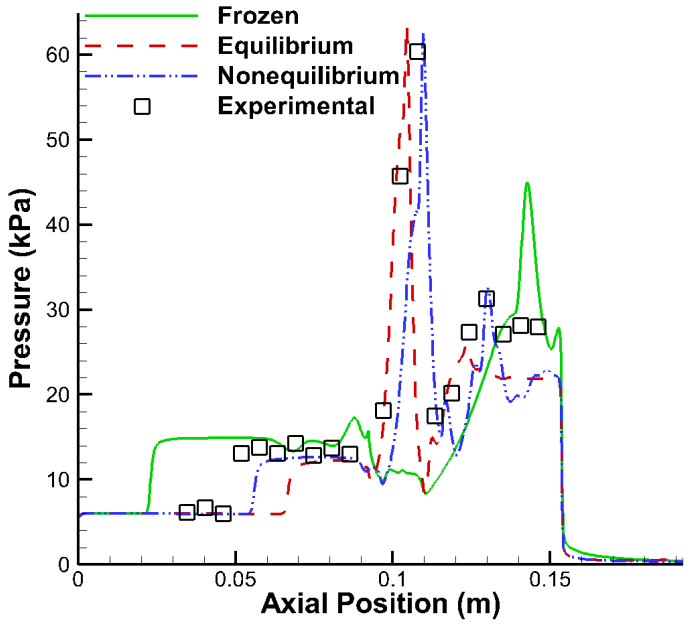

(a) Surface pressure

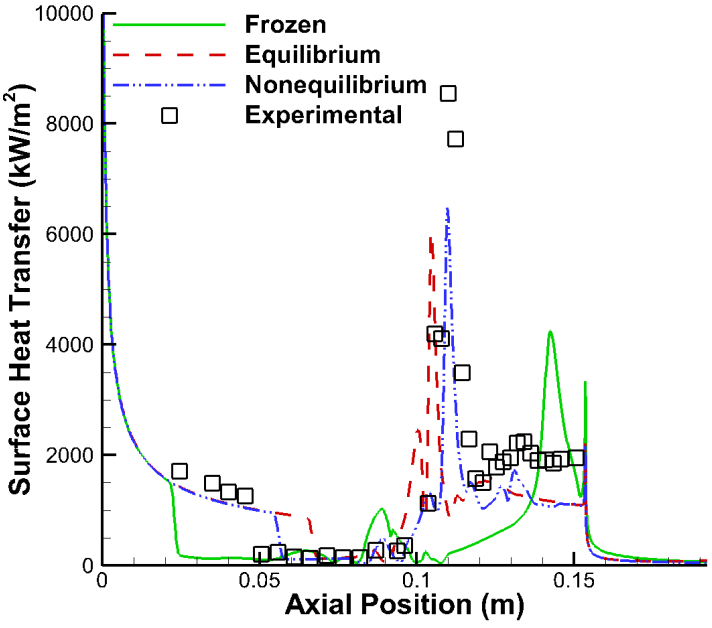

(b) Surface heat transfer

Figure 3.13: Run 46 surface properties.

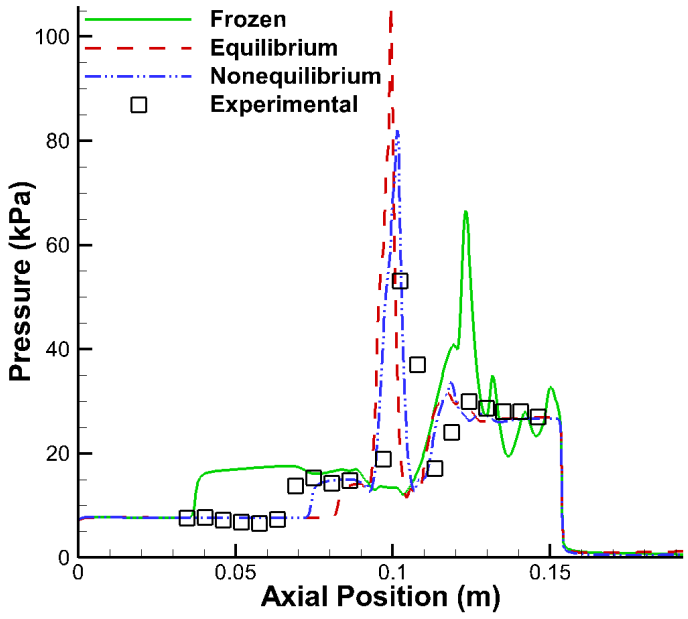

(a) Surface pressure

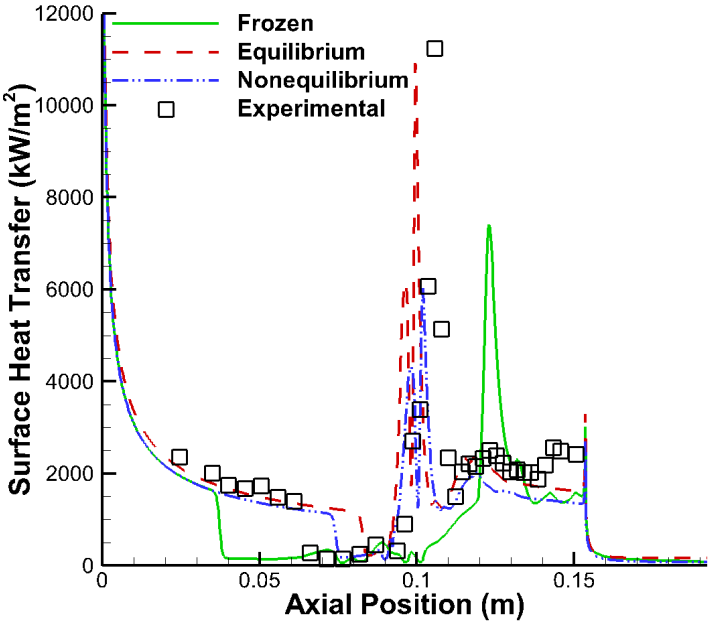

(b) Surface heat transfer

Figure 3.14: Run 43 surface properties.

The location of the onset of separation for each case is shown in Table 3.3. The table shows that the separation point occurs earliest for the frozen solutions and latest for the equilibrium solutions. The difference in separation point location is a few centimeters. The validation in the location of separation points shows sensitivity to the thermochemistry modeling.

The CUBRC separation points were determined by averaging the data point before the pressure rise and the data point where a pressure rise is first seen. There are significant differences in the separation points computed with the nonequilibrium approach and the CUBRC experiments, except for Run 90.

Table 3.3: Axial location of separation (m)

Run:	Nonequilibrium	Equilibrium	Frozen	CUBRC
90	0.058	0.067	0.023	0.058
90 (RE Wall)	0.050	0.060	0.021	
88	0.075	0.080	0.033	0.066
46	0.054	0.064	0.021	0.048
43	0.073	0.080	0.036	0.066

3.5.3 Aerothermodynamic Loading

The resulting pressure and shear stress values along the double-cone surface are integrated over the surface area to calculate the total drag, shown in Table 3.4. The percent differences are calculated using Eq. 3.1. For all five cases, the percentage difference in drag between the equilibrium and nonequilibrium solutions is less than 2% suggesting that the details of thermochemistry modeling are relatively unimportant for this parameter. Frozen thermochemistry significantly over predicts drag in comparison to the nonequilibrium thermochemistry approach. For the Run 90 case,

use of the radiative equilibrium wall has no effect on drag with equilibrium thermochemistry, but leads to a significant increase in drag difference with the frozen flow approach.

$$Percent\ Difference = \frac{X_1 - X_2}{\frac{X_1+X_2}{2}} \times 100 \tag{3.1}$$

Table 3.4: Total drag (N)

Run:	Nonequilibrium	Equilibrium	Frozen	% Difference Noneq./Eq.	% Difference Noneq./Frozen
90	526	524	508	-0.48	-3.52
90 (RE)	525	522	489	-0.48	-7.09
88	597	597	623	0.10	4.26
46	1170	1160	1154	-1.15	-1.68
43	1430	1430	1451	0.43	1.37

The resulting surface heat transfer values are integrated over the surface area to calculate the total heating rate for each case, shown in Table 3.5. Run 90 shows large percent differences in the heating rate, especially between the nonequilibrium and frozen cases. The percent difference between the nonequilibrium and equilibrium case almost doubles when the RE wall condition is applied while the frozen case remains relatively unchanged. Run 88 shows the most extreme changes in heating rate when the thermochemistry models are altered. Run 46 also shows significant differences in heating rate when the thermochemistry models are altered. Run 43 shows large differences between nonequilibrium and equilibrium flow when compared to the frozen solution. Run 43 also shows a significant increase between the nonequilibrium and equilibrium solution. Run 43 is especially interesting when Table 3.5 is compared to Fig. 3.14(b). Though the nonequilibrium and frozen surface properties

look dramatically different, when integrated the total heating rate is only slightly altered. These results show that thermochemistry models have a very significant effect on heating rate for high and low enthalpy oxygen flows, high enthalpy nitrogen flows, and high enthalpy air flows. Most importantly, these results stress the importance of carefully considering thermochemistry models when dealing with all high enthalpy freestream properties. Tables 3.4 - 3.5 also indicates that heating rate is much more sensitive to thermochemical modeling than drag.

Table 3.5: Heating rate (kW)

Run:	Nonequilibrium	Equilibrium	Frozen	% Difference Noneq./Eq.	% Difference Noneq./Frozen
90	29.2	31.2	21.6	6.62	-29.9
90 (RE)	18.0	20.3	13.3	12.0	-30.0
88	67.2	88.1	55.7	27.0	-18.7
46	91.4	95.2	82.6	4.07	-10.1
43	118	147	116	21.5	-2.31

The CUBRC pressure data are integrated over the surface area to calculate pressure drag for each case and compared to the CFD results, shown in Table 3.6. The CFD results are integrated over the exact same area, between the first and last pressure port. It is important to note that the integrated experimental measurements is an approximation based off the number of experimental ports. The radiative equilibrium wall condition is omitted because it does not represent a condition studied experimentally. Runs 90 and 43 show relatively low differences, less than 10%, between the experimental results and the different chemistry models. Runs 88 and 46 show larger differences, greater than 10%, between experimental results and the different chemistry models. Despite Runs 90 and 43 showing lower percent differences,

Table 3.6 shows clear differences for each thermochemistry model. The larger percent differences also correlate with the surface plots that show the largest differences.

Table 3.6: Experimental pressure drag compared to simulations (kPa)

Run:	Noneq.	Eq.	Frz.	CUBRC	%Difference CUBRC/Noneq.	%Difference CUBRC/Eq.	%Difference CUBRC/Frz.
90	513	510	500	474	7.90	7.32	5.34
88	577	576	610	517	11.0	10.8	16.5
46	1150	1140	1130	1370	-17.5	-18.3	-19.2
43	1400	1400	1430	1330	5.13	5.13	7.25

The experimental heat transfer values are integrated over the surface area to determine the experimental heating rate and compared to the CFD results, shown in Table 3.7. The CFD values are integrated over the exact same area. Again, the integrated experimental data is an approximation based off the number of experimental ports. The radiative equilibrium wall condition is also omitted from this study. In each case, the frozen solution shows the largest percent difference when compared to experiments. Run 90 shows the lowest, though significant, percent differences in partial heating rate values. Run 88 also shows significant differences between experiments and CFD solutions. Run 46 shows the most extreme differences between experiments and CFD solutions, with differences upwards of 55%. Run 43 also shows extreme differences between experiments and CFD results. Not unlike Tables 3.4-3.5, the percent differences in Table 3.7 are much larger when compared to Table 3.6, indicating that heating rate is much more significant than drag. These results show that thermochemistry models have a very significant effect on heating rate for high and low oxygen flows, high enthalpy nitrogen flows, and high enthalpy air flows.

It is significant that while the three chemistry models bound the experimentally

Table 3.7: Experimental heating rate compared to simulations (kW)

Run:	Noneq.	Eq.	Frz.	CUBRC	%Difference CUBRC/Noneq.	%Difference CUBRC/Eq.	%Difference CUBRC/Frz.
90	28.6	28.6	21.0	31.1	-8.38	-8.38	-38.8
88	65.8	86.5	54.3	78.7	-17.9	9.44	-36.7
46	89.6	93.5	81.0	144	-46.6	-42.5	-56.0
43	116	144	113	169	-37.2	-16.0	-39.7

measured separation regions, they do not do so for the integrated pressure drag and heating rate. All three chemistry models consistently over predict or under predict the heating rate, while each model besides Run 88 consistently over or under predict the pressure drag. This failure to bound the measurements strongly suggests a basic inconsistency between the experiments and the simulations that is most likely related to inaccurate and/or incomplete characterization of the freestream in the experiments. Additional inconsistencies have been deduced in sensitivity analysis reported by Kieweg et al. and Ray et al. [37] [38].

3.5.4 Extent of Nonequilibrium

With a goal of trying to better understand the differences between the simulations and the experiments, the extent of thermal and chemical nonequilibrium, is characterized for Runs 46, 88, 90, and 90 RE. The extent of thermal nonequilibrium is characterized by the temperature ratio T_{tr}/T_v. The extent of chemical nonequilibrium is characterized by the density ratio between equilibrium chemistry and that calculated by LeMANS under the nonequilibrium thermochemistry approach. The equilibrium chemistry value is calculated using the Law of Mass Action, Eq. 3.2, in which α^* is the degree of dissociation which is equal to the atomic mass fraction [39].

The constants used in Eq. 3.2 are shown in Table 3.8.

$$\frac{(\alpha^*)^2}{1-\alpha^*} = \frac{exp\left(-\frac{\theta_d}{T}\right)}{\rho}\left\{m_a\left(\frac{\pi m_a k}{h^2}\right)^{\frac{3}{2}}\theta_r\sqrt{T}\left[1-exp\left(-\frac{\theta_v}{T}\right)\right]\frac{\left(Q_{el}^a\right)^2}{Q_{el}^{aa}}\right\} \tag{3.2}$$

Table 3.8: Values for Eq. 3.2 [39]

Species	θ_d (K)	θ_r (K)	θ_v (K)	Q_{el}^a	Q_{el}^{aa}
O_2	59500	2.08	2280	9	3
N_2	113000	2.9	3390	4	1

For simplicity, the extent of nonequilibrium is evaluated only for the pure oxygen and pure nitrogen cases. The extent of thermal nonequilibrium is shown in Figs. 3.15 and 3.16. Each Run shows significant amounts of thermal nonequilibrium even in the freestream. For Run 90, Fig. 3.15, the two sets of contours are similar indicating weak dependence on the specific wall surface model. Here, the total region of thermal nonequilibrium is the largest and this correlates with the largest differences in heating rates predicted by the frozen and nonequilibrium flow models. The contours for Run 88, Fig. 3.16(a), show the highest levels of nonequilibrium temperature ratio and this is the condition with the widest range of heating rate values. In Run 46, Fig. 3.16(b), the temperature ratio remains less than one on the first cone but then displays similar trends to Run 90 on the second cone. There is no obvious correlation with the fact that Run 46 has relatively low variation in heating rate between the three thermochemistry approaches.

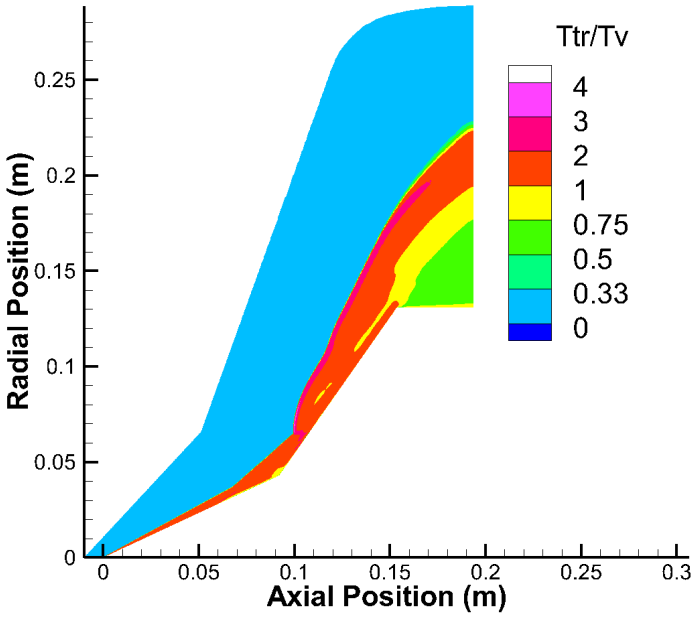

(a) Run 90 (nonequilibrium)

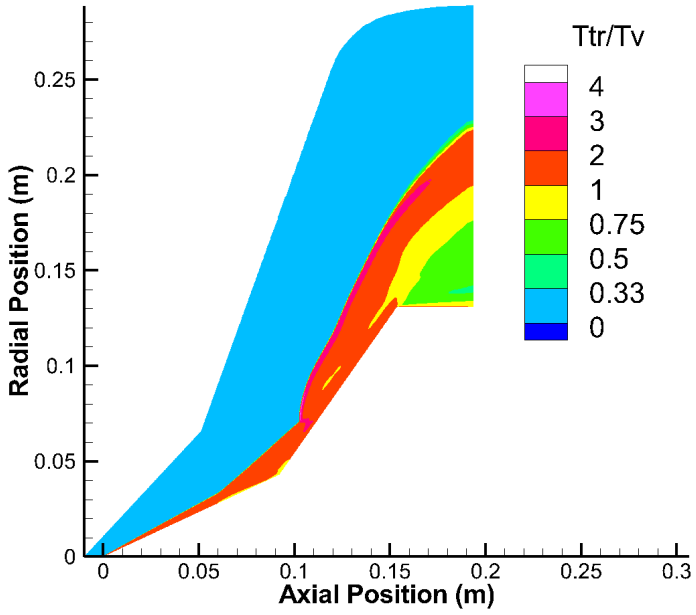

(b) Run 90 RE wall (nonequilibrium)

Figure 3.15: Extent of thermal nonequilibrium for Run 90.

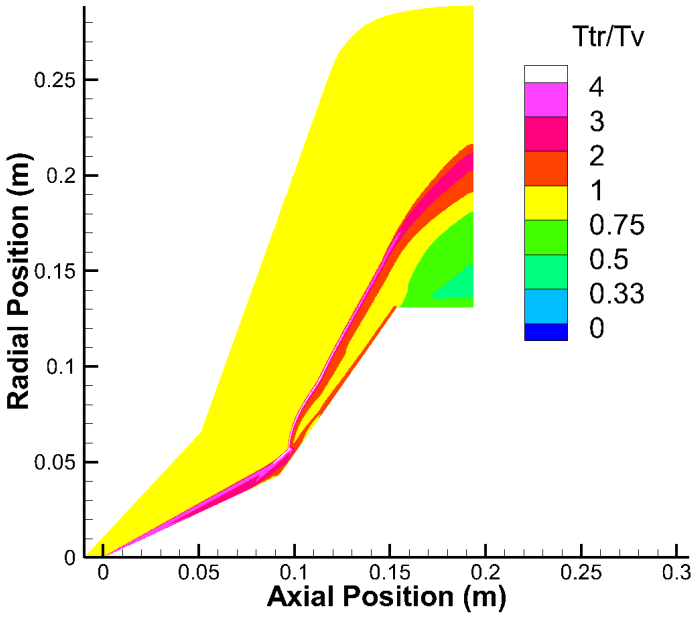

(a) Run 88 (nonequilibrium)

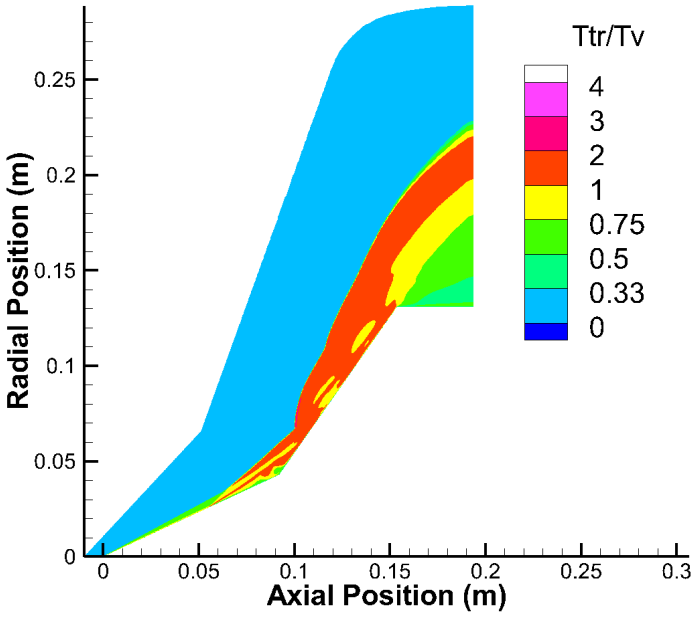

(b) Run 46 (nonequilibrium)

Figure 3.16: Extent of thermal nonequilibrium for Run 88 and 46.

The extent of chemical nonequilibrium is shown in Figs. 3.17 and 3.18. Runs 90 and 46, Figs. 3.17(a), 3.17(b), and 3.18(b), display significant regions of chemical nonequilibrium behind the second detached shock, but in each case equilibrium is recovered at the cone surfaces. This suggests that chemical nonequilibrium plays a minor role in the surface properties for these cases. Run 88, Fig. 3.18(a), has the strongest degree of chemical nonequilibrium and it is maintained all the way to the surface. This is the case that also has the widest spread in heating rate between the different thermochemistry models.

Overall, the analysis of thermal and chemical nonequilibrium provides a conclusion that is not unexpected: the conditions of Run 88, for which there is the greatest variation in surface properties for the three different modeling approaches, is the one with the highest enthalpy and, because it is also a pure oxygen flow, the highest level of thermochemical activity. However, it is worth noting that Run 46 in nitrogen has a similar enthalpy to Run 88, but significantly less thermochemical activity and clearly reduced variation in heating rate with thermochemical model. With a 50% difference in vibrational energy spacing between nitrogen and oxygen, and an almost 100% difference in chemical bond strength, it is clear that any general evaluation of the role of the importance of thermochemistry modeling must account for the specific thermochemical properties of the gas involved.

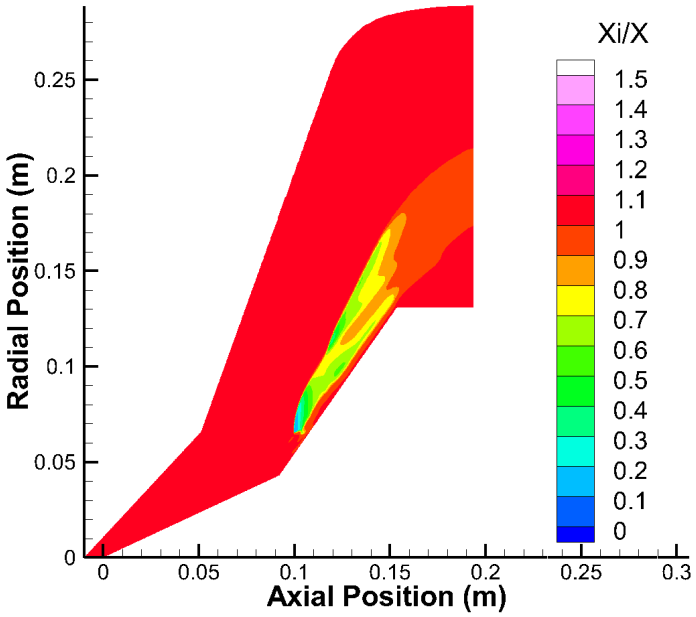

(a) Run 90 (nonequilibrium)

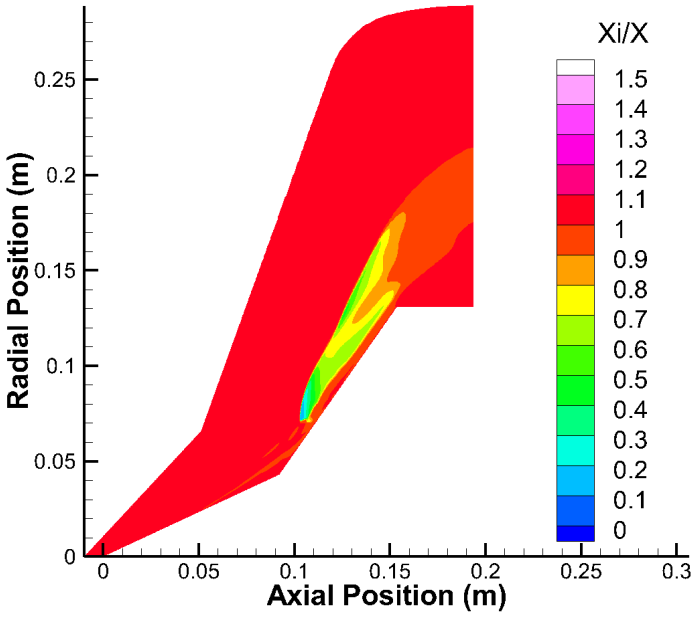

(b) Run 90 RE wall (nonequilibrium)

Figure 3.17: Extent of chemical nonequilibrium for Run 90.

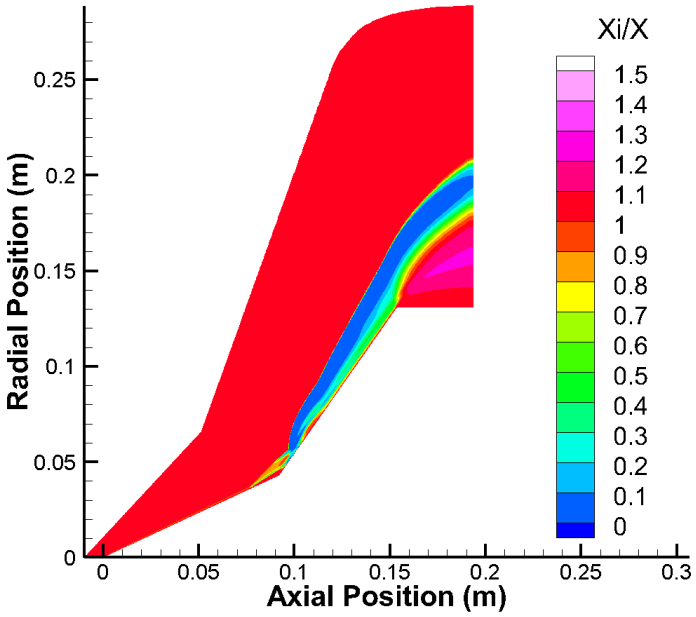

(a) Run 88 (nonequilibrium)

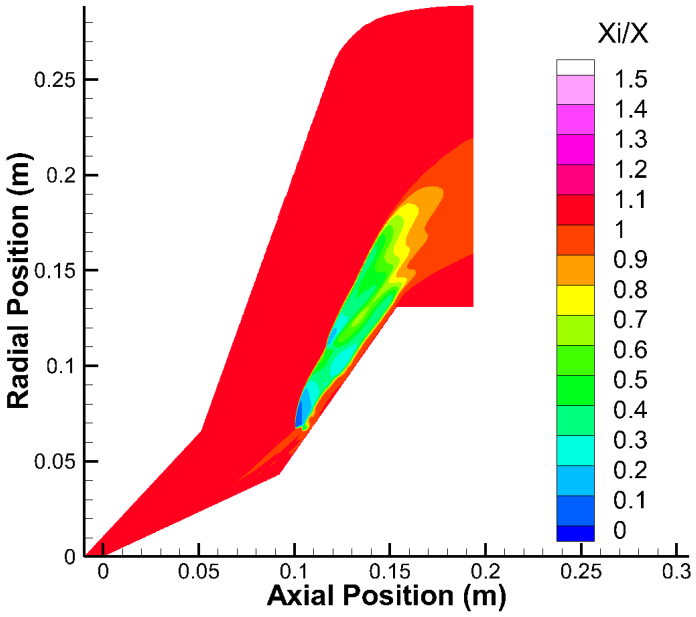

(b) Run 46 (nonequilibrium)

Figure 3.18: Extent of chemical nonequilibrium for Runs 88 and 46.

3.6 Chapter Summary

The influence of different assumptions for thermochemistry modeling in hypersonic flow over a double-cone was investigated. The thermochemical model used in this study utilizes Millikan-White with the high-temperature corrections of Park to model vibrational relaxation time and captures thermochemical nonequilibrium effects by means of the 2T model. These results showed that the flow properties of frozen thermochemistry models have greater translational temperatures while equilibrium models have the lowest. The possibility of unsteady flow is also observed in some frozen cases. The surface property analysis demonstrated a delay in flow separation when the thermochemistry model moved closer to equilibrium. It also showed the significant sensitivity to thermochemistry modeling for all high enthalpy cases and low enthalpy oxygen cases. In general, the drag analysis showed that similar results were obtained with the nonequilibrium and equilibrium approaches while frozen thermochemistry produced larger differences. The heating rate analysis demonstrated significant differences between the equilibrium, nonequilibrium, and frozen thermochemistry models and that high enthalpy oxygen cases are especially sensitive. Lastly, the extent of nonequilibrium study gives the impression that thermal nonequilibrium is more sensitive than chemical nonequilibrium. It also suggests that the extent of nonequilibrium is proportional to the freestream enthalpy and that the wall model has no effect on the amount of nonequilibrium in the flow field.

These results indicate that some of the double-cone cases investigated at CUBRC are much more sensitive to the details of thermochemistry than others. For example,

high enthalpy oxygen flow appears to be the most sensitive of the cases considered. In addition, sensitivity to thermochemistry varies across different aspects of the flows. While the total drag is relatively insensitive to thermochemistry, the separation point is more sensitive, and the total heating rate showed variations of up to $\pm$ 30% between the different thermochemistry models.

All three chemistry models consistently over predict or under predict pressure drag and heating rate in comparison to the experimental data for almost all cases examined. These trends indicate a basic difference between the actual experiments and the simulations. Due to the inconsistencies in the trends observed, it must be concluded that the double-cone experiments examined are limited in their practicality for validation of the thermochemistry models utilized in this study.

CHAPTER 4

Double-Cone Part II: A LENS-XX Study

The effect of thermochemical kinetics modeling on hypersonic flow over a double-cone geometry is investigated in the following chapter. The double-cone is simulated using three different approaches based on the Park thermochemistry model: nonequilibrium flow, equilibrium flow, and frozen flow for 5-species air at four different freestream conditions. A comparison of Park and MMT thermochemistry models is also made. The effects of the different thermochemical models on the flow field and surface properties are specific areas of interest. The resulting aerothermodynamic loads are compared to experiments performed in the CUBRC LENS-XX facility.

4.1 Introduction

The motivation for this chapter is much like Chapter 3, to study the effects of thermochemistry modeling for hypersonic flow. This chapter also studies the double-cone, but differs from Chapter 3 in that it investigates experiments conducted in CUBRC's newer LENS-XX facility. The LENS-XX facility is of interest because it

has a wide range of relevant hypersonic freestream conditions available, shown in Fig. 3.2. An overview of CUBRC and the double-cone experimental set up and flow field can be found in Section 3.2.

In order to assess the accuracy of nonequilibrium models in predicting aerothermodynamic loads in hypersonic flight, this study specifically focuses on hypersonic shock wave laminar boundary layer interactions. Though the hypersonic shock wave boundary layer interactions in transitional and turbulent flows are important, the laminar boundary layer restriction allows for a more straight-forward assessment of the nonequilibrium models without the added complexity and cost of modeling the transitional and turbulent boundary layers.

In order to determine the sensitivity of the flow and surface properties to thermochemistry modeling, several different double-cone cases are studied. Each case consists of 5-species air mixtures at different freestream conditions.

The current chapter focuses on assessment of the models when applied to conditions studied in the CUBRC LENS-XX facility. Chapter 3 studied the effects of Park 2T thermochemistry modeling on hypersonic flow over a double-cone for the older CUBRC LENS-I facility. Chapter 3 showcased inconsistencies between CFD and experimental measurements of surface properties and, therefore, concluded that the double-cone cases utilized in those studies are limited in their usefulness to validate thermochemistry models. One of the differences between the two LENS facilities is the amount of nonequilibrium in the freestream. LENS-XX produces a freestream that is in thermochemical equilibrium whereas LENS-I generates flow that is in both thermal and chemical nonequilibrium. There should therefore be significantly less

uncertainty in the freestream conditions for LENS-XX. One objective of the current chapter is to determine if CFD can better reproduce the measurements made in the LENS-XX facility, due to a better characterized freestream.

The current chapter will also investigate two different chemical kinetics models. The two models considered are the older Park 2T model and the newer MMT chemical kinetics model [8, 43]. The first objective is to study any difference in integrated surface properties between the two models, such as drag and heating rate. The second objective is to compare surface properties to determine if Park or MMT can better reproduce results measured at the CUBRC LENS-XX facility. The Park model is also altered in order to determine if the LENS-XX double-cone cases are sensitive to thermochemistry modeling, similar to Chapter 3. The MMT model was recently developed to take into account rotational energy and was found to be consistent with the dominant underlying mechanisms of dissociation [43]. The Park and MMT thermochemistry models are discussed in Section 2.2.

This chapter will begin by explaining each numerical approach used in the study. Each test case condition is then defined and the importance of thermochemistry modeling is showcased by examining the resulting flow properties for each Park thermochemistry model. Any sensitivity in surface properties when the Park model is altered is then discussed. The Park and MMT model are then compared to each other and experimental measurements. The chapter ends with conclusions based on trends observed.

4.2 Numerical Approach

The numerical simulations presented in this study are performed using the CFD code LeMANS, which was developed at the University of Michigan to simulate hypersonic reacting flows. A complete overview of LeMANS can be found in Ref. [42] or Section 2.2 of this dissertation.

The investigation of the importance of thermochemistry modeling is similar to Chapter 3. The thermochemical model used in this study also utilizes Millikan-White with the high-temperature corrections of Park to model vibrational relaxation time and captures thermochemical nonequilibrium effects by means of Park's 2T model. This study also considers three different thermochemical regimes using the Park model: nonequilibrium, equilibrium, and frozen. The current chapter differs from Chapter 3 in that it also applies the new MMT thermochemistry model. Details of the Park and MMT models can be found in Section 2.2.

4.3 Test Case Descriptions

Each double-cone case and the freestream conditions generated in the LENS-XX facility considered in this study are shown in Table 4.1 [75]. These four cases are chosen to study a wide range of air conditions from relatively low to high enthalpies. Each case is also chosen for their good agreement between experimental results and past nonequilibrium models; reasonable agreement on the front cone indicates that the data and freestream conditions are valid, see Fig. 3.9.

The geometry of the double-cone is shown in Fig. 3.5 and consists of a 25° first

Table 4.1: LENS-XX freestream properties and composition given in terms of species mass-fractions [75]

Run:	Mach	h_0 (MJ/kg)	ρ_∞ (g/m^3)	T_∞ (K)	$T_{v\infty}$ (K)	T_{wall} (K)	N_2	O_2
1	12.2	5.44	0.499	175	175	300	0.765	0.235
2	10.9	9.65	0.984	389	389	300	0.765	0.235
6	11.46	15.23	2.045	573	573	300	0.765	0.235
4	12.82	21.77	0.964	652	652	300	0.765	0.235

cone and a 55° second cone. The computational grid, shown in Fig. 3.6, consists of approximately 300,000 cells with 636 cells along the wall for which the solutions have been demonstrated to be independent. The grid convergence study consisted of a coarse grid, approximately 160,000 cells, and a fine grid, approximately 600,000 cells. An RMS study between the surface pressure and surface heat transfer for each grid produced a max percent difference of 1.0% and 1.2%, respectively. Due to the short run time of the experiments, each case is modeled as an isothermal wall for consistency with the CUBRC results.

4.4 Park Results

The following sections discuss the computational results obtained when the Park 2T model, discussed in Section 2.2, is applied to the CUBRC LENS-XX experiments. The Park 2T model effects on the flow field and surface properties are specific areas of interest. The integrated surface properties are compared to the CUBRC experiments.

4.4.1 Flowfield Results

Pressure contours from the nonequilibrium and equilibrium solutions for Run 6 are shown in Fig. 4.1. Each case demonstrates steady flow results. These pressure contours are representative of the other nonequilibrium and equilibrium Runs. For each Run, as illustrated in Fig. 4.1, the equilibrium cases produce smaller shock angles.

The time-averaged pressure contours for the frozen flow Run 6 case are shown in Fig. 4.2. This case produces unsteady flow, which is not uncommon and is illustrated in Refs. [36, 72, 73]. When compared to the nonequilibrium solution in Fig. 3.7, the frozen case shows greater shock angles. These larger shock angles are due to vibrational energy increasing the ratio of specific heats. The stronger shocks also produce adverse pressure gradients that lead to earlier points of flow separation.

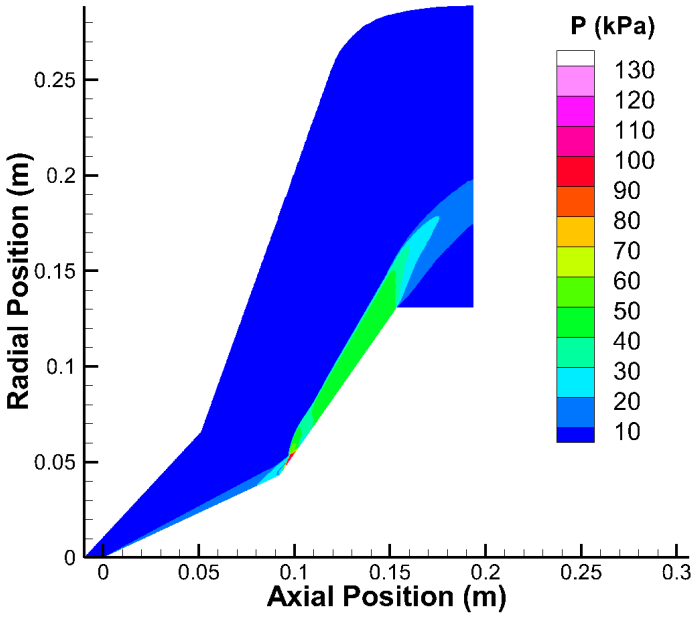

(a) Pressure contours (Run 6 nonequilibrium)

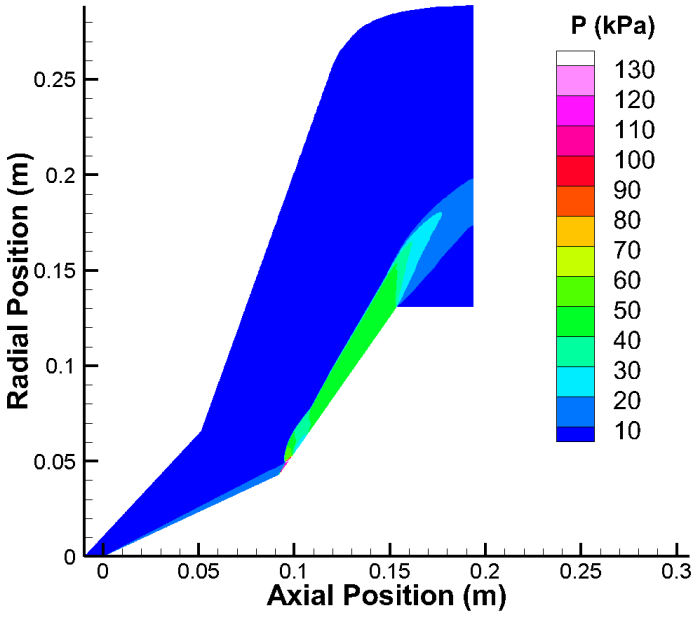

(b) Pressure contours (Run 6 equilibrium)

Figure 4.1: Results for the Nonequilibrium and Equilibrium cases.

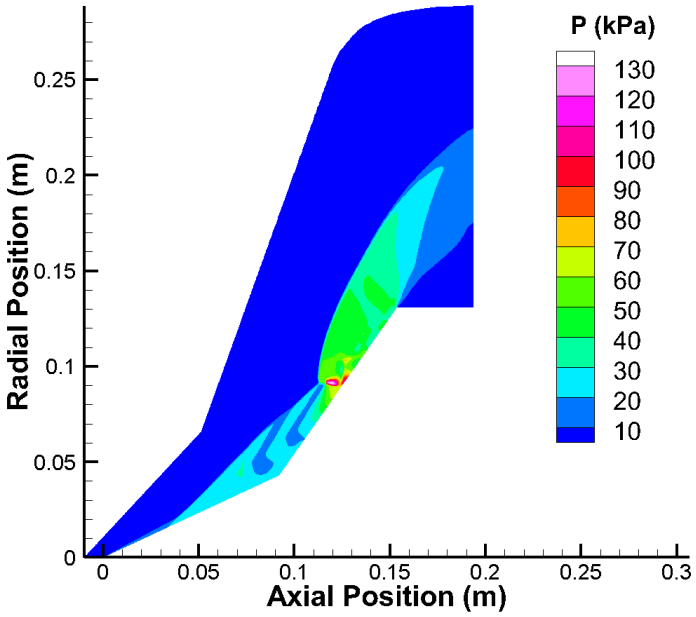

Figure 4.2: Pressure contours for the Run 6 frozen case.

4.4.2 Surface Properties

The effects that each Park thermochemistry modeling approach has on the surface of the double-cone, in terms of pressure and heat transfer, are discussed below. The unsteady flow cases use time-averaged results. The experimental results were produced at the CUBRC LENS-XX facility [75]. An in-depth evaluation of the resulting drag and heating rate is also discussed.

Each case is, in part, chosen for its agreement with prior CFD analysis. An example of this comparison is shown in Fig. 3.9 for the Run 1 test case. The results in Fig. 3.9 are compared to prior analysis by Nompelis et al. [84]. An RMS comparison between the two simulations shows a difference of 3.9% in surface pressure and a 2.1% difference in surface heat transfer.

Run 1 is a low enthalpy air case. The surface properties are shown in Fig. 4.3. The nonequilibrium pressure calculated by LeMANS shows little agreement with the experimental values in the separated region. The computational heat transfer slightly under predicts the experimental heat transfer values on the forward cone, but shows good agreement with experimental values in the separated flow region. The surface properties produced by LeMANS shows clear, though small, differences in each thermochemistry model. The results indicate that separation occurs earliest in the frozen case and latest for the equilibrium case. These solutions also show lower peaks in pressure and surface heat transfer for the equilibrium case and larger peaks for the frozen case. The simulations for Run 1 show mixed agreement with the experimental values and relatively small differences in thermochemistry models. While this case may not show the most dramatic differences, it is interesting in that the frozen and nonequilibrium cases are more similar to one another, with the equilibrium solution showing more significant differences.

Run 2 is a mid-level enthalpy air case. The surface properties are shown in Fig. 4.4. The nonequilibrium solution is again consistent with prior CFD analysis presented in Ref. [84]. The nonequilibrium pressure values produced by LeMANS shows fair agreement with the experimental measurements on the forward cone while the nonequilibrium heat transfer solution slightly under predicts the experimental measurements. Run 2 shows relatively good agreement of the computations with experiments. The surface properties produced by LeMANS shows clear differences between each thermochemistry model, indicating that this mid-level enthalpy air case is a good experiment in showcasing the importance of thermochemistry modeling.

Run 6 is also a mid-level enthalpy air case. The surface properties are shown in Fig. 4.5. The frozen solution is unsteady and the results are time-averaged. The nonequilibrium solution is again consistent with Ref. [84]. The nonequilibrium surface pressure does a reasonable job of capturing the experimental measurements on the forward cone while poorly capturing the data in the separated flow region. LeMANS, again, slightly under predicts the surface heat transfer measurements on the forward cone and poorly captures the data in the separated flow region. Run 6 shows clear differences in each thermochemistry model, again demonstrating the importance of thermochemistry modeling.

Run 4 is a high enthalpy air case. The surface properties are shown in Fig. 4.6. The nonequilibrium solution is again consistent with Ref. [84]. The nonequilibrium surface pressure produced by LeMANS shows good agreement with experimental measurements on the front cone and in the separated flow region. However, LeMANS slightly under predicts surface heat transfer measurements on the forward cone and little agreement overall with experimental measurements. Run 4 shows clear differences in each thermochemistry model, making this high enthalpy air simulation an interesting case in showcasing the importance of thermochemistry modeling.

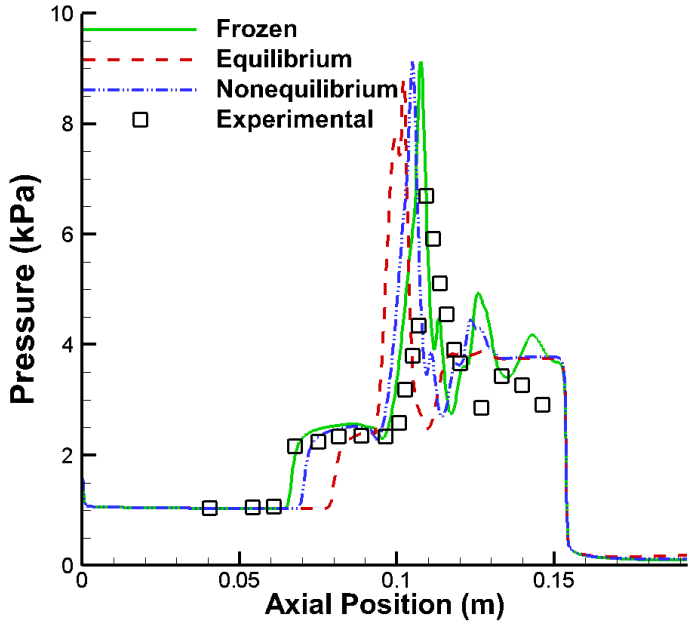

(a) Surface pressure

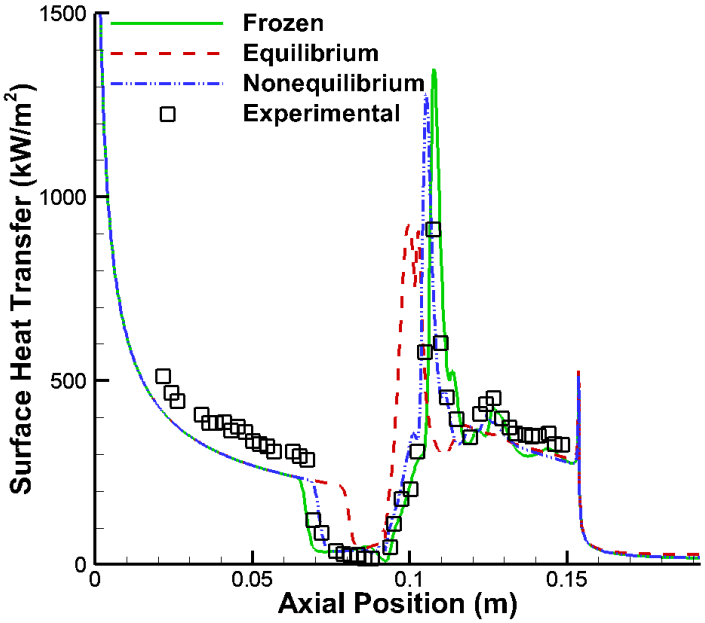

(b) Surface heat transfer

Figure 4.3: Run 1 surface properties.

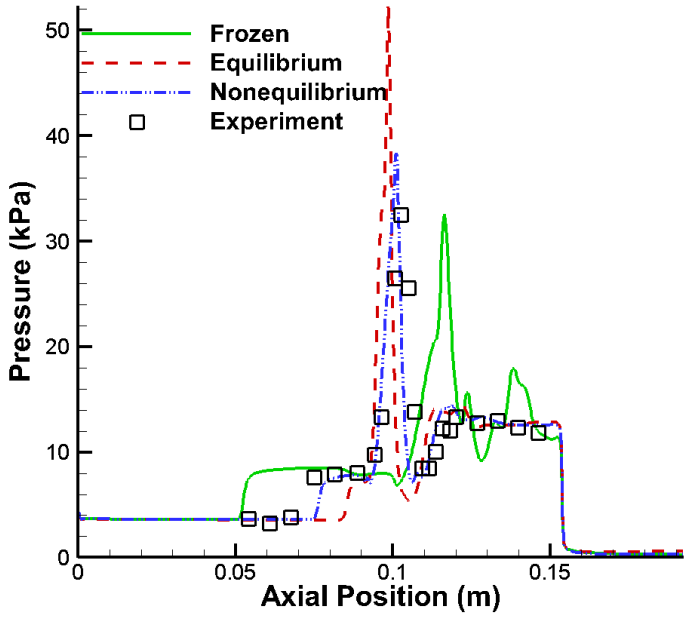

(a) Surface pressure

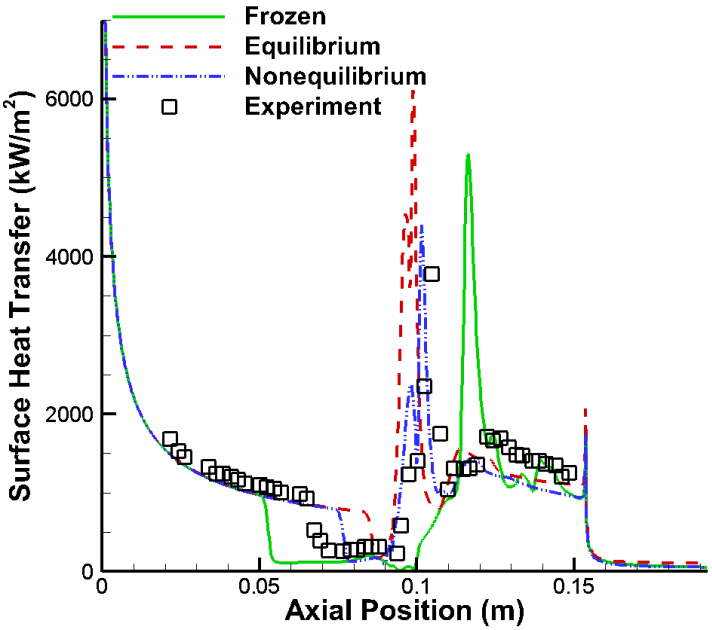

(b) Surface heat transfer

Figure 4.4: Run 2 surface properties.

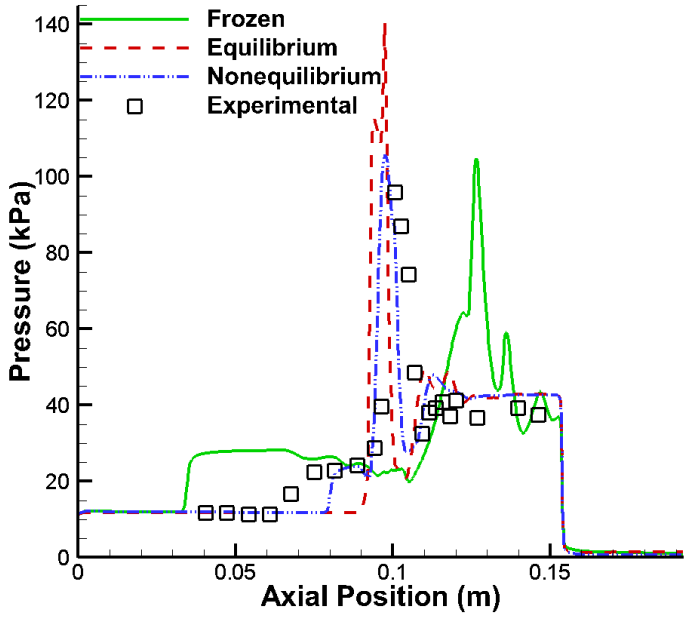

(a) Surface pressure

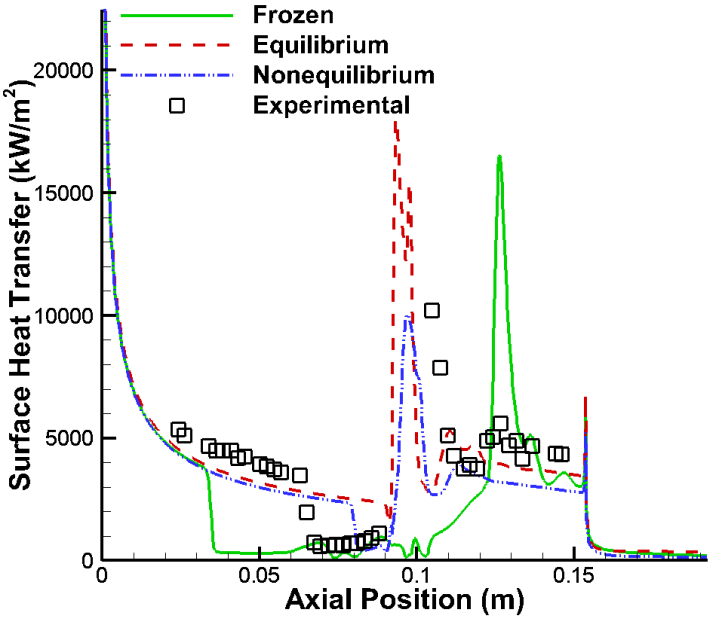

(b) Surface heat transfer

Figure 4.5: Run 6 surface properties.

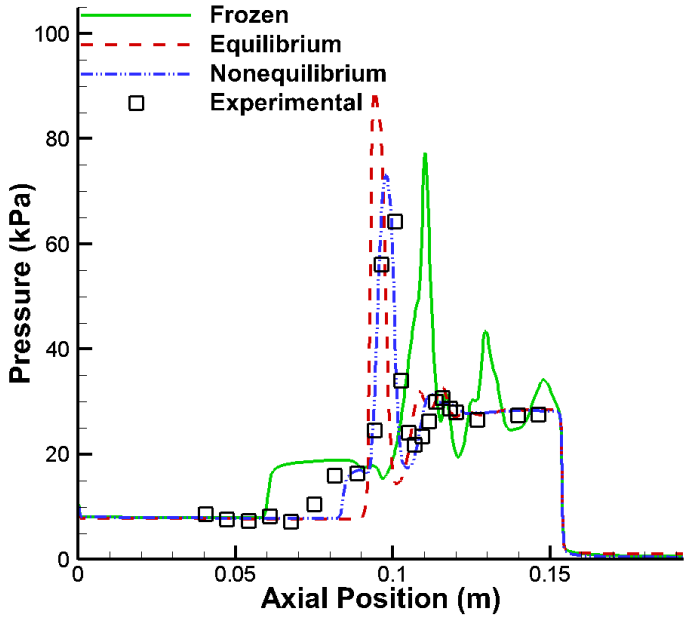

(a) Surface pressure

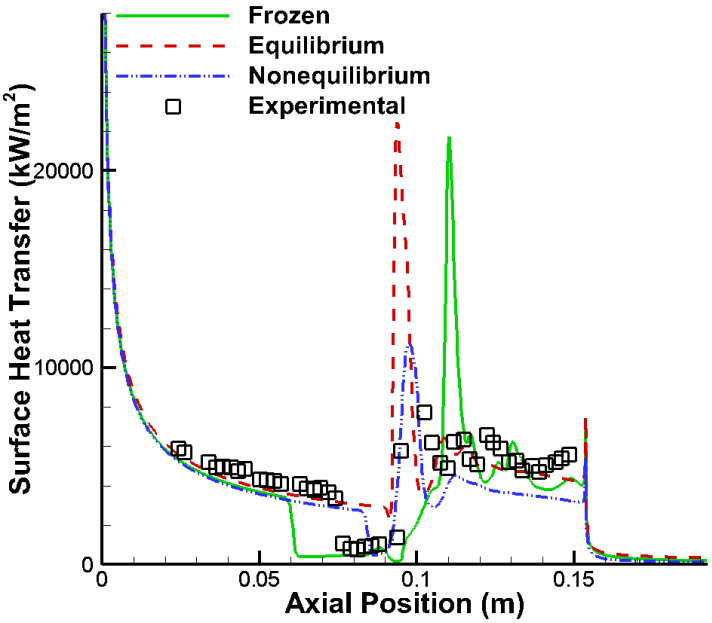

(b) Surface heat transfer

Figure 4.6: Run 4 surface properties.

4.4.3 Aerothermodynamic Loading

The computed pressure and shear stress values along the double-cone surface are integrated over the surface area to calculate the total drag for each case, shown in Table 4.2. The percent differences are calculated using Eq. 3.1. For all four cases, the percentage difference in drag between the equilibrium and nonequilibrium solutions is less than 2% suggesting that the details of thermochemistry modeling are relatively unimportant for this parameter. Frozen thermochemistry significantly over predicts drag in comparison to the nonequilibrium thermochemistry approach, except for Run 6.

Table 4.2: Total Drag (N)

Run:	Nonequilibrium	Equilibrium	Frozen	%Difference Noneq./Eq.	%Difference Noneq./Frozen
1	206	203	210	-1.81	1.59
2	687	688	712	0.145	3.50
6	2280	2300	2290	0.880	0.440
4	1520	1540	1610	1.32	5.92

The computed surface heat transfer values are integrated over the surface area to calculate the total heating rate for each case, shown in Table 4.3. Run 1 shows the least change in heating rate values when the thermochemistry models are altered. This is also the case with the most similar surface property values. Run 4 shows largest percent differences in the heating rate, especially between the nonequilibrium and equilibrium cases. This is also the case with the widest range in surface properties. Run 6 shows the greatest overall changes in heating rate when the thermochemistry models are altered. Run 2 also shows significant differences in heating rate between the nonequilibrium and equilibrium solutions while the difference between

the nonequilibrium and frozen solutions are minimal. These results show that thermochemistry models have a very significant effect on high and low enthalpy air flows. Tables 4.2 - 4.3 also indicate that heating rate is much more sensitive to thermochemical modeling than drag, which was also concluded in Chapter 3. Further, there is not usually a monotonic trend in Tables 4.2 - 4.3 when moving from frozen to nonequilibrium to equilibrium, which complicates assessment of sensitivity to thermochemistry modeling.

Table 4.3: Heating Rate (kW)

Run:	Nonequilibrium	Equilibrium	Frozen	%Difference Noneq./Eq.	%Difference Noneq./Frozen
1	25.0	26.0	25.1	3.92	0.399
2	85.8	98.7	86.6	14.1	0.905
6	247	321	258	30.0	4.45
4	285	391	341	37.2	19.7

The CUBRC measurements of pressure are integrated over the surface area to calculate pressure drag for each case and compared to the CFD results, shown in Table 4.4. The CFD results are integrated over the exact same area, between the first and last pressure measurement ports. Runs 2, 4, and 6 show relatively small differences, less than about 10%, between the experimental results and the different chemistry models. Run 1 shows the largest differences, greater than about 10%, between experimental results and the different chemistry models. Regardless of Runs 2, 4 and 6 showing lower percent differences, Table 4.4 shows clear differences between each thermochemistry model and the CUBRC data. The larger percent differences also correlate with the cases in which surface profiles that show the largest differences.

The experimental heat transfer values are integrated over the surface area to de-

Table 4.4: Experimental pressure drag compared to simulations (kPa)

Run:	Noneq.	Eq.	Frz.	CUBRC	%Difference Noneq./CUBRC	%Difference Eq./CUBRC	%Difference Frz./CUBRC
1	199	194	202	171	15.1	12.6	16.6
2	662	661	689	641	3.22	3.07	7.22
6	2220	2240	2250	2020	9.43	10.3	10.8
4	1470	1480	1560	1410	4.17	4.84	10.1

termine the experimental heating rate and compared to the CFD results, shown in Table 4.5. The CFD values are integrated over the exact same area as for the measurements. Runs 1 and 2 shows the lowest, though still significant, percent differences in partial heating rate values. Run 4 shows greatest differences between experiments and CFD solutions. Run 6 shows the largest range between experiments and CFD solutions, with differences upwards of 22%. Interestingly, Table 4.5 also shows that the integrated frozen solutions of Runs 4 and 6 accurately capture the predicted heating rate, even though the surface profiles do not fit the experimental measurements. Unlike Tables 4.2-4.3, the percent differences in Table 4.5 are similar when compared to Table 4.4, indicating that heating rate is as significant as drag when compared to experimental values. These results show that thermochemistry models have a very significant effect on heating rate for high and low enthalpy air flows.

Table 4.5: Experimental heating rate compared to simulations (kW)

Run:	Noneq.	Eq.	Frz.	CUBRC	%Difference Noneq./CUBRC	%Difference Eq./CUBRC	%Difference Frz./CUBRC
1	24.6	25.6	24.7	23.4	5.00	8.98	5.41
2	84.3	97.4	85.1	90.0	6.54	7.90	5.60
6	241	316	253	254	5.25	21.8	0.394
4	279	385	334	335	18.2	13.9	0.299

4.5 Modified Marrone-Treanor Results

The double-cone cases with MMT thermochemistry results are discussed below and compared to Park. The test cases are defined above in Table 4.1. The section below will compare surface properties and integrated surface properties to determine, one, if there are any differences between the Park and MMT thermochemistry models for the double-cone, and two, if the MMT thermochemistry model can better reproduce experimental results measured at the CUBRC LENS-XX facility. The Park results here are determined by the nonequilibrium case because chemistry rates and the vibrational relaxation times are unaltered. The flow field results are identical to Fig. 4.1(a).

4.5.1 Surface Properties

Run 1 is the low enthalpy air case and the results are shown in Fig. 4.7. The resulting surface properties between Park and MMT thermochemistry are identical. An RMS study of surface pressure and surface heat transfer show a less than 0.1% difference each. These results indicate that there are no significant differences between the models at this low enthalpy and that the MMT thermochemistry model is no better at reproducing the experimental results than the Park thermochemistry model.

Run 2 is the mid-level enthalpy air case. The results are shown in Fig. 4.8. The difference in surface properties between Park and MMT thermochemistry is slightly more prevalent for this case when compared to Run 1, but still minimal. An RMS study of surface pressure and surface heat transfer show a less than 1% difference

each. These results indicate there are no significant differences between each model at this mid-level enthalpy and that the MMT thermochemistry model also fails to reproduce the experimental results.

Run 6 is also a mid-level enthalpy air case. The results are shown in Fig. 4.9. The resulting surface pressure for Park is identical to MMT. However, the differences between surface heat transfer are noteworthy, especially at maximum surface heat transfer, for this mid-level enthalpy case. An RMS study of surface pressure shows a less than 1% difference. The RMS difference in surface heat transfer is about 2%, but has a max percent difference of 8%. These surface plots also suggest that the MMT thermochemistry model can not reproduce the experimental results.

Run 4 is a high enthalpy air case. The results are shown in Fig. 4.10. The differences between the Park and MMT surface properties are minimal, but still greater than Runs 1 and 2. An RMS study of surface pressure shows a less than 1% difference. While the RMS difference in surface heat transfer is about 2%, similar to Run 6, the max percent difference is only 3%. These surface plots also indicate that the MMT model fails to reproduce the experimental results.

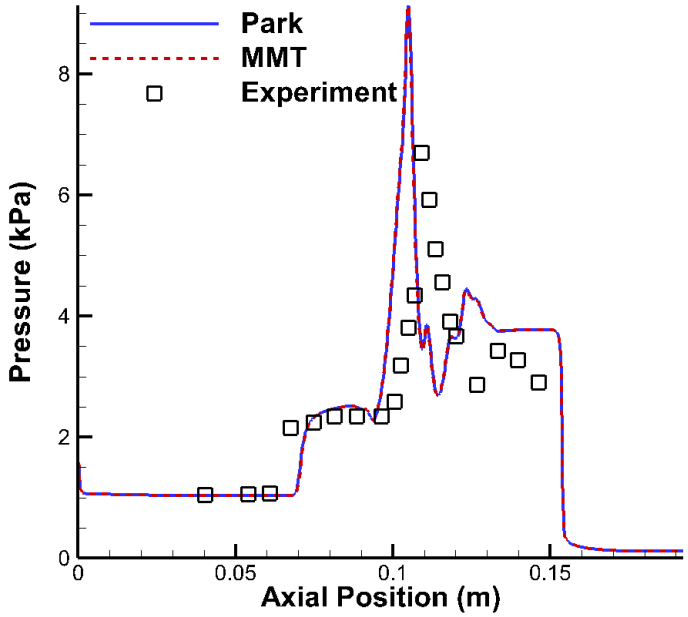

(a) Surface pressure

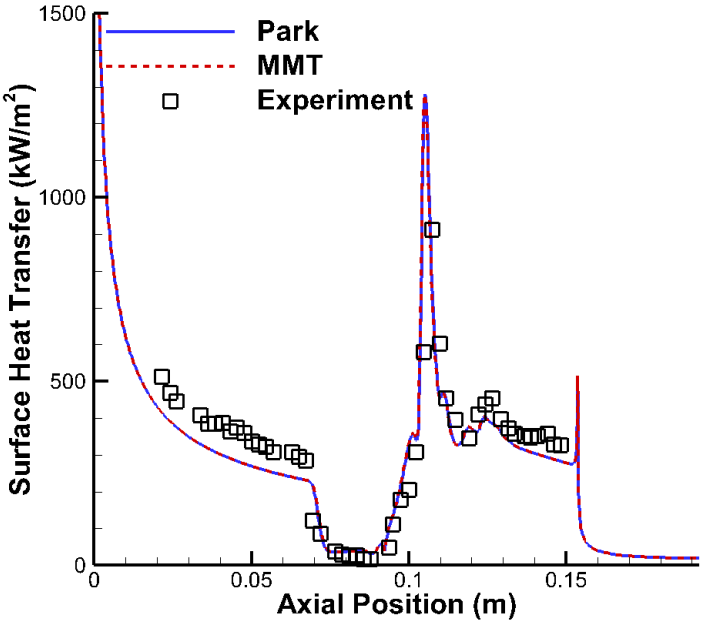

(b) Surface heat transfer

Figure 4.7: Run 1 comparison of Park and MMT.

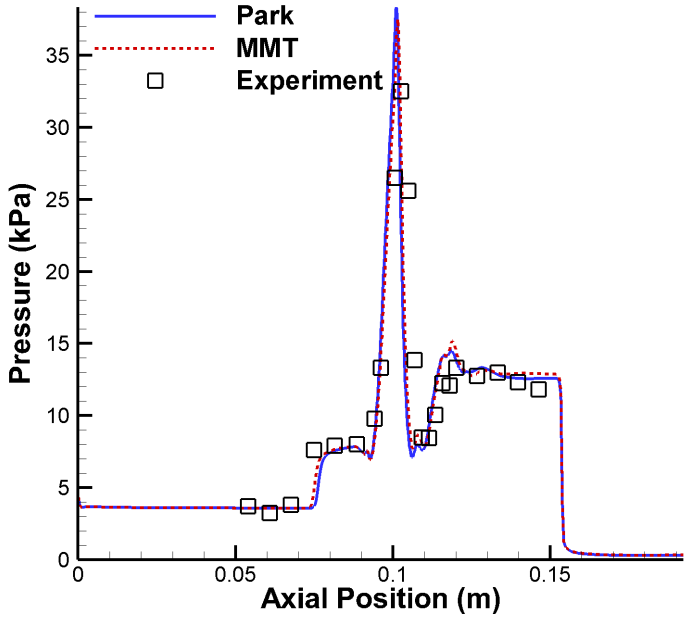

(a) Surface pressure

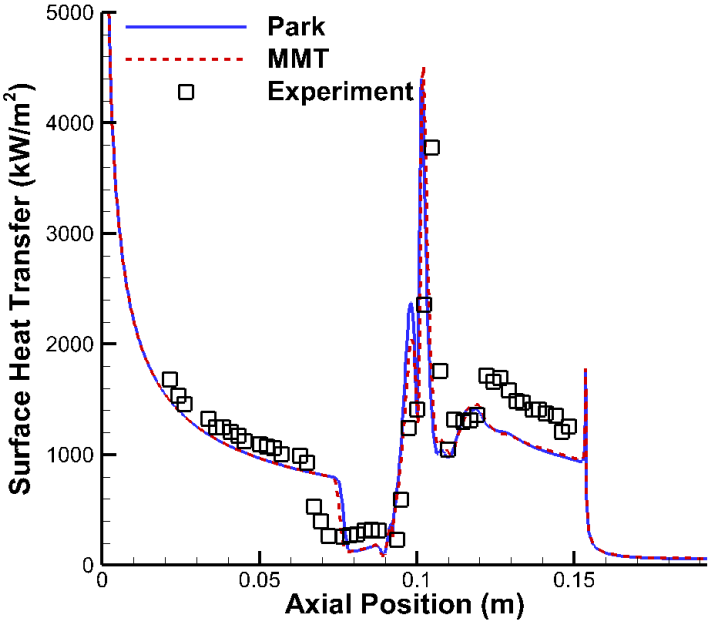

(b) Surface heat transfer

Figure 4.8: Run 2 comparison of Park and MMT.

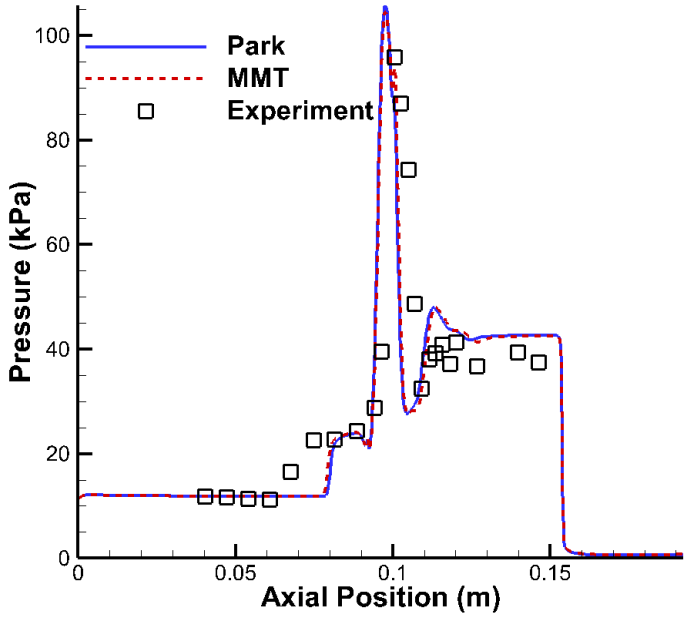

(a) Surface pressure

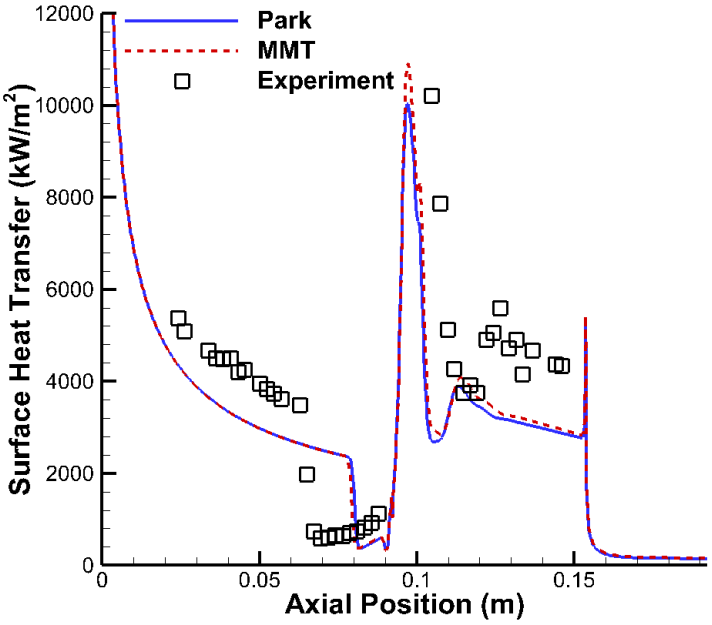

(b) Surface heat transfer

Figure 4.9: Run 6 comparison of Park and MMT.

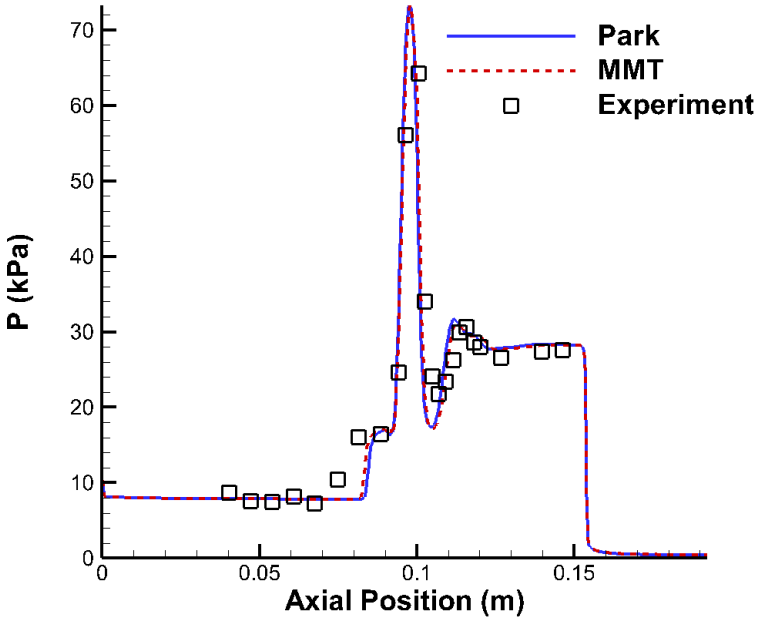

(a) Surface pressure

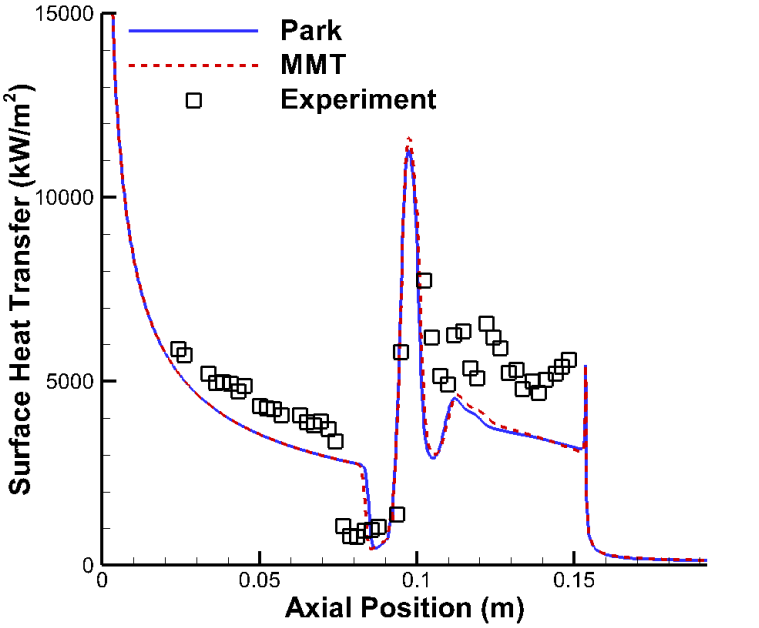

(b) Surface heat transfer

Figure 4.10: Run 4 comparison of Park and MMT.

4.5.2 Aerothermodynamic Loading

The integrated surface properties are shown in Tables 4.6-4.7. The integrated values are calculated in the same way as for Tables 4.2-4.3. These tables confirm that the differences in surface properties between the two thermochemistry models are minimal, generally less than 1%. However, Run 6 shows the largest percent difference when comparing surface heat transfer indicating that this mid-level enthalpy case is more sensitive. Run 2 also shows a larger percent difference in surface pressure than surface heat transfer, but these values are still minimal.

Table 4.6: Comparison of total drag (N) between Park and MMT

Run	Park	MMT	% Difference
1	206.6	206.6	-0.01
2	687.4	695.9	1.22
6	2280	2277	-0.12
4	1522	1520	-0.14

Table 4.7: Comparison of heating rate (kW) between Park and MMT

Run	Park	MMT	% Difference
1	25.00	25.06	0.24
2	85.77	86.15	0.44
6	246.7	257.2	4.16
4	285.3	289.5	1.46

The small differences in pressure when compared to surface heat transfer are unsurprising. The main differences between the Park and MMT models concerns the rate at which air molecules are dissociating and recombining. Molecular dissociation and recombination involves the absorption and release of energy in the form of heat, which can then be transfered to the surface. Therefore, the differences between the Park and MMT thermochemistry models are more likely to occur in terms of sur-

face heat transfer than surface pressure. However, results from Chaudhry et al. [56] illustrate larger differences in surface heat transfer than those shown here with the double-cone, see Fig. 4.11. The current work utilizes the MMT-VNB model shown in Fig. 4.11. These differences might arise from the differing geometries. Significantly, Chaudhry et al. explain that the major contribution to the differences in the two models has to do with the freestream conditions, or more specifically, their corresponding altitude. This is because altitude is directly related to freestream density which is directly related to collision rate. Chaudhry et al. demonstrate that major differences between the two models occur at altitudes between 35-45 km, which corresponds to a freestream density that is a factor of 16 higher (or an altitude that is 5-10 km lower) than the LENS-XX double-cone cases above. This is also suggested in Fig. 4.9 and Table 4.7 where the double-cone case with the highest freestream density, Run 6, shows the largest difference in surface heat transfer predicted by the Park and MMT models. To further investigate this claim, a double-cone case with a freestream density corresponding to an altitude of 45 kilometers, consistent with Chaudhry et al., is analyzed and the results are shown in Fig. 4.12. Unsurprisingly, the differences in surface pressure are minimal. An RMS study of the surface pressure and surface heat transfer show a difference of less than 1% in each case. However, the differences in surface heat transfer now become more apparent with local differences reaching 65% in the separation region, illustrating that the double cone's sensitivity to the chemical kinetics model is dependent on the freestream density. This is due to the increase in collision rate which is related to the increase in freestream density. The increase in collision rate leads to more chemical reactions taking place in the flow. However,

the increase in density is not so much to put the flow in an equilibrium state. The increase in chemical reactions in this region was found to be recombination dominate by Chaudhry et al. [56]. The recombination of air species produces energy in the form of heat. Therefore, it is unsurprising that increasing the freestream density of the double-cone produced larger differences in surface heat transfer between the Park and MMT thermochemistry models.

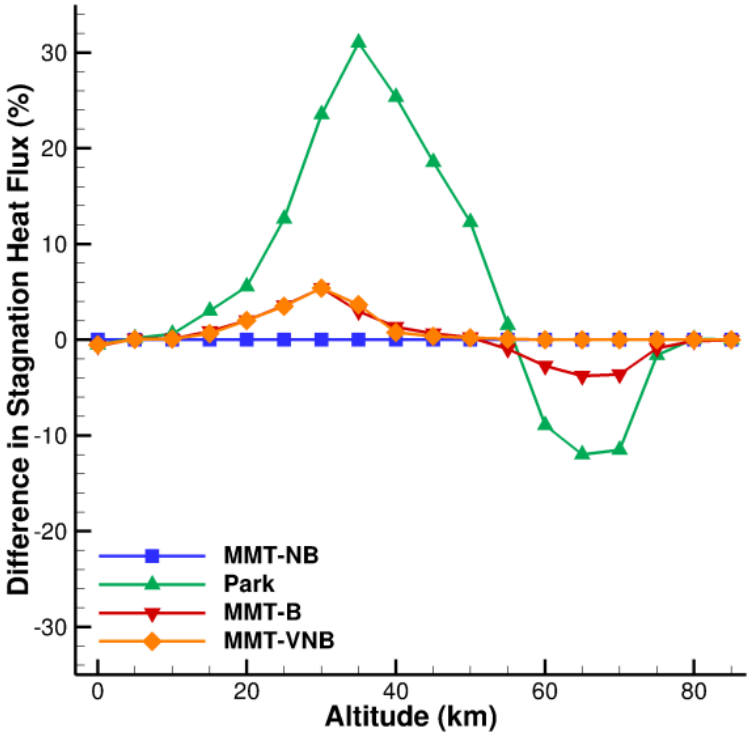

Figure 4.11: Relative heat flux difference vs MMT-NB [56].

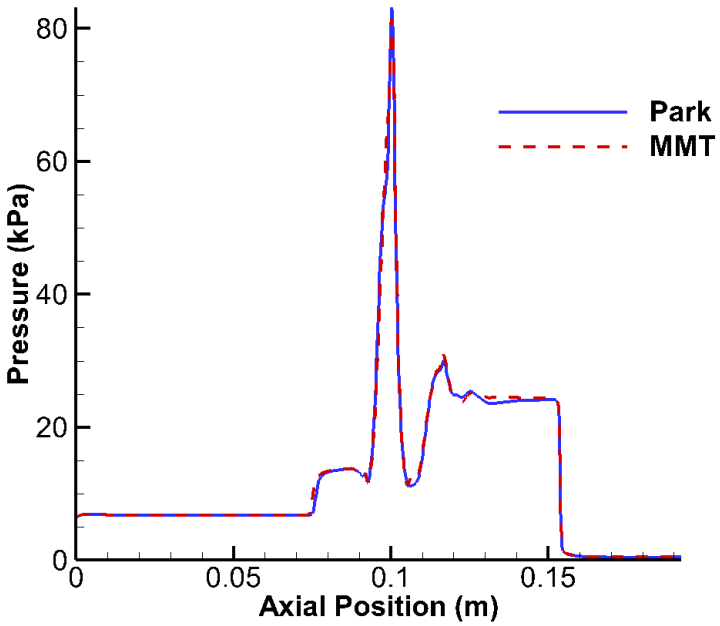

(a) Surface pressure

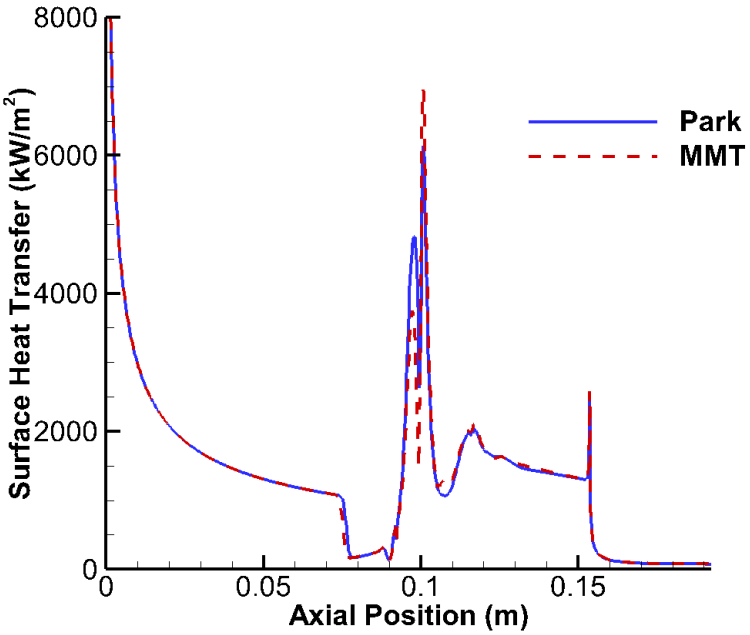

(b) Surface heat transfer

Figure 4.12: Comparison of Park and MMT for a double-cone at 45 km.

4.6 Chapter Summary

The influence of different assumptions for thermochemistry modeling using the Park 2T model in hypersonic air flows over a double-cone was studied. Each double-cone experiment was conducted at the newer CUBRC LENS-XX facility that provides freestream conditions that are in thermochemical equilibrium. Unsteady flow was observed in some frozen cases. The surface property analysis demonstrated a delay in flow separation when the thermochemistry model moved closer to equilibrium. It also showed significant sensitivity to thermochemistry modeling for all mid and high enthalpy double-cone cases. In general, the drag analysis showed that similar results were obtained with the nonequilibrium, equilibrium and frozen approaches. The heating rate analysis demonstrated significant differences as high as 37% between the equilibrium, nonequilibrium, and frozen thermochemistry models.

These results indicate that some of the double-cone cases investigated at the CUBRC LENS-XX facility are much more sensitive to the details of thermochemistry modeling than others. High enthalpy air cases appear to be the most sensitive of the cases considered. This sensitivity varies across different aspects of the flow. The total heating rate showed variations of greater than 30%. This is in contrast to the difference in total drag that had a maximum of 6%, indicating that heating rate is much more sensitive. This is due to the differences in the rate of chemical reactions between the three regimes. Chemical reactions include molecular dissociation and recombinations, which require energy in the form of heat. Therefore, it is unsurprising to see more significant differences in surface heat transfer when compared to surface

pressure.

A comparison of the Park and MMT thermochemistry models was also studied. By comparing the surface properties of the two models, it was determined that surface pressure was relatively unaffected when compared to surface heat transfer. This result was unsurprising, considering the main differences in the Park and MMT thermochemistry models has to do with heat exchange. It was also determined that the main contributor to the small differences in surface heat transfer between the two models has to do with the relatively low freestream density of each double-cone experiment. Increasing the freestream density increased the collision rate, leading to more chemical reactions in the flow that was still in a state of nonequilibrium by the time it reached the wall. This region of flow was found to be recombination dominate. Therefore, the differences in the Park and MMT thermochemistry models became more apparent in the form of surface heat transfer. Lastly, it was illustrated that the MMT thermochemistry model also failed to reproduce experimental measurements.

Despite the expectation that LENS-XX should produce freestream conditions with less uncertainty than those in LENS-I, due to the claimed absence of thermochemical nonequilibrium, it is shown that CFD consistently over predicted the surface properties. Additional inconsistencies are shown by other researchers in Refs. [37,38]. These trends suggest there is a basic difference between the experiments and the simulations for both CUBRC facilities. Due to the inconsistencies observed in the current chapter and in Chapter 3, it must be concluded that the CUBRC double-cone experiments considered in this dissertation are limited in their usefulness for the evaluation of thermochemistry models utilized for analysis of hypersonic flows.

It is therefore surmised that new hypersonic experiments are needed in facilities with a well-characterized freestream and that employ advanced diagnostics for characterization of both the surface properties and the flow field. Computational analyses should be employed to determine suitable geometries and flow conditions. Sensitivity analyses can be used to indicate the level of measurement fidelity required to discriminate between different thermochemistry models.

CHAPTER 5

Sensitivity Analysis of the Thermochemical Kinetics

This chapter serves as a follow up to the conclusions of Chapter 4. A sensitivity analysis of thermochemistry models for hypersonic flow over a cylinder is investigated. A CFD analysis is used to model Mach 5 and Mach 7 flow over a cylinder, where freestream properties are representative of experiments to be conducted in the Hypervelocity Expansion Tube (HET) at the California Institute of Technology (CalTech). The analysis is performed using the Sandia National Laboratory's toolkit code Dakota. The objective of the sensitivity study is to vary reaction rates to help identify rate inputs that most influence key quantities of interest.

5.1 Introduction and Motivation

In the previous chapters, the double-cone was investigated to study the effects of thermochemistry modeling because of its simple geometry and its shock wave bound-

ary layer interaction. However, the investigation was unable to reproduce experimental data, likely due to inaccurate characterization of some aspects of the experiments, making the double-cone limited in its usefulness for validating thermochemistry models for the studied cases.

In order to better assess the computational models, the current chapter will conduct a sensitivity analysis on the thermochemistry model. This analysis will help identify the key reactions that may be tested by future experiments to be conducted in the CalTech facility. It may also help experimentalists to better understand the accuracy required from their diagnostics to be able to differentiate between different models. An example of large uncertainty values for thermochemistry experiments is shown in Fig. 5.1. Figure 5.1 compares the post normal shock relaxation of molecular oxygen for the Park 2T and State-to-State (STS) thermochemical models against experimental measurements. The two models show clear differences, but both are bounded by the measurement uncertainties. Therefore, an evaluation to which model provides a better prediction cannot be made. The results of the sensitivity study described in this chapter may aid experimentalists in lowering uncertainties like these to provide computationalists a better understanding of which thermochemical approaches are necessary for accurate results.

A simple geometry that can be used to conduct a sensitivity analysis on thermochemistry models is a cylinder in cross flow. Though the cylinder does not produce a shock wave boundary layer interaction, the geometry allows for post shock conditions to be easily evaluated at a low computational cost. In addition, cylinder flows involve expansion and flow separation regions that broaden the range of phenomena. The

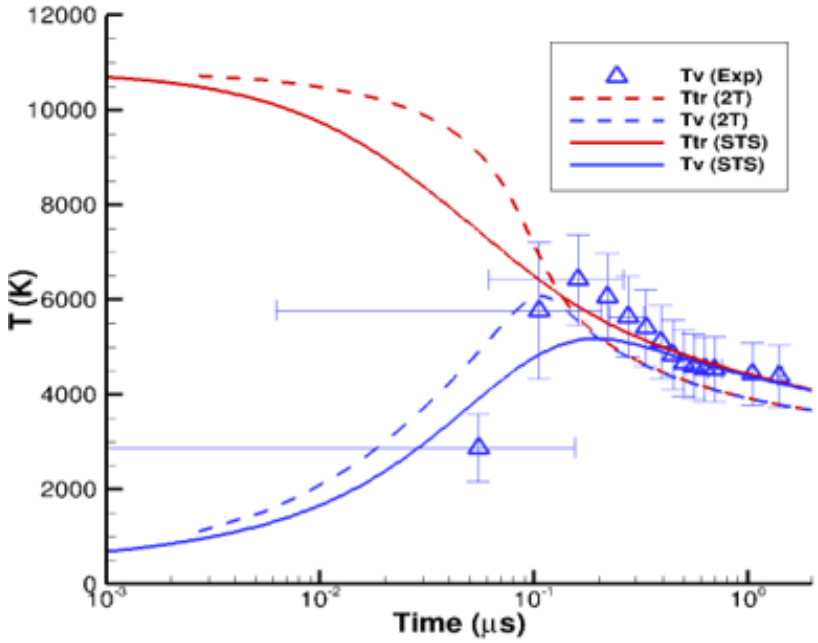

Figure 5.1: Mach 13 shock tube profile of molecular oxygen relaxation [85].

specific cylinder will be investigated in the HET facility. A schematic of the HET facility and a sample x-t diagram are shown in Figs. 5.2 and 5.3, respectively. Details regarding the operation of the facility and its capabilities can be found in Ref. [86]. The HET diagnostics include piezoelectric pressure transducers and temperatures extracted from spectrum fitting [86,87]. Details of the experimental setup can be found in Ref. [87] and are discussed below.

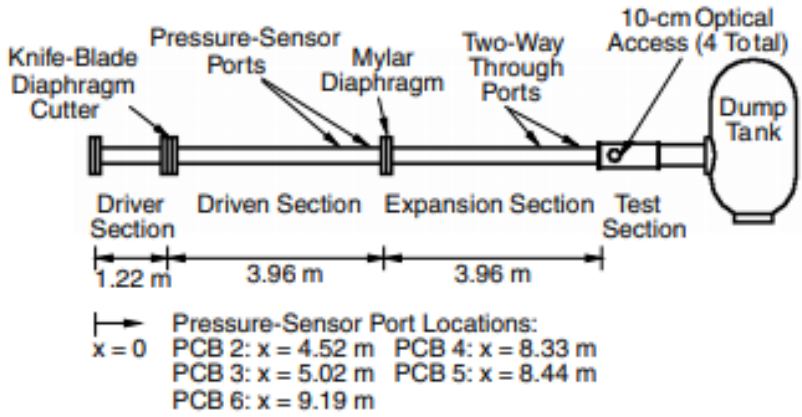

Figure 5.2: HET schematic [86].

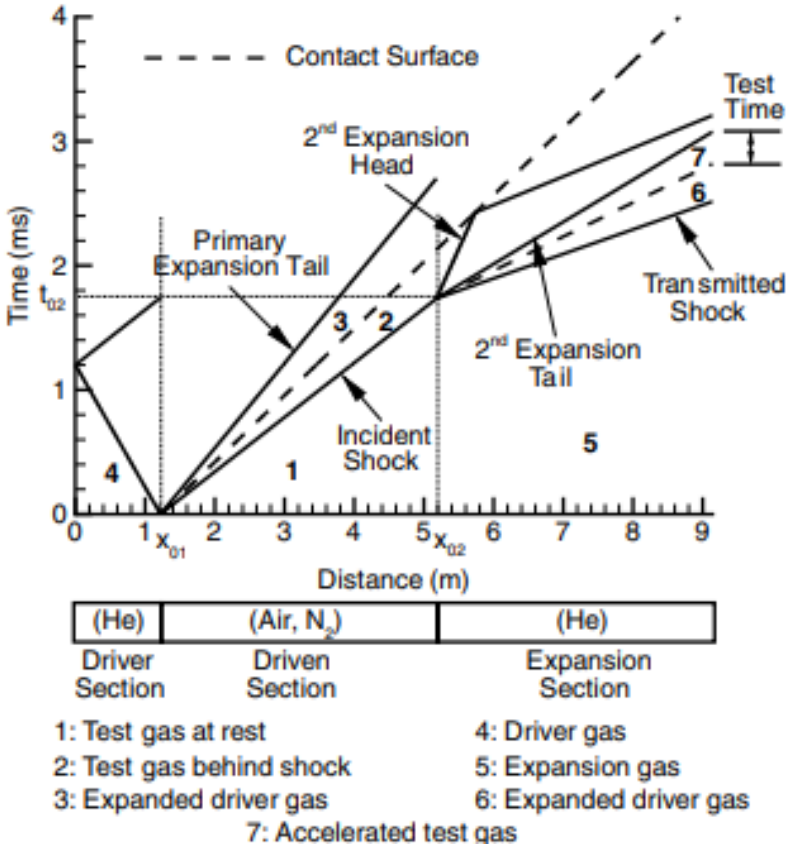

Figure 5.3: Sample x-t diagram of the calculated gas dynamic process for a Mach 5.1 test flow [86].

In order to illustrate the potential effects thermochemistry models have on QoIs, Mach 5 and Mach 7 cylinder cases in air are studied by adjusting reaction rates for five of the most common reactions in air: (1) O_2 dissociation with partner N_2 (2) O_2 dissociation with partner O (3) O_2 dissociation with partner O_2, and the first and second Zeldovich reactions (4) N_2 exchange with partner O and (5) NO exchange with partner O. The QoIs in the current work include the surface pressure, surface heat transfer, number density of NO at the wall, stagnation line rotational temperature, and total drag and heating rate. An in depth discussion on the inputs and QoIs is provided below.

The current chapter will explain the numerical approach used in this study, describe the test cases, examine the resulting flow properties for the cylinder, explain the strategy of the sensitivity study, discuss the sensitivities of the QoIs, and will end with conclusions based on trends observed.

5.2 Numerical Approach

The hypersonic flow component of the numerical simulations in this chapter are performed using the CFD code LeMANS, detailed in Section 2.2, with the Park 2T model. This chapter investigates a wide range of thermochemical regimes between equilibrium, nonequilibrium, and frozen flow by altering chemistry rates calculated by Eq. 2.20.

The sensitivity analysis in this study is performed by Dakota, detailed in Section 2.3. The integration of Dakota with LeMANS accounts for a major portion of the current work. Sensitivity is investigated through polynomial chaos expansion (PCE), a stochastic expansion method. Dakota utilizes PCE to automatically change reaction rates, calculated by Eq. 2.20, for every LeMANS simulation. Since the investigation only considers a relatively small number of input parameters, five, PCE is more efficient than a random sampling method [37,66]. After the Dakota PCE simulation is complete, and LeMANS simulations have been run, Dakota quantifies the sensitivities each input has on a QoI by means of global Sobol indices. This method will identify which input parameters most influence output quantities of interest. The input file of Dakota utilizes a sparse grid level of two and sets upper and lower bounds of the

reaction rates by two orders of magnitude from their standard value. The order of polynomials is five. These inputs are chosen to optimize computational expense and quality of results. The resulting computational expense includes approximately 80 LeMANS simulations and a total of approximately 2000 core hours per hypersonic cylinder case.

5.3 Hypersonic Flow Over a Cylinder

Each cylinder case and its freestream conditions generated in the HET facility considered in this study are shown in Table 5.1 [86]. Here, the nomenclature for the HET case is introduced where the first two letters and numbers represent the freestream Mach number and enthalpy, respectively. The third represents the test gas, air: 76.5% N_2 and 23.5% O_2 by mass fraction. These cases are chosen because air at these high enthalpy levels produces nonequilibrium thermochemistry phenomena that can be examined. These were also the cases suggested by Professor Joanna Austin, the principle investigator at HET. The freestream conditions were calculated in Ref. [87] assuming perfect gas. The freestream enthalpies of the two cylinder cases are mid-level, between Runs 1 and 2 of CUBRC's LENS-XX experiments shown in Table 4.1. A laminar flow model is also used, which is consistent with Ref. [87]. The unit Reynolds number for these cylinder cases are on the same order of magnitude, 10^5, as all of the LENS-XX double-cone cases where the laminar model is known to be appropriate.

The geometry specifications of the cylinder consist of a 0.03175 m (1.25 in) diam-

Table 5.1: Cylinder freestream conditions [87]

Case	M7-H8-A	M5-H6-A
Test Gas	Air	Air
Mach	7.18	4.87
h_0, MJ/kg	8.14	6.23
U_∞, m/s	3922	3283
T, K	743	1129
p, Pa	807	3513
ρ_∞, g/m^3	3.79	10.84
t_{Test}, μs	163	311
Re, 1/m	4.3×10^5	7.9×10^5
$U_{s,accel}$, m/s	4728	3968

eter and a 0.0762 m (3 in) span. The two dimensional computational grid consists of approximately 60,000 cells with 200 cells along the wall. The grid is shown in Fig. 5.4. The grid convergence study consists of a coarse grid, approximately 30,000 cells, and a fine grid, approximately 120,000 cells. An RMS comparison between the surface pressure and surface heat transfer for each grid produced a maximum percent difference much less than 1%. Due to the short run time of the experiment, the case is modeled as an isothermal wall at 300 K to replicate the HET experiments. The wall is non catalytic.

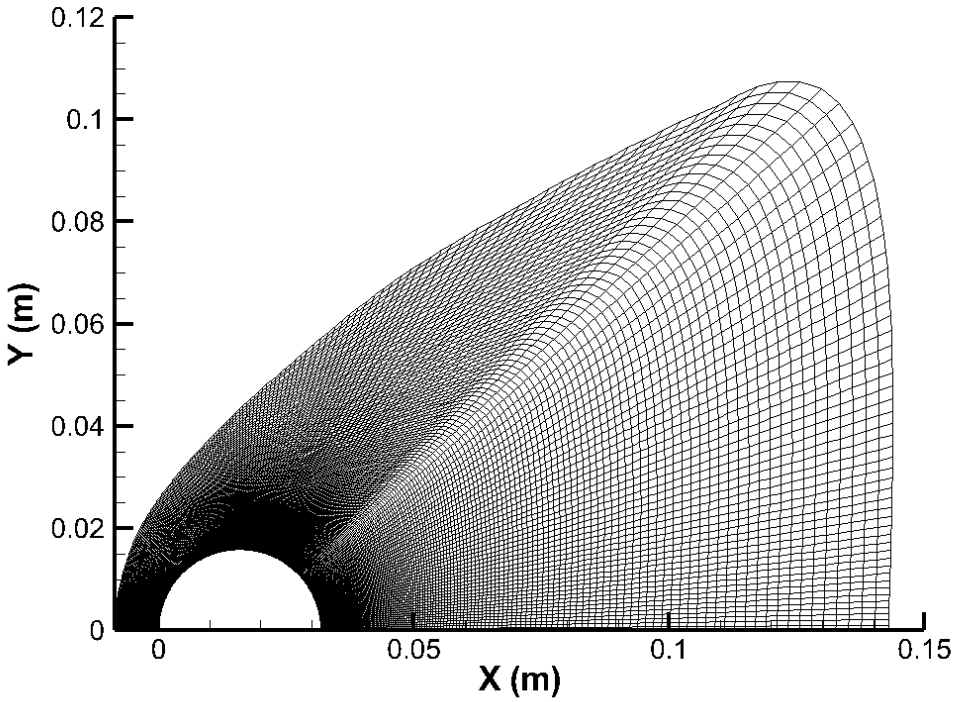

Figure 5.4: Hypersonic cylinder grid.

5.4 Results

The results for the hypersonic cylinder flows are shown here. This section includes a synopsis of the cylinder's flow field and surface properties, in terms of surface pressure and surface heat transfer. These results serve as a foundation for the proceeding section on sensitivity analysis.

5.4.1 Flowfield Results

The temperature contours for the M7-H8-A case are shown in Fig. 5.5. The M7-H8-A temperature results are representative of the M5-H6-A case. These temperature

contours illustrate the simplicity of the cylinder flow field. The flow field consists of a bow shock that increases pressure and temperature and gradually decreases as the shock strength weakens and the flow expands. These flow properties are still large by the time the flow reaches the surface, making the study of surface properties important. The contours also capture the trailing edge of the cylinder where flow separation and recirculation occur. These flow phenomena lead to interesting characteristics in the sensitivity study discussed below.

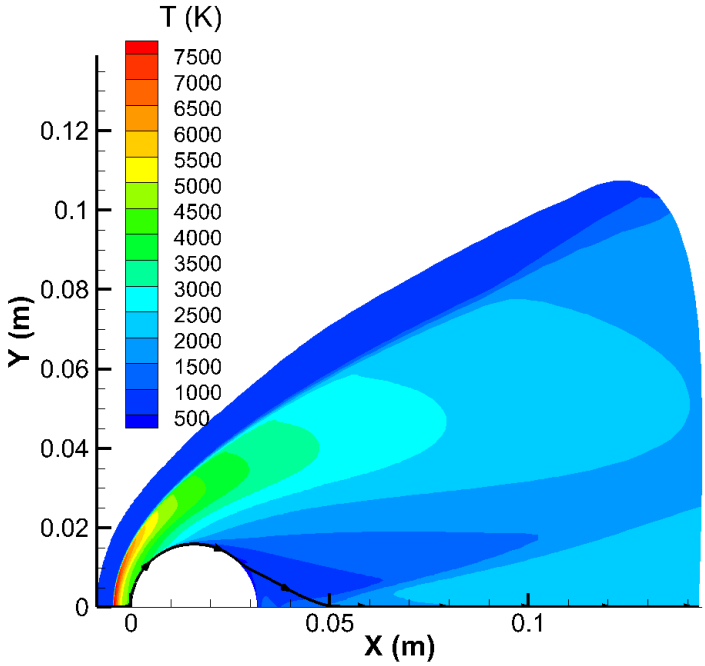

Figure 5.5: M7-H8-A cylinder temperature contours with surface streamline.

A major objective of the sensitivity analysis is to determine how different reactions affect QoIs. This requires some understanding of the chemical reactions taking place in the flow field. Figure 5.6 shows the change in the chemical makeup along the stagnation line in terms of species mass fraction for 5-species air. Figure 5.6(a) illustrates molecular oxygen dissociation, that produces atomic oxygen. Shortly af-

ter, nitric oxide is formed due to the first Zeldovich reaction. The dissociation and exchange of nitric oxide molecules then leads to a small increase in atomic nitrogen. Figure 5.6(b) illustrates the formation of oxygen molecules near the wall and a significant amount of atomic oxygen and nitric oxide. Atomic nitrogen is insignificant near the surface.

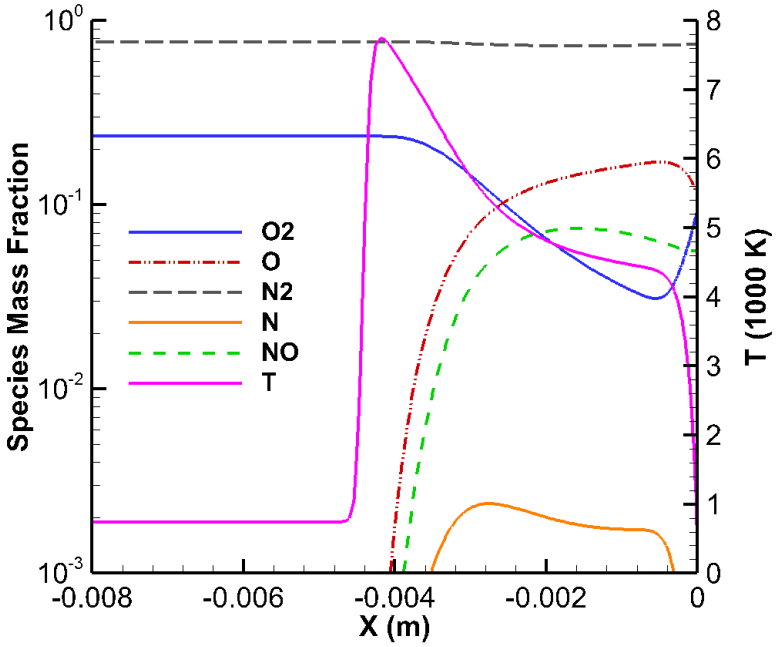

(a) Full stagnation line properties

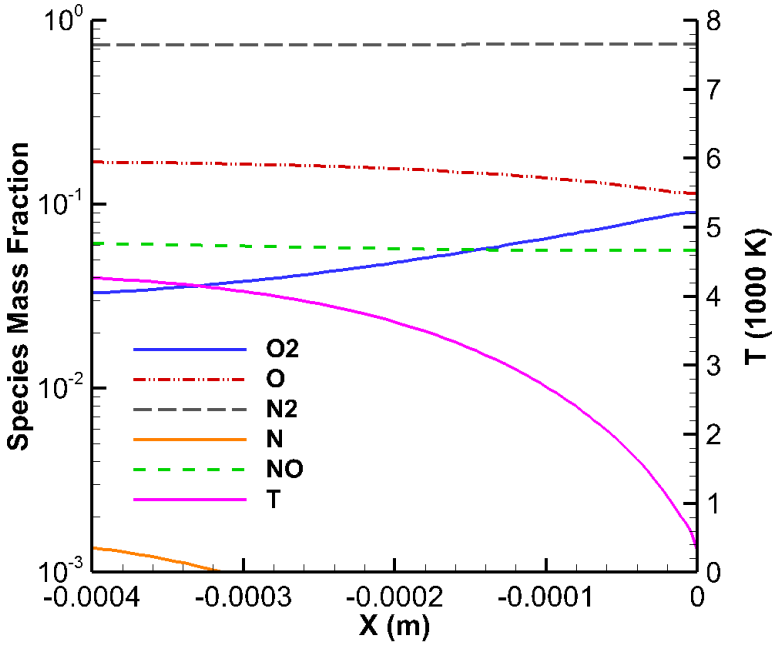

(b) Near wall stagnation line properties

Figure 5.6: Stagnation line properties for the M7-H8-A cylinder with standard reaction rates.

The net chemistry rates for the five key reactions for both cylinder cases are also presented below. Figure 5.7 shows the net reaction rates on a stream line just above the stagnation point, shown in Fig. 5.5, to approximately half way around the cylinder, where the five net reaction rates reach zero and before the flow reaches the wake. Each cylinder case shows that the net O_2-N_2 reaction is the most active right after the shock and again as the flow starts to move around the surface. It is also shown that the net O_2-O_2 reaction is the least active overall. Figure 5.7(a) shows that the O_2-O and N_2-O net reactions are similar after the shock, however as the flow moves over the surface of the cylinder the O_2-O reaction begins to dominate. The NO-O net reaction is also significant post shock, but reaches zero as the flow moves over the cylinder. Figure 5.7(b) is similar to Fig. 5.7(a), but differs in the post shock region where the N_2-O net reaction is more active than the O_2-O net reaction. Also, the net reactions of O_2-O and O_2-N_2 are similar as the flow moves over the surface of the cylinder. Further illustration of the net reaction rates in the flow field can be found in Appendix A.1, Figs. A.3-A.7, where the most active reactions agree with Fig. 5.7.

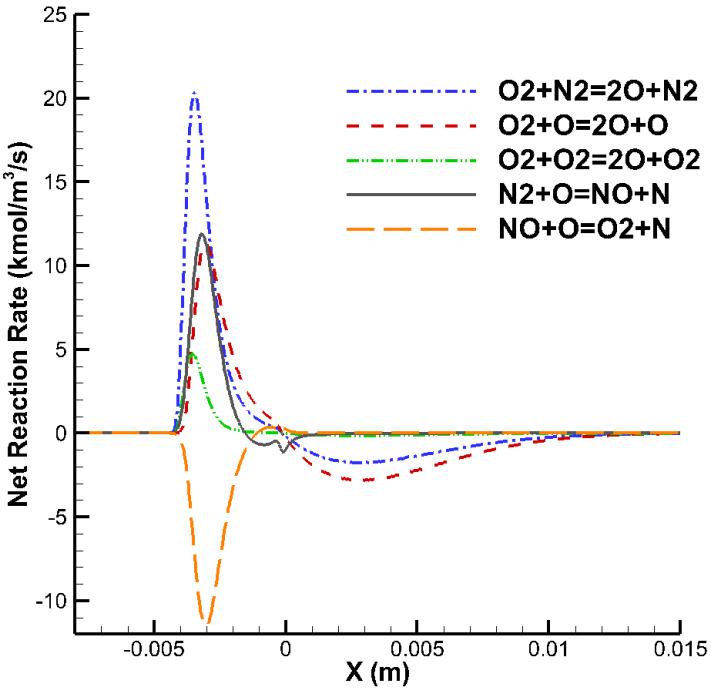

(a) M7-H8-A cylinder

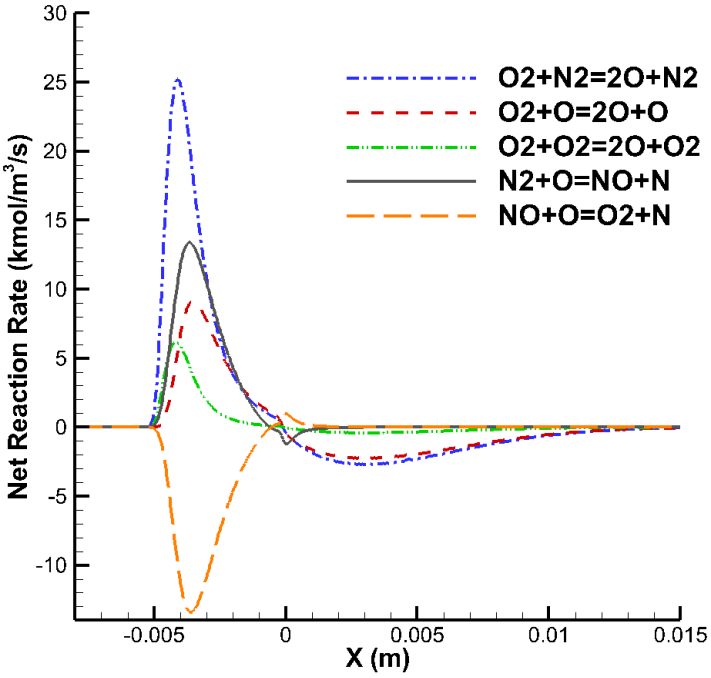

(b) M5-H6-A cylinder

Figure 5.7: Net reaction rates along a streamline.

5.4.2 Surface Properties

M7-H8-A is a high enthalpy air case. The surface properties are shown in Figs. 5.8 and 5.9 and display expected results. The M7-H8-A surface profiles are representative of the M5-H6-A surface profiles. The M5-H6-A surface profiles are shown in Section A.1 for reference. The surface pressure calculated by LeMANS shows a peak at the stagnation point and a gradual decline around the cylinder. The surface heat transfer also shows a peak at the stagnation point and a gradual decline as the flow expands. The surface properties also show a slight increase at the trailing edge, further indicating complicated flow physics at this location and showcasing the importance of a sensitivity study in this region. The flow physics are illustrated by the streamlines shown in Fig. 5.10 and confirm recompression and potentially recirculation near the trailing edge of the cylinder. Figures 5.8-5.9 also show HET's mid-span locations of experimental measurement ports at 0, 30, 60, and 90 degrees.

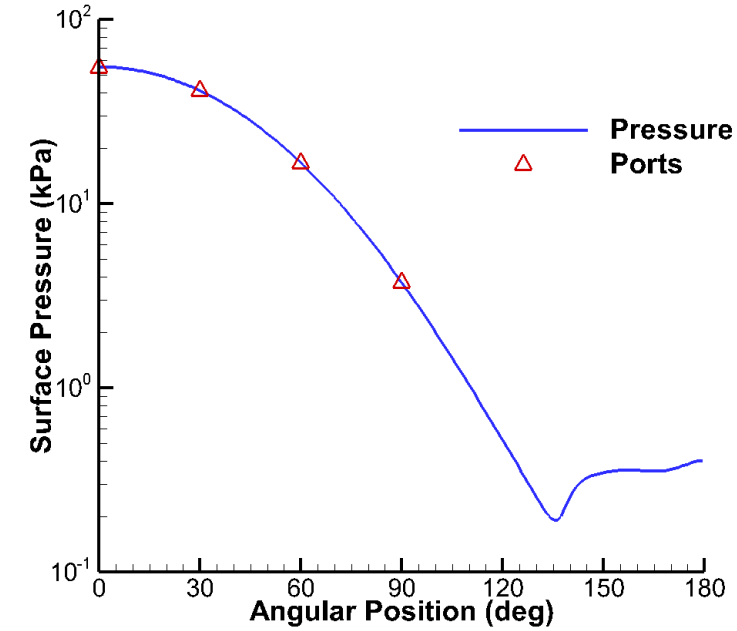

Figure 5.8: M7-H8-A surface pressure with experimental measurement locations.

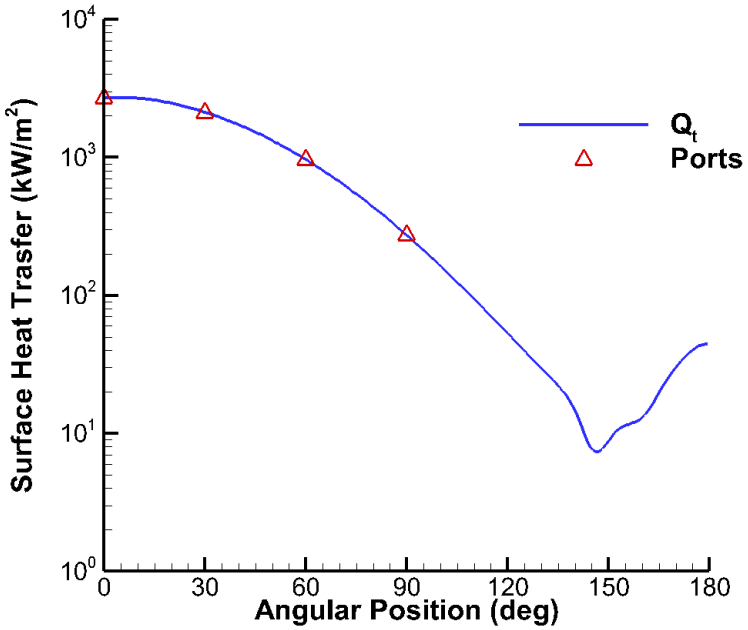

Figure 5.9: M7-H8-A surface heat transfer with experimental measurement locations.

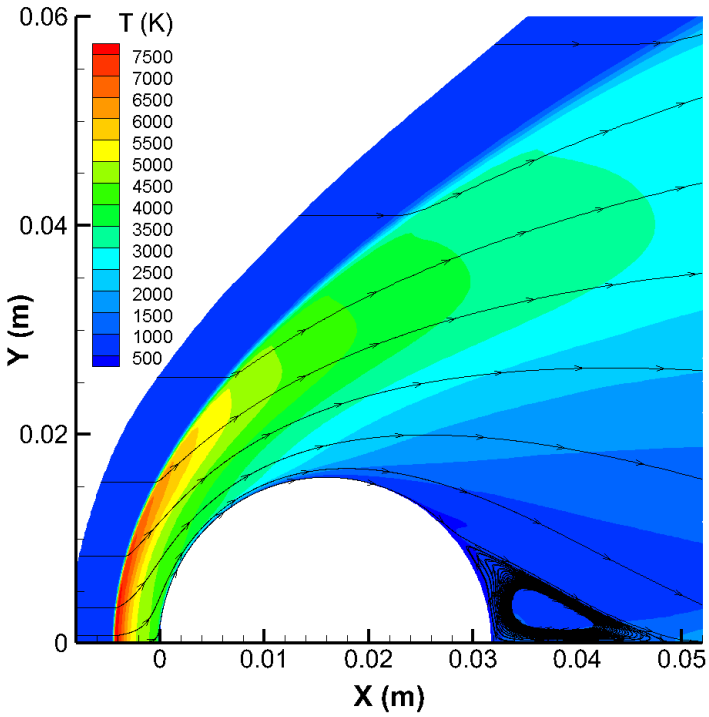

Figure 5.10: M7-H8-A streamlines.

5.5 Sensitivity Analysis Results

The previous section discussed the baseline flow field and surface properties of the hypersonic cylinder flows. The analysis produced the expected results and suggest complicated flow physics near the trailing edge of the cylinder, making this region important for the proceeding sensitivity analysis. The following section will discuss the input parameters and QoI for the PCE sensitivity study and provides an in-depth discussion of the results.

5.5.1 Input Parameters

The sensitivity analysis considers five input parameters, which are the forward reaction rates of O_2 dissociation with partner N_2, O_2 dissociation with partner O, O_2

dissociation with partner O_2, and the first two Zeldovich reactions, N_2 exchange with partner O and NO exchange with partner O. Dakota is programmed such that the PCE method varies the chemistry rates by no more than three orders of magnitude. Other reactions are currently not considered to save computational cost. The O_2-N_2, O_2-O, and O_2-O_2 reactions are considered for a few reasons:

1. Primary focus is on O_2 dissociation because it has a weaker bond than N_2.

2. O_2-N_2 is considered because N_2 is the dominant species in air.

3. O_2-O_2 is considered because O_2 is the second most common species in air.

4. O_2-O is considered because of O_2 dissociation.

The oxygen atoms can then interact with other species, either in the flow or on the surface. It is well known that atomic oxygen significantly affects flow and surface properties, so these reactions need to be understood in detail. The two Zeldovich reactions are considered for a few reasons. The first reason is that the first Zeldovich reaction, $N_2 + O \longrightarrow NO + N$, is a primary reaction that destroys N_2. The bond strength of N_2 is so strong that breaking it all at once is rare. The first Zeldovich reaction provides a pathway, because the NO bond is about 6 eV, compared to 10 eV for N_2, so the energy required to activate the reaction is only about 4 eV. Second, the density of NO will be measured in the CalTech experiments. Lastly, Fig. 5.6 illustrates that NO forms near the wall. Post-shock dissociation of O_2 is also shown in Fig. 5.6.

5.5.2 Quantities of Interest

Several QoIs are considered for the sensitivity analysis. These QoIs coincide with the HET facility and its ability to measure surface pressure, surface heat transfer, number density of NO, and stagnation line rotational temperature. Even though surface properties are only measured in HET at locations of 0, 30, 60, and 90 degrees around the cylinder, the current work investigates these QoIs at every 10 degrees on the cylinder to help identify locations of interest. The rotational temperature is measured in HET on the stagnation streamline at locations of 2.3 mm, 2.8 mm, and 3.3 mm upstream of the stagnation point. Due to the use of the Park 2T model in LeMANS, rotational temperature is assumed to be in equilibrium with translational temperature. Therefore, translational temperature is used to represent the rotational temperature as the QoI. This is a safe assumption considering the relatively low temperature values of the hypersonic cylinder, less than 8,000 K, and is explained further in Park's paper on the limitations of his 2T model in Ref. [88]. The number density of NO at the wall is also considered a QoI due to the presence of NO near the wall, shown in Fig. 5.6. Total drag is also a QoI and is calculated by integrating the entire profile of surface pressure and surface shear stress. Total heating rate is also considered a QoI because of its potential impact on material response and is calculated by integrating the entire profile of surface heat transfer over the cylinder area.

5.5.3 Sobol Indices

The sensitivities are quantified via Sobol indices, described in Section 2.3 and the results are discussed below. A high Sobol index suggests that the particular reaction dominates the QoI. Surface heat transfer, surface pressure, and surface number density of NO have their Sobol index presented versus their location on the cylinder. Translational/Rotational temperature, drag, and heating rate have their Sobol index quantified in a bar chart.

The sensitivity of surface heat transfer is quantified in Fig. 5.11 for both hypersonic cylinder flows. For the M7-H8-A case, the O_2-N_2 reaction dominates surface heat transfer at the stagnation point. This result is partially explained when Fig. 5.7(a) is considered. O_2-N_2 is a primary reaction that destroys O_2. The properties along the stagnation line in Fig. 5.6 also show the formation of O_2 near the wall. As the flow moves over the cylinder, recombination begins to take effect via the O_2-N_2 and O_2-O reactions, shown by the negative values in Fig. 5.7(a). Negative values in Fig. 5.7 indicates reactions are proceeding in the backward direction. This recombination releases energy in the form of heat which can be transfered to the surface. Similarly, the O_2-N_2 reaction dominates the stagnation point for the M5-H6-A case. However, in this instance, the Zeldovich reactions are also contributing to the production of molecules and, therefore, releasing heat. The high contribution to surface heat transfer via the Zeldovich reactions is consistent with Fig. 5.7(b). This case also shows an increase in the O_2-O reaction Sobol indices as the flow moves over the cylinder, which again agrees with Fig. 5.7 where this reaction begins to dominate

along with O_2-N_2. Also of note in Fig. 5.11 is the region leading up to and after 140 deg. At this location, the Sobol indices begin to change rapidly. This is due to the onset of flow separation and recirculation in this region, shown in Fig. 5.10. This phenomenon can be a result of the change in reaction rates, as shown in Chapters 3 and 4, and can lead to some unsteadiness in the flow. As a result, each LeMANS simulation converges to a slightly different solution which leads Dakota to indicate this area of the cylinder is sensitive.

While the Sobol indices indicate that a QoI is sensitive to a particular parameter, they do not indicate the degree of how much a Sobol index value affects the QoI. To study this effect, a number of additional LeMANS simulations are performed in which the reaction rates of four of the five key reactions (O2-O2 is omitted) are increased and decreased one at a time by two orders of magnitude. Based on the comparison of these new results to the baseline case, the overall impact on surface heat transfer is shown in Tables 5.2 and 5.3 at the experimental measurement locations. Tables 5.2 and 5.3 again show that the O_2-N_2 and O_2-O reactions are the most dominant with percent differences of up to 34% and 24% for the M7-H8-A and M5-H6-A cylinders, respectively, while the O_2-O_2, N_2-O, and NO-O reactions produce relatively much lower percent differences. While the overall percent difference for the first and second Zeldovich reactions are relatively small, Tables 5.2 and 5.3 show that these two reactions are more impactful for the M5-H6-A case than the M7-H6-A case, also shown in Fig. 5.11.

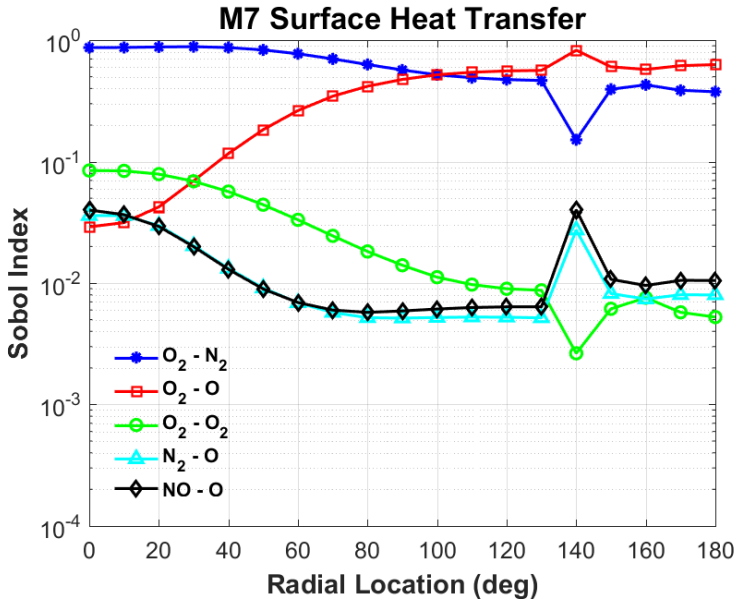

(a) M7-H8-A surface heat transfer Sobol indices

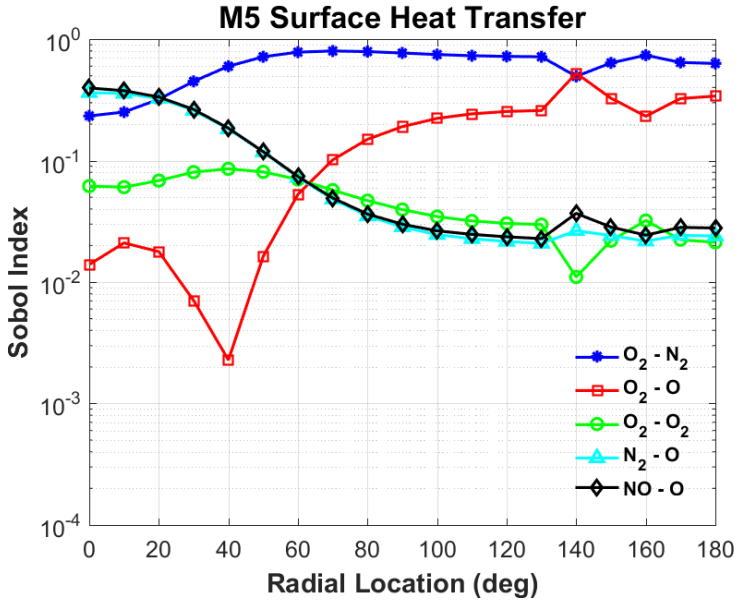

(b) M5-H6-A surface heat transfer Sobol indices

Figure 5.11: Hypersonic cylinder surface heat transfer Sobol indices.

The sensitivity of surface pressure is quantified in Fig. 5.12 for both the M7-H8-A and M5-H6-A hypersonic cylinders. At the stagnation point, both hypersonic cylinder cases illustrate that the O_2-O reaction is the most dominant along with the O_2-N_2 reaction. This result can be traced back to the stagnation line properties and

Table 5.2: M7-H8-A percent difference in surface heat transfer

Angle deg	O_2-N_2	O_2-O	N_2-O	NO-O
0	33.4	32.1	0.88	1.44
30	34.2	32.8	0.06	1.14
60	27.6	27.6	2.11	0.36
90	14.2	17.5	3.96	0.08

Table 5.3: M5-H6-A percent difference in surface heat transfer

Angle deg	O_2-N_2	O_2-O	N_2-O	NO-O
0	21.9	11.6	3.30	2.35
30	24.1	12.7	2.77	2.06
60	24.4	10.5	1.30	1.34
90	20.3	5.18	0.28	0.66

the relation between surface pressure and number density. Figure 5.6(b) shows that atomic oxygen is quickly recombining near the wall. Pressure is also proportional to species number density. As a result of the rapid change in molecular oxygen number density, the sensitivity of surface pressure is going to be dominated by these two reactions. As the flow moves down stream of the cylinder, the Sobol index of the O_2-N_2 reaction begins to overtake the O_2-O reaction for the M5-H6-A cylinder. It should be noted that while the Sobol indices in this downstream region are quantitatively different, Sobol indices on the same order of magnitude are qualitatively similar. Consequently, the O_2-O_2, and the two Zeldovich reactions are relatively unimportant when compared to the other two reactions.

Additionally, based on the additional LeMANS simulations in which individual rates were increased and decreased by two orders of magnitude, the overall impact of surface pressure is shown in Tables 5.4 and 5.5 at the experimental measurement locations. Tables 5.4 and 5.5 display very low percent differences indicating that

surface pressure is not sensitive to the change in flow chemistry. This was also shown for the double-cone flows in Chapters 3 and 4. Therefore, a high Sobol index in Fig. 5.12 does not indicate that the particular reaction significantly influences surface pressure.

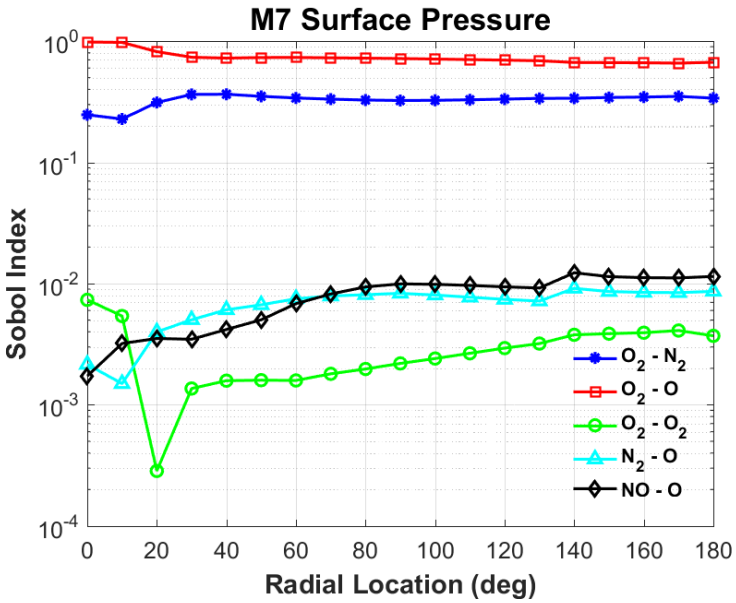

(a) M7-H8-A surface pressure Sobol indices

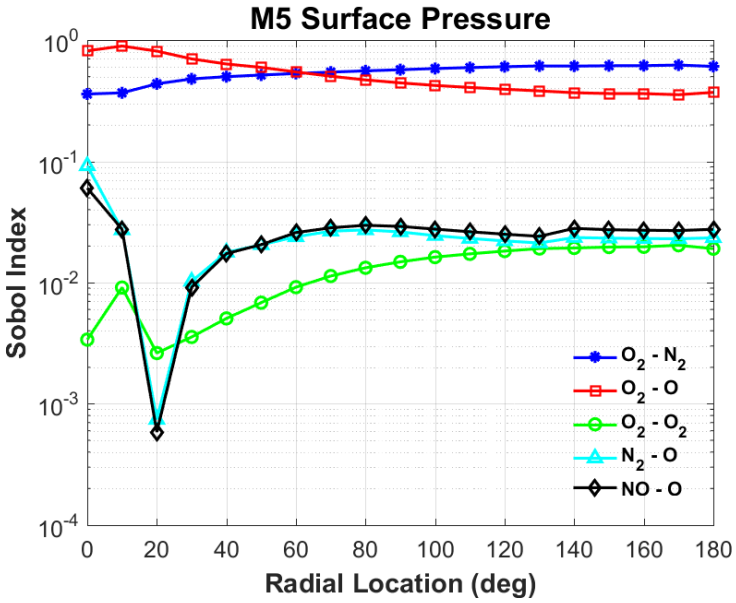

(b) M5-H6-A surface pressure Sobol indices

Figure 5.12: Hypersonic cylinder surface pressure Sobol indices.

Table 5.4: M7-H8-A percent difference in surface pressure

Angle deg	O_2-N_2	O_2-O	N_2-O	NO-O
0	0.88	0.89	0.06	0.04
30	0.19	0.17	0.17	0.18
60	2.73	0.74	0.45	0.54
90	5.24	0.66	1.12	0.98

Table 5.5: M5-H6-A percent difference in surface pressure

Angle deg	O_2-N_2	O_2-O	N_2-O	NO-O
0	1.10	0.52	0.08	0.02
30	0.74	0.41	0.06	0.06
60	0.48	0.01	0.05	0.25
90	1.27	0.68	0.25	0.42

The sensitivity of surface number density of NO is shown in Fig. 5.13 for both hypersonic cylinder cases. The results here are unsurprising. Namely, the two Zeldovich reactions dominate the number density of NO on the surface of the cylinder. The results also suggest that the O_2-O_2 reaction is relatively unimportant for this QoI. This is because NO requires atomic oxygen, which is more likely to arise from the other four reactions, as shown in Fig. 5.7. Also of note is that the O_2-N_2 and O_2-O reactions also heavily influence the surface number density of NO for the M7-H8-A case, while these two reactions do not become important for the M5-H6-A case until further around the cylinder. This phenomenon is most likely related to the difference in dominant net reaction rates in Fig. 5.7. Unlike the M7-H8-A case, the M5-H6-A case shows that the O_2-O reaction is not as active as the first and second Zeldovich and O_2-N_2 reactions post shock, leading Dakota to indicate the O_2-O reaction is not as sensitive.

These results are also illustrated in Table 5.6 and Table 5.7. These tables showcase the overall impact of surface NO number density for each reaction at the experimental measurement locations based on the additional simulations in which individual rates are increased and decreased by two orders of magnitude. Tables 5.6 and 5.7 show that not only are the first and second Zeldovich reactions the most dominant, as they produce an overall percent difference between approximately 120-190%, the O_2-O reaction for Table 5.7 is less dominant when compared to Table 5.6, also shown in Fig. 5.13. These large percent differences indicate that NO surface number density is highly influenced by the rate input.

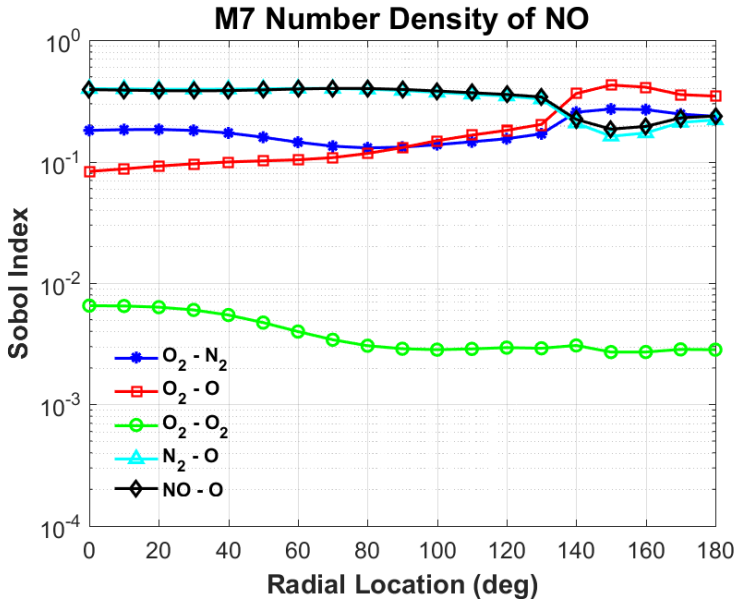

(a) M7-H8-A surface number density of NO Sobol indices

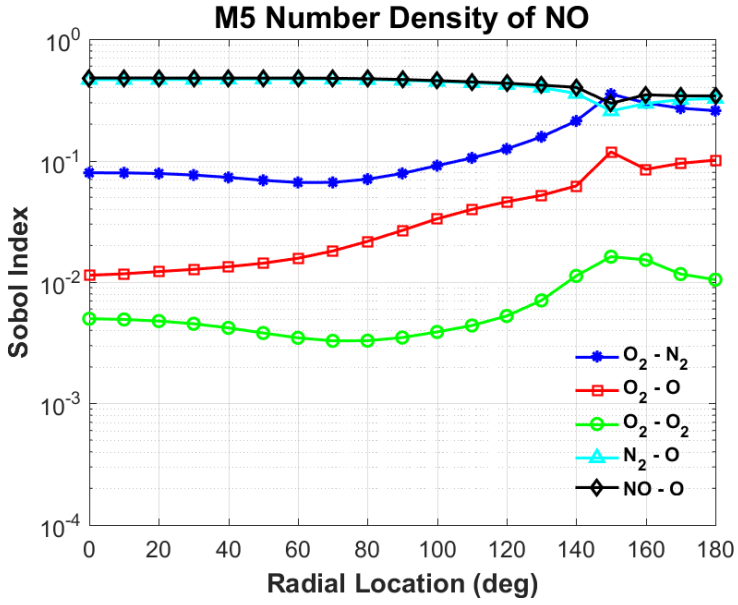

(b) M5-H6-A surface number density of NO Sobol indices

Figure 5.13: Hypersonic cylinder surface number density of NO Sobol indices.

The remaining QoIs for the M7-H8-A cylinder are shown in Fig. 5.14 and involve total drag, total heating rate, and rotational temperature at locations of 2.3 mm (T1), 2.8 mm (T2), and 3.3 mm (T3) upstream of the stagnation point. For this case, both drag and heating rate are dominated by the O_2-N_2 and O_2-O reactions. This

Table 5.6: M7-H8-A percent difference in surface number density of NO

Angle deg	O_2-N_2	O_2-O	N_2-O	NO-O
0	29.2	42.0	171	150
30	33.5	46.2	172	152
60	40.3	51.5	174	154
90	45.7	54.4	175	155

Table 5.7: M5-H6-A percent difference in surface number density of NO

Angle deg	O_2-N_2	O_2-O	N_2-O	NO-O
0	22.8	26.9	182	117
30	24.1	28.2	183	118
60	25.7	30.5	184	119
90	26.2	32.4	184	119

result coincides with the dominant reactions in Figs. 5.7, 5.11(a), and 5.12(a). It is likely that if a particular reaction dominates surface pressure or surface heat transfer, it will also dominate total drag or total heating rate, respectively. The O_2-N_2 and O_2-O reactions also dominate the determination of rotational temperature. This can be explained by considering Fig. 5.7. The O_2-N_2 and O_2-O reactions are likely the fastest chemical reactions behind the shock. These are dissociation reactions that remove a lot of energy from the flow. This energy loss accounts for the decrease in both T_{tr} and T_{vib} behind the shock. The first and second Zeldovich reactions are also active behind the shock, however Fig. 5.7 shows that the two reactions are likely canceling each other out. Therefore, the value of T_{r} is most influenced by the rates of the O_2-N_2 and O_2-O reactions.

Similarly, the remaining QoIs for the M5-H6-A cylinder are shown in Fig. 5.15. For this case the O_2-N_2 and O_2-O reactions reactions dominate total drag and coincide with Fig. 5.12(b). Unlike the M7-H8-A cylinder case, however, the heating rate is

dominated by the O_2-N_2 and O_2-O reactions and the two Zeldovich reactions. This coincides with Fig. 5.7 and illustrates how sensitive the amount of chemical activity is to the freestream condition. The rotational temperature is again dominated by the O_2-N_2 and O_2-O reactions, for similar reasons as the M7-H8-A case.

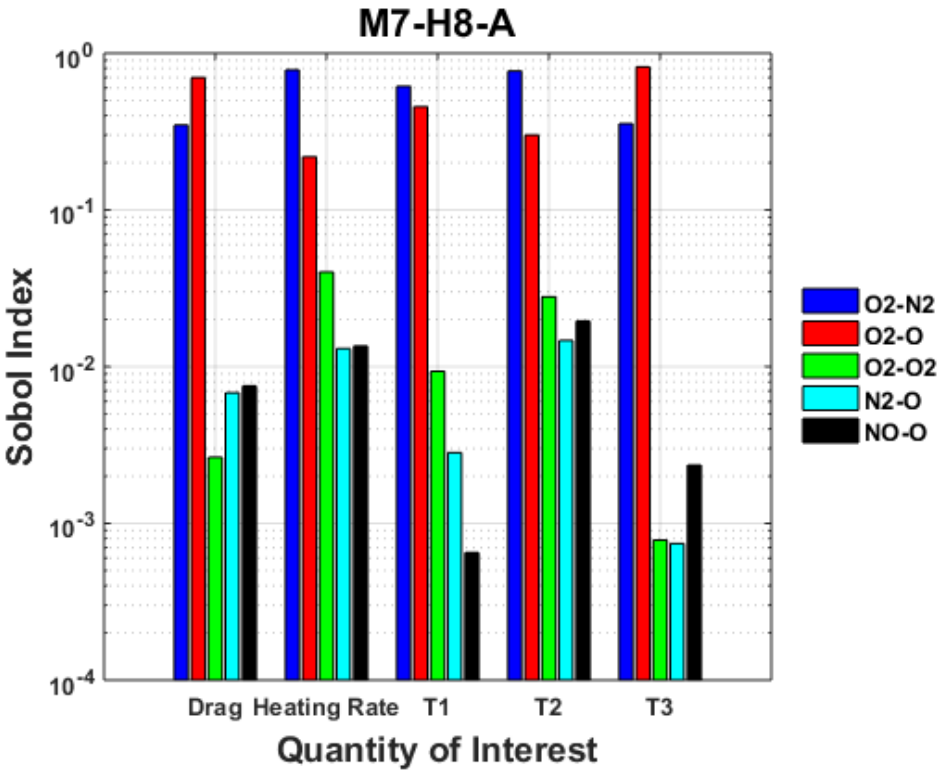

Figure 5.14: M7-H8-A Sobol indices.

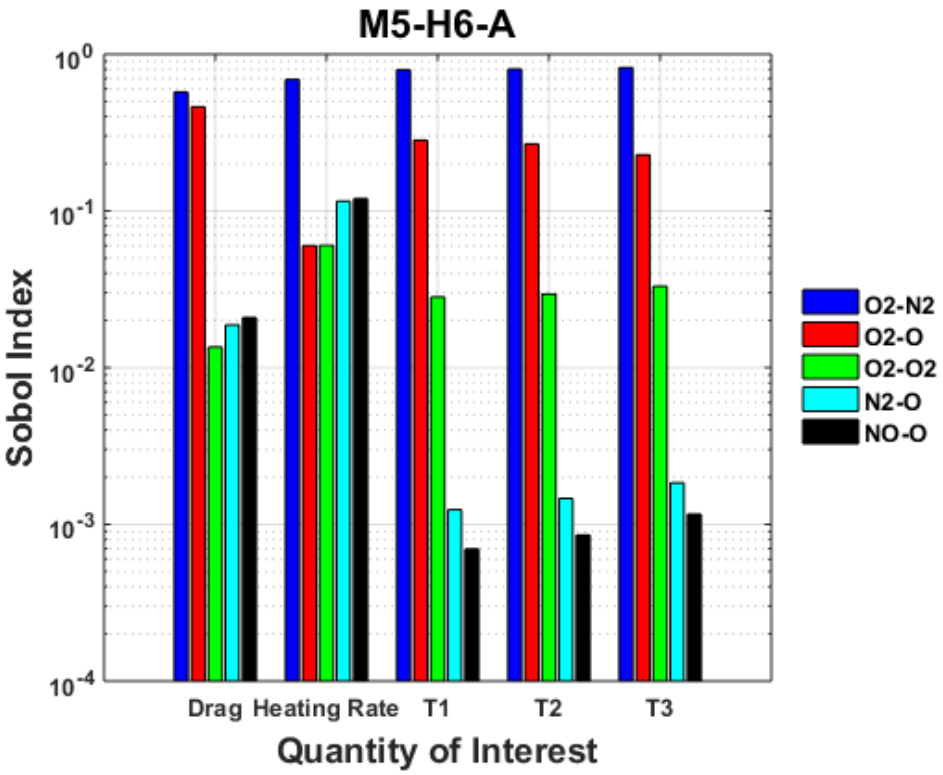

Figure 5.15: M5-H6-A Sobol indices.

Additionally, the overall impact of the remaining QoIs for each cylinder based on the additional simulations in which individual rates are increased and decreased by two orders of magnitude are shown in Tables 5.8 and 5.9 at the experimental measurement locations for rotational temperature. Tables 5.8 and 5.9 again show that drag is relatively uninfluenced when compared to heating rate, as expected considering the overall impact of surface pressure in Tables 5.4 and 5.5 and the extreme impact of surface heat transfer in Table 5.2 and 5.3. Tables 5.8 and 5.9 also show that rotational temperature is strongly impacted overall, with percent differences up to 27%.

Table 5.8: M7-H8-A percent difference in QoIs

QoI	O_2-N_2	O_2-O	N_2-O	NO-O
Drag	0.113	0.502	0.178	0.154
Heating Rate	31.3	30.5	0.529	0.991
T1	20.8	22.2	1.00	0.891
T2	25.0	26.5	0.455	0.877
T3	17.9	9.53	1.78	0.192

Table 5.9: M5-H6-A percent difference in QoIs

QoI	O_2-N_2	O_2-O	N_2-O	NO-O
Drag	0.956	0.41	0.07	0.04
Heating Rate	23.4	11.4	2.33	1.87
T1	20.0	17.4	0.68	0.64
T2	23.6	16.6	0.19	0.25
T3	26.4	11.4	0.30	0.40

5.6 Chapter Summary

A sensitivity analysis of thermochemical kinetics models for hypersonic flow over a cylinder was investigated. LeMANS was used to model the M7-H8-A and M5-H6-A cylinder flows, with freestream properties that can be generated in the HET facility at the California Institute of Technology. The CFD analysis utilized Park's 2T model to model thermal nonequilibrium. The sensitivity analysis was performed using Sandia National Laboratory's sensitivity code Dakota by means of a PCE algorithm. The PCE study altered the reaction rates by adjusting the rates for five of the most common chemical reactions in air, O_2 dissociation with partner N_2, O_2 dissociation with partner O, O_2 dissociation with partner O_2, and the two Zeldovich reactions, N_2 exchange with partner O and NO exchange with partner O, to help identify rate inputs that most influence QoIs. The quantities of interest were surface pressure, surface heat transfer, surface number density of NO, total drag, total heating rate, and rota-

tional temperature. The rotational temperature was represented by the translational temperature consistent with the use of Park's 2T model. The sensitivity each input had on a QoI was quantified via Sobol indices, which were also calculated by Dakota.

The relatively simple cylinder configuration allowed for the flow field to be easily evaluated at low cost. The temperature contours consisted of a bow shock in front of the cylinder that increases pressure and temperature and gradually decreased as the shock weakened. The flow field also captured the trailing edge of the cylinder where flow separation begins to occur. The surface pressure investigation showed a peak at the stagnation point and a gradual decline downstream. The surface heat transfer also showed a peak at the leading edge and a gradual decline downstream. Each surface property also showed a slight increase near the trailing edge, further suggesting flow recompression and recirculation and making the location of interest.

The sensitivity results illustrate how complicated understanding hypersonic flows can be and indicate that different freestream conditions will influence which chemical reactions dominate QoIs. For the M7-H8-A case, surface pressure and surface heat transfer were dominated by the O_2-N_2 and O_2-O reactions, and, therefore, so were total drag and total heating rate. The surface number density of NO was dominated by the two Zeldovich reactions, which was expected. The rotational temperature was also dominated by the O_2-N_2 and O_2-O reactions because they were proceed most rapidly behind the shock while the first and second Zeldovich reactions canceled each other out. The M5-H6-A case also had surface pressure, surface heat transfer, total drag, and total heating rate dominated by the O_2-N_2 and O_2-O reactions. However, unlike the M7-H8-A case, the two Zeldovich reactions were also dominant in surface

heat transfer and total heating rate, illustrating the influence freestream properties have on chemical reactions. It was also noted that while a particular reaction might dominate surface pressure and drag, these quantities are not very influential overall, also shown in Chapters 3 and 4. The results also suggested flow separation and recirculation around 140 deg. Lastly, the Sobol indices showed that the O_2-O_2 reaction was not dominant in any of the QoIs considered in this study.

Given the results of this Chapter, the CalTech HET experiments should be useful for evaluation of thermochemistry modeling. Though surface pressure and total drag were insensitive to the alteration of the thermochemical kinetics model, each other QoI was sensitive. The overall effect on rotational temperature at the HET measurement locations were almost 30%, indicating that the relatively large Sobol indices for the O_2-N_2 and O_2-O reactions are associated with large variations in rotational temperature. Likewise, the overall impact on surface heat transfer and surface NO number density are large at the experimental measurement locations with percent differences up to 35% for surface heat transfer and up to 185% for surface NO number density, again indicating that the large Sobol indices for particular reactions are associated with significant changes in these QoIs. Additionally, each cylinder case showed different reactions dominating QoIs. Each of these takeaways indicate that the accuracy of freestream measurements and the thermochemical kinetics model are important.

Furthermore, results from the sensitivity analysis can help inform diagnostics development. Specific property measurements of interest include the concentration of atomic oxygen. Each QoI is heavily influenced by the concentration of atomic oxygen

on the surface and in the flowfield, shown throughout the Chapter, indicating that low uncertainty measurements of atomic oxygen that can be reproduced by numerical simulations is important. The large percent differences in Tables 5.6 - 5.9 indicate sensitivity to the thermochemistry model, suggesting that low uncertainty measurements of T_{tr} and the concentration of NO are important and should also be considered. Having low uncertainties in these measurements will help computationalists distinguish differences between thermochemistry models.

The difference in sensitive properties for the two cylinder cases suggest that several other factors should be considered to better understand hypersonic flows. First, it would help our understanding of sensitive input reaction rates if the sensitivity investigation was conducted over a wider range of freestream conditions. For this approach a random-sampling method might be more efficient than PCE. Second, other geometries should be considered to determine if the same input reactions dominate slender bodies as they do for the blunt cylinder. Lastly, a larger set of reactions should be considered for the sensitivity study.

CHAPTER 6

Conclusion and Future Directions

"Go then, there are other worlds than these."

Stephen King, *The Gunslinger*

This chapter serves to summarize this dissertation and specific results from Chapters 3 - 5. Next, the major research contributions from this dissertation are discussed. Lastly, recommendations for future work are provided along with a list of published journal and conference papers by the author.

6.1 Dissertation Summary and Conclusions

Chapter 1 provided an introduction for the presented work. It included a brief history of hypersonics that laid a foundation for the motivation of the presented work. Past and current hypersonic research topics were discussed. Additionally, this chapter discussed the unique challenges of studying computational hypersonics and the overall scope of the dissertation.

Chapter 2 gave a description of the numerical modeling of hypersonic gas dynamics. Specifically, the Chapter began by providing a discussion on thermodynamic

equilibrium and the underlying physics associated with nonequilibrium flow phenomena typically found in hypersonic flow environments. Next, a description of the CFD code LeMANS was provided with specifics such as the Navier-Stokes equations, thermodynamic and transport properties, and Park's 2T and MMT thermochemistry models. Lastly, a discussion on the numerical toolkit Dakota and how it can be used to conduct a sensitivity analysis was provided.

Chapter 3 investigated the effects of thermochemistry modeling for hypersonic flow over a double-cone. Park's 2T model was utilized and the chemistry rates were altered. Freestream properties were measured at CUBRC's LENS-I facility and were in a state of thermochemical nonequilibrium. Surface properties, such as pressure, heat transfer, drag, and heating rate, were then compared and it was determined that thermochemistry modeling plays an important role, especially at high freestream enthalpies. Contours of thermal and chemical nonequilibrium were also provided to better illustrate that any general evaluation of the role of the importance of thermochemistry modeling must account for the specific thermochemical properties of the gas involved. Computational results also consistently over predicted or under predicted pressure drag and heating rate in comparison to the experimental data. Due to these inconsistencies, it was concluded that the LENS-I double-cone cases examined are limited in their usefulness for validation of thermochemistry models.

Chapter 4 further investigated the effects of thermochemistry modeling for hypersonic flow over a double-cone. However, the freestream conditions considered in this Chapter were generated in CUBRC's LENS-XX facility, where properties are in a state of thermochemical equilibrium. Park's 2T model was utilized and the

chemistry rates were altered to induce equilibrium, nonequilibrium, and frozen flows. Surface properties were compared and again it was determined that thermochemistry models play an important role. Computational results also failed to reproduce the experiments, despite thermochemical equilibrium in the freestream. Additionally, this chapter utilized the newly implemented MMT model in LeMANS to investigate the difference between it and Park's 2T model. The difference between the two models were minimal, a result of the freestream density. This indicated that the MMT model also failed to reproduce experimental results, further indicating that the double-cone is limited in its usefulness in validating thermochemistry models.

To reduce the inconsistencies between CFD and experiments, like those observed in Chapters 3 - 4, Chapter 5 reported on a sensitivity analysis on the thermochemical kinetics for hypersonic flow over a cylinder. The sensitivity analysis was conducted via PCE and quantified by Sobol indices. The freestream properties were representative of experiments to be conducted in the HET facility at CalTech. The results showed that, generally, the O_2-N_2 and O_2-O reactions dominated surface pressure, surface heat transfer, drag, heating rate, and rotational temperature, while the two Zeldovich reactions dominated the surface number density of NO. The O_2-O_2 reaction was found to be less important than the other four reactions. Surface pressure and drag were also found to be insensitive overall. The results also suggested flow separation and recirculation near the trailing edge of the cylinder. Given these findings, the CalTech HET experiments should be useful for the evaluation of thermochemistry modeling.

6.2 Research Contributions

The previous Section provided a summary of each chapter of this dissertation. The following Section discusses the major contributions of the research, which can be characterized as follows:

- **Investigation into the effects of thermochemistry modeling for hypersonic double-cone flows:** The CUBRC LENS-I and LENS-XX double-cone cases were investigated and determined that thermochemistry models play a significant role in determining surface properties, especially at high free stream enthalpies.

- **Comparison of CUBRC's LENS-I and LENS-XX double-cone experiments:** The LENS-XX double-cone simulations were investigated and compared to the LENS-I simulations to determined if the thermochemical equilibrium condition of the freestream in the LENS-XX facility could help CFD reproduce experimental measurements. Each CFD simulation consistently over predicted or under predicted experimental results, suggesting that the double-cone experiments considered in this dissertation are limited in their usefulness for validating thermochemistry models.

- **Comparison of Park's 2T and MMT thermochemistry models:** CUBRC's LENS-XX double-cone experiments were utilized to compare the Park 2T and MMT thermochemistry models. Each model produced similar surface profiles due to the freestream density. The freestream density correlates to a regime

where recombination and dissociation differences are not important. These results again indicated that the double-cone is limited in its usefulness for the validation of thermochemistry models.

- **Development of coupled numerical tools:** A coupled CFD-numerical toolkit framework was developed, allowing Dakota to interact with LeMANS to conduct a sensitivity analysis.

- **Sensitivity analysis on thermochemical kinetics:** The rates of the O_2-N_2, O_2-O_2, O_2-O, and the first two Zeldovich reactions were altered individually by the PCE method to determine their effects on QoIs. The sensitivities were quantified via Sobol indices to determine which reactions dominate particular QoIs.

- **Usefulness of the CalTech HET experiments:** The sensitivity analysis results informs researchers which reactions dominate QoIs. The information can help guide the CalTech HET experiments. For example, the uncertainty in surface pressure measurements can be much higher than the uncertainty in surface number density of NO because surface pressure is not very sensitive to the change in reaction rates when compared to the surface number density of NO. The takeaways in this section also indicate that the accuracy of freestream measurements and the thermochemical kinetics model are important. Given these results, the CalTech HET experiments should be useful for evaluation of thermochemistry models.

6.3 Recommendations for Future Work

The modeling approach for each CFD simulation presented in this dissertation have been thoroughly discussed to evaluate assumptions. These assumptions include laminar flow models, 5-species air models, 2D and axisymmetric grids, and others. However, these assumptions open the door for future work in the area of thermochemistry modeling for hypersonic air flows and is discussed below.

One major recommendation is investigating the effects of plasma and the 11-species air model. As discussed in Section 1.1, vehicles approaching velocities in excess of Mach 10 produce a layer of plasma around the flight vehicle that hinders communications. The plasma can interact with the wall, initializing catalytic reactions between the gas-phase molecules and atomic species bound to the surface. These chemical reactions release atoms of the surface material into the gas-phase, which can alter the chemical pathways associated with plasma formation. Therefore, the study of plasma would ideally coincide with a study of surface-fluid interactions. This study can be accomplished by utilizing a material response code such as MOPAR-MD, mentioned briefly in Section 3.4, by fully coupling the flow and material simulations.

There are also discrepancies when dealing with the thermochemistry model of a partially ionized hypersonic flow field that should be examined. One major discrepancy are the rates at which chemical reactions take place. Historically, the rates published by Park in Ref. [8] have been the most popular. However, these rates were determined empirically from experiments ranging in temperature from 300 K to 7000 K, presenting uncertainties when extrapolating to higher temperatures. Park himself

mentions that his 2T approach may be inadequate for the analysis of an ionized flowfield [88]. This suggests that there is still a great deal of uncertainty regarding the range of applicability of the underlying thermochemical models governing the physics of these ionized flows. Therefore, quantifying the uncertainties of the various thermochemical model parameters on the observed plasma density for hypersonic flows is suggested. This can be accomplished by utilizing the uncertainty quantification tools in Dakota.

Additional work on the sensitivity study in Chapter 5 is also suggested. First, a wider range of freestream conditions would allow researchers to have a better understanding of the correlation between freestream properties and dominant reactions. Ideally, each simulation could be compared to experimental measurements. Second, all 17 reactions in 5-species air should be examined to understand dominant reactions in their entirety. This can be accomplished by looking at the chemical production rates from a single simulation and relaying relevant reactions as inputs to Dakota. If the number of relevant reactions exceeds five, a random-sampling method, such as Latin Hypercube Sampling, is suggested over PCE to lower computational cost. A study of computational time between PCE and Latin Hypercube Sampling could also prove useful for future sensitivity studies. Third, different geometries should be considered to determine how dominant reactions change. CalTech should also consider measuring cylinder properties at additional locations, specifically around the 140 degree mark given the sensitivity of flow separation to the reaction rate. Lastly, the effects of turbulence should eventually be considered for the hypersonic cylinder given that these experiments are new when compared to the double-cone where the

laminar model is understood to be sufficient.

APPENDIX

APPENDIX A

Hypersonic Cylinder

The surface plots of the HET M7-H8-A and M5-H6-A cylinder experiments produced similar results. Section 5.4 only addressed the M7-H8-A cylinder. Additionally, only the net reaction rates for a single streamline was shown in Section 5.4 for both cylinders. The following Appendix serves as a reference for the M5-H6-A cylinder surface properties and the contours for the net reaction rates for both hypersonic cylinders.

A.1 Additional Properties

The M5-H6-A cylinder is a mid enthalpy air case. The surface properties are shown in Figs. A.1 and A.2. The surface properties calculated by LeMANS are similar to the M7-H8-A case and shows a peak at the stagnation point and a gradual decline downstream. The surface heat transfer also peaks at the stagnation point and gradually declines downstream. Figures A.1 and A.2 also show a slight increase at the trailing edge, similar to the M7-H8-A case, again indicating that this region is experiencing flow recirculation. Additionally, The contours of the net reaction rates

for each chemistry input is also shown in Figs. A.3-A.7 to give the reader an additional illustration of the chemistry taking place in the flow field of each hypersonic cylinder case.

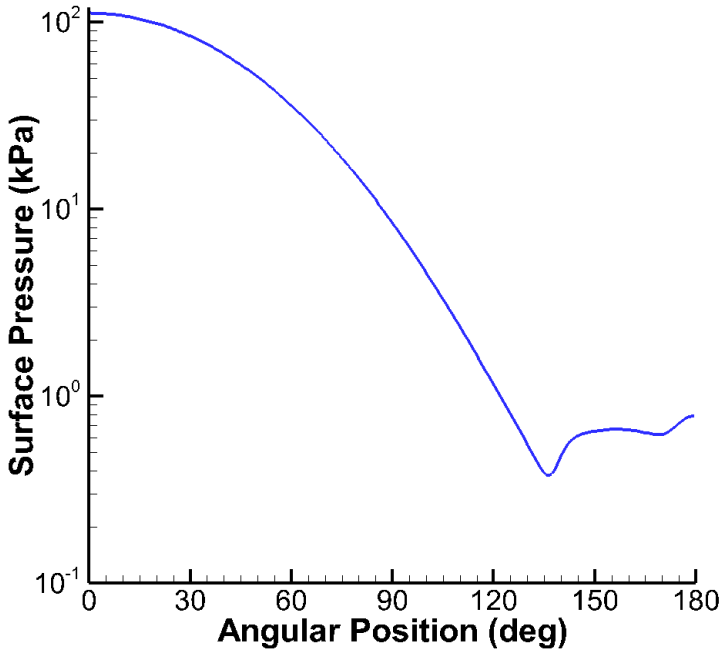

Figure A.1: M5-H6-A surface pressure.

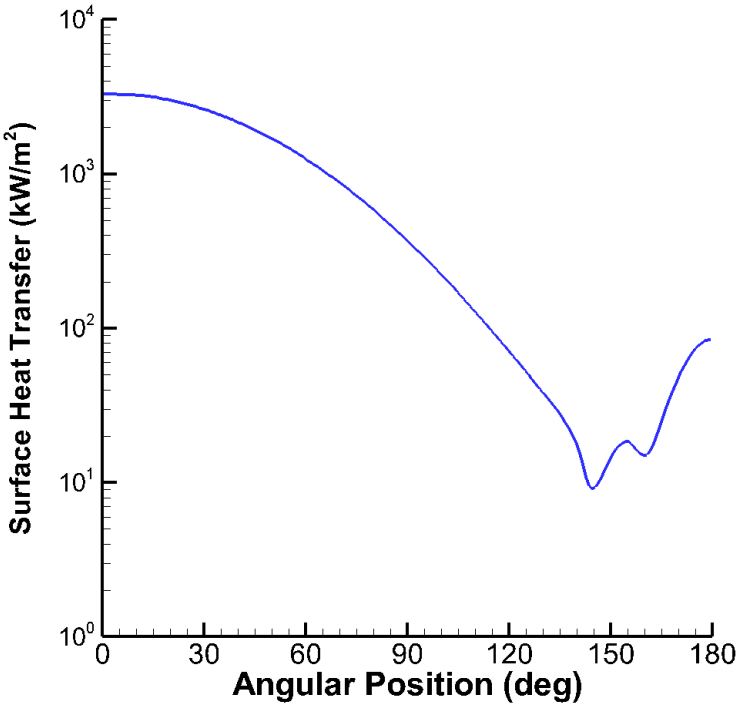

Figure A.2: M5-H6-A surface heat transfer.

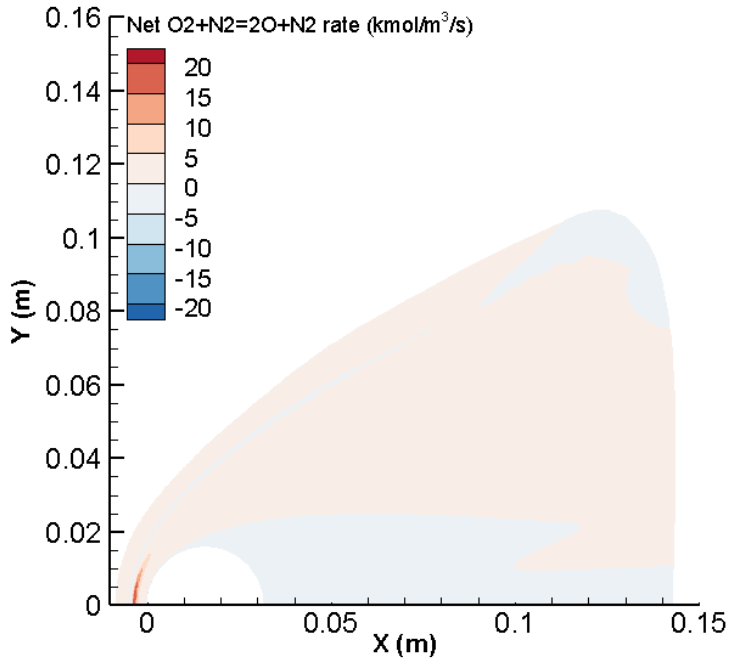

(a) M7-H8-A cylinder

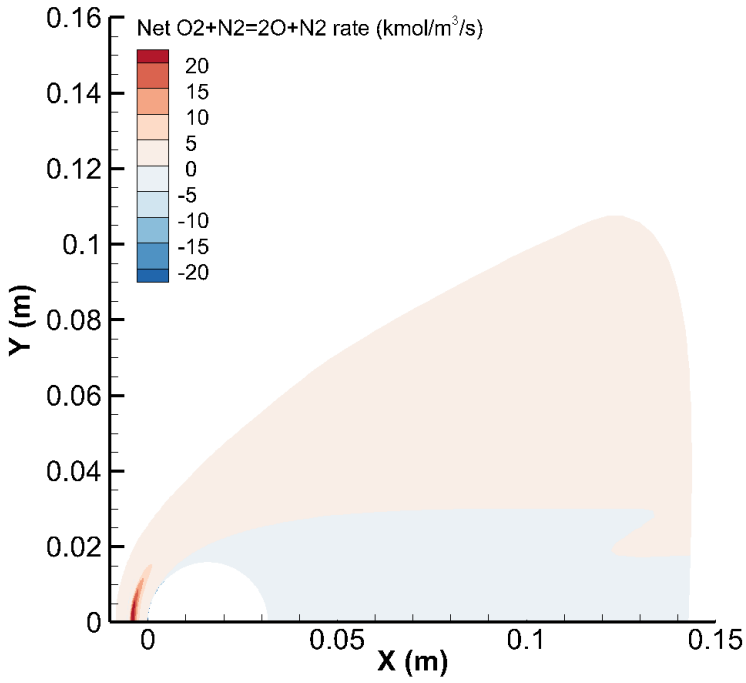

(b) M5-H6-A cylinder

Figure A.3: Net reaction rate of O_2 dissociation with partner N_2.

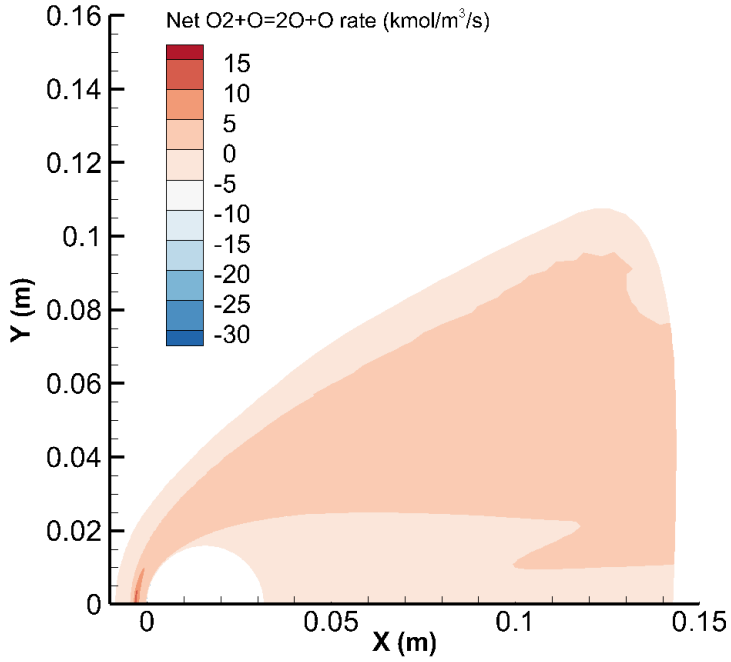

(a) M7-H8-A cylinder

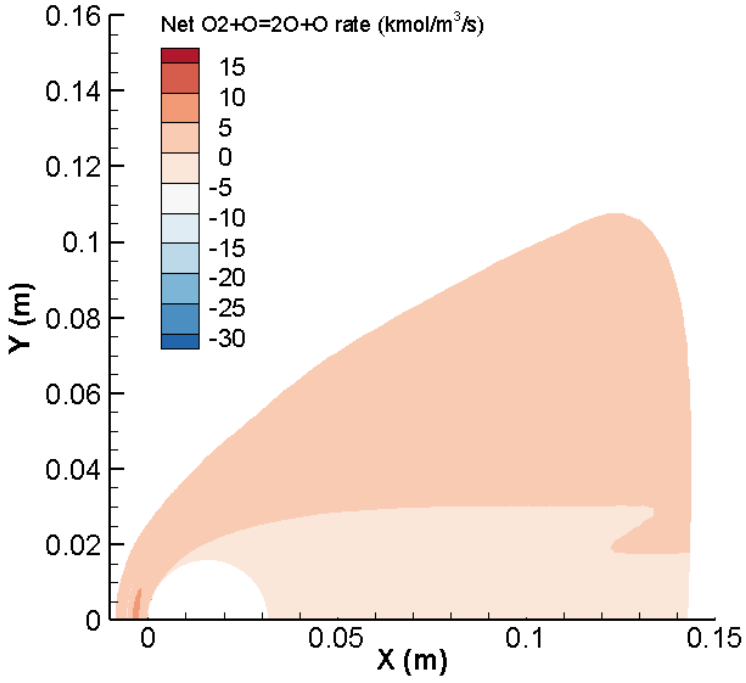

(b) M5-H6-A cylinder

Figure A.4: Net reaction rate of O_2 dissociation with partner O.

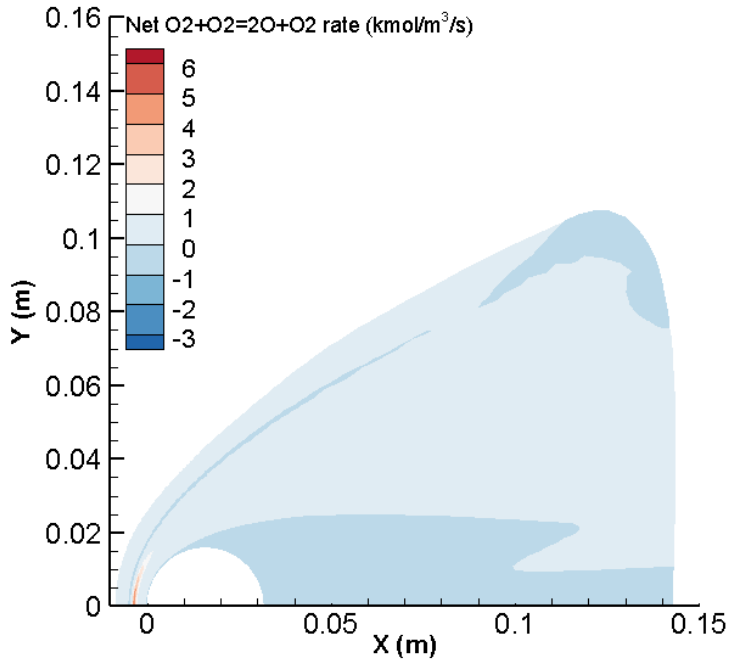

(a) M7-H8-A cylinder

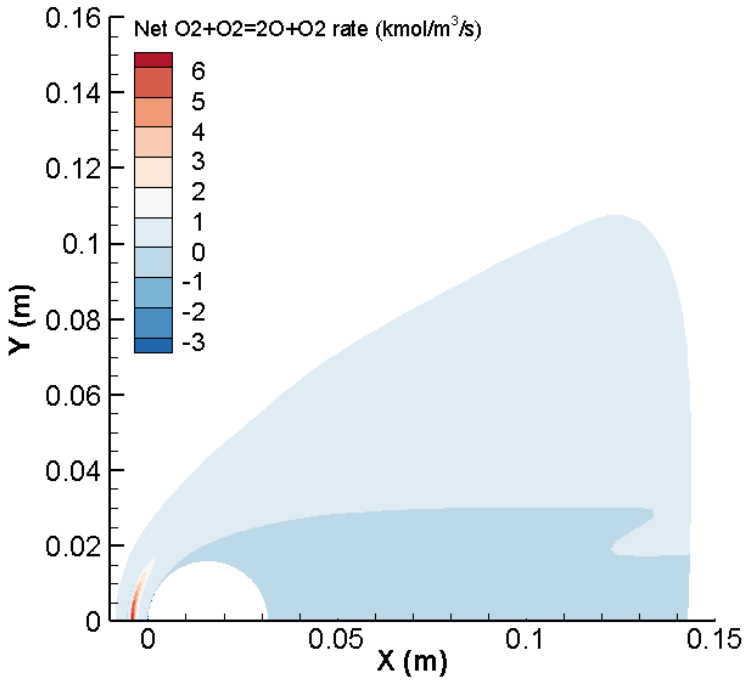

(b) M5-H6-A cylinder

Figure A.5: Net reaction rate of O_2 dissociation with partner O_2.

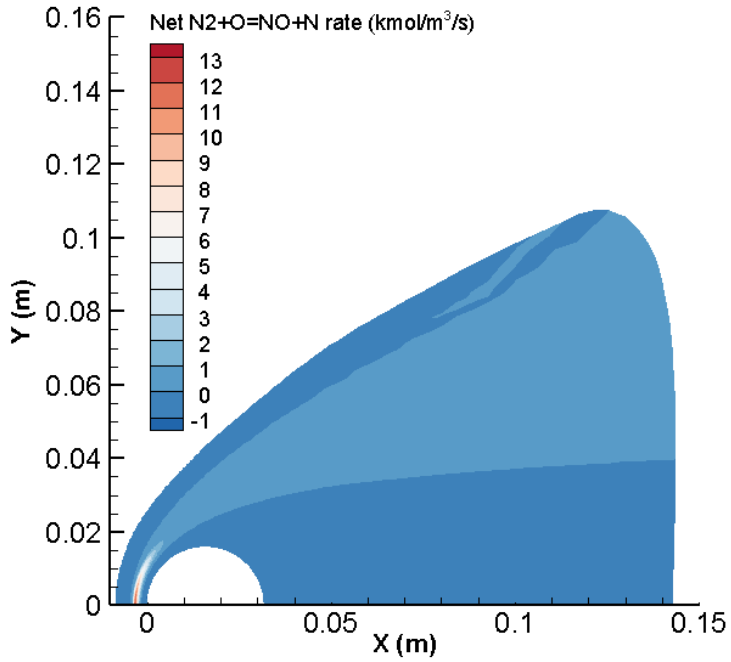

(a) M7-H8-A cylinder

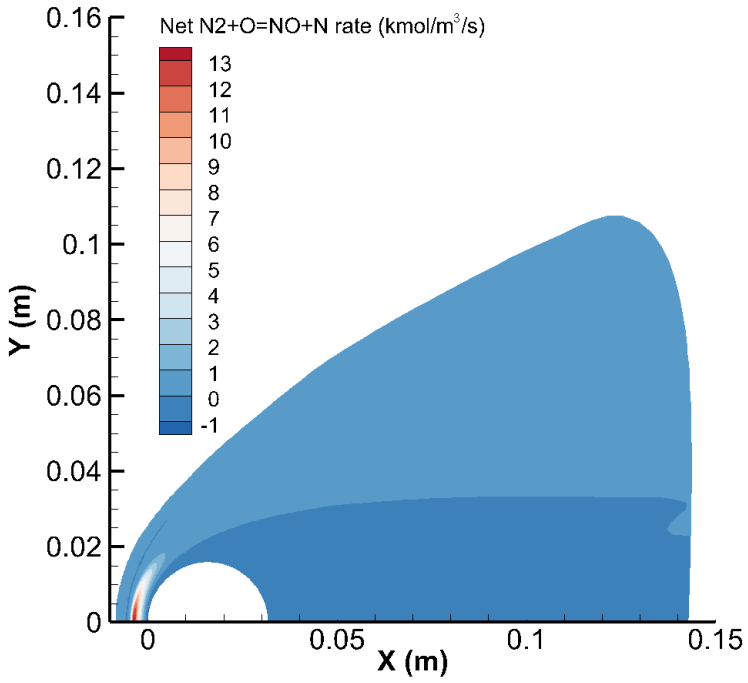

(b) M5-H6-A cylinder

Figure A.6: Net reaction rate of the first Zeldovich reaction.

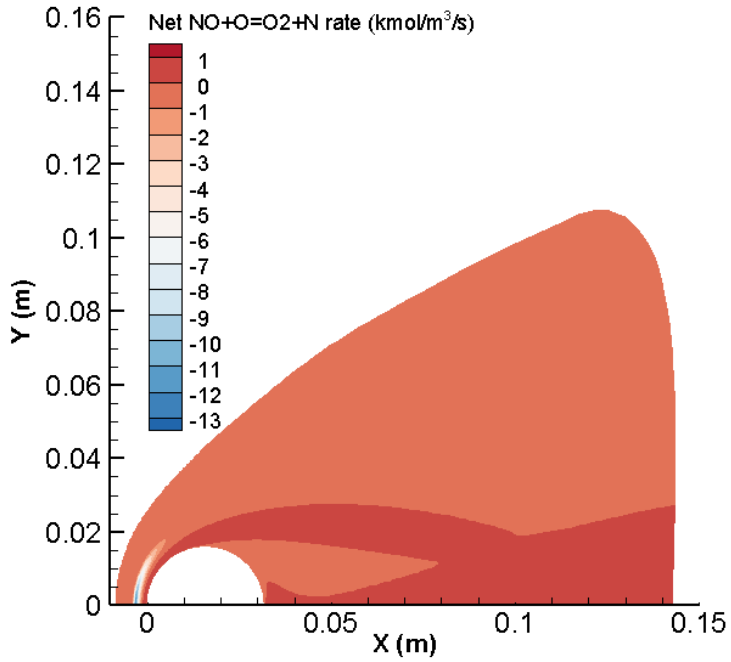

(a) M7-H8-A cylinder

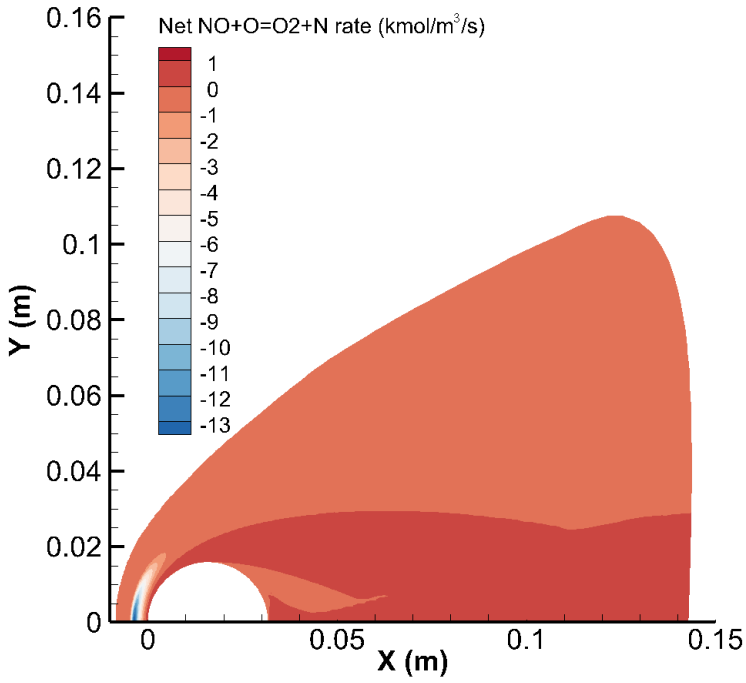

(b) M5-H6-A cylinder

Figure A.7: Net reaction rate of the second Zeldovich reaction.

BIBLIOGRAPHY

[1] Marren, D. and Lu, F., *Advanced Hypersonic Test Facilities*, American Institute of Aeronautics and Astronautics, 2002.

[2] Matthews, D. L., "Interferometric Measurement in the Shock Tube of the Dissociation Rate of Oxygen," *The Physics of Fluids*, Vol. 2, No. 2, 1959, pp. 170–178.

[3] Byron, S. R., "Measurement of the Rate of Dissociation of Oxygen," *The Journal of Chemical Physics*, Vol. 30, No. 6, 1959, pp. 1380–1392.

[4] Rink, J. P., Knight, H. T., and Duff, R. E., "Shock Tube Determination of Dissociation Rates of Oxygen," *The Journal of Chemical Physics*, Vol. 34, No. 6, 1961, pp. 1942–1947.

[5] Park, C., "Assessment of a Two-Temperature Kinetic Model for Dissociating and Weakly Ionizing Nitrogen," *Journal of Thermophysics and Heat Transfer*, Vol. 2, No. 1, 1988, pp. 8–16.

[6] Park, C., "Two-Temperature Interpretation of Dissociation Rate Data for N_2 and O_2," *26th Aerospace Sciences Meeting*, AIAA Paper 1988-458, 1988, p. 458.

[7] Park, C., "Assessment of Two-Temperature Kinetic Model for Ionizing Air," *Journal of Thermophysics and Heat Transfer*, Vol. 3, No. 3, 1989, pp. 233–244.

[8] Park, C., *Nonequilibrium Hypersonic Aerothermodynamics*, John Wiley and Sons, Inc., New York, 1990.

[9] Park, C., "Review of Chemical-Kinetic Problems of Future NASA Missions, I: Earth Entries," *Journal of Thermophysics and Heat Transfer*, Vol. 7, No. 3, 1993, pp. 385–398.

[10] Park, C., Howe, J. T., Jaffe, R. L., and Candler, G. V., "Review of chemical-kinetic problems of future NASA missions. II - Mars entries," *Journal of Thermophysics and Heat Transfer*, Vol. 8, No. 1, 1994, pp. 9–23.

[11] Chaudhry, R. S., Bender, J. D., Valentini, P., Schwartzentruber, T. E., and Candler, G. V., "Analysis of Dissociation and Internal Energy Transfer in High-Energy N_2+O_2 Collisions using the Quasiclassical Trajectory Method," *46th AIAA Thermophysics Conference*, AIAA Paper 2016-4319, 2016.

[12] Chaudhry, R. S., Bender, J. D., Schwartzentruber, T. E., and Candler, G. V., "Quasiclassical Trajectory Analysis of N2+O2 and Implications for Hypersonic CFD," *47th AIAA Thermophysics Conference*, AIAA Paper 2017-3167, 2017.

[13] Chaudhry, R. S., Bender, J. D., Schwartzentruber, T. E., and Candler, G. V., "Quasiclassical Trajectory Analysis of Nitrogen for High-Temperature Chemical Kinetics," *Journal of Thermophysics and Heat Transfer*, Vol. 32, No. 4, 2018, pp. 833–845.

[14] Mehta, A., "Hypersonics 'Highest Technical Priority' for Pentagon RD head," *Defense News*, March 2018.

[15] AP, "Russia reports successful test launch of hypersonic missile," *Defense News*, October 2020.

[16] Mehta, A., "Is the Pentagon moving quickly enough on hypersonic defense?" *Defense News*, March 2019.

[17] Walker, S., Sherk, J., Shell, D., Schena, R., Bergmann, J., and Gladbach, J., "The DARPA/AF Falcon Program: The Hypersonic Technology Vehicle #2 (HTV-2) Flight Demonstration Phase," *15th AIAA International Space Planes and Hypersonic Systems and Technologies Conference*.

[18] Dolvin, D., "Hypersonic International Flight Research and Experimentation (HIFiRE) Fundamental Science and Technology Development Strategy," *15th AIAA International Space Planes and Hypersonic Systems and Technologies Conference*.

[19] Chang, K., "Astronauts Dock With Space Station After Historic SpaceX Launch," *New York Times*, 31 May 2020.

[20] Speier, R. H., Nacouzi, G., Lee, C., and Moore, R. M., *Hypersonic missile nonproliferation: hindering the spread of a new class of weapons*, Rand Corporation, 2017.

[21] Harvey, J., Holden, M., and Wadhams, T., "Code Validation Study of Laminar Shock/Boundary Layer and Shock/Shock Interactions in Hypersonic Flow, Part B: Comparison with Navier–Stokes and DSMC Solutions," *39th Aerospace Sciences Meeting and Exhibit*, AIAA Paper 2001-1031.

[22] Holden, M., Wadhams, T., MacLean, M., and Walker, B., "Experimental Studies in the LENS Supersonic and Hypersonic Tunnels for Hypervelocity Vehicle Performance and Code Validation," *15th AIAA International Space Planes and Hypersonic Systems and Technologies Conference*, AIAA Paper 2008-2505.

[23] Knight, D., Longo, J., Drikakis, D., Gaitonde, D., Lani, A., Nompelis, I., Reimann, B., and Walpot, L., "Assessment of CFD capability for prediction of hypersonic shock interactions," *Progress in Aerospace Sciences*, Vol. 48, 2012, pp. 8–26.

[24] Olejniczak, J., "Computational and Experimental Study of Nonequilibrium Chemistry in Hypersonic Flows," *PhD thesis, University of Minnesota*, 1997.

[25] Druguet, M.-C., Candler, G., and Nompelis, I., "Comparison of Physical Models in Computations of High-Enthalpy Double-Cone Flows," *9th AIAA/ASME Joint Thermophysics and Heat Transfer Conference*, AIAA Paper 2006-3419.

[26] Holden, M. S., *Experimental Research and Analysis in Supersonic and Hypervelocity Flows in the LENS Shock Tunnels and Expansion Tunnel*, AIAA Paper 2015-3660.

[27] Holden, M. S., Wadhams, T. P., MacLean, M. G., and Dufrene, A. T., "Measurements of Real Gas Effects on Regions of Laminar Shock Wave/Boundary Layer Interaction in Hypervelocity Flows for "Blind'Code Validation Studies," *21st AIAA Computational Fluid Dynamics Conference*, AIAA Paper 2013-2837, 2013.

[28] Satchell, M. J., Layng, J. M., and Greendyke, R. B., "Numerical Simulation of Heat Transfer and Chemistry in the Wake behind a Hypersonic Slender Body at Angle of Attack," *Aerospace*, Vol. 5, No. 1, 2018.

[29] Gillman, E. D., Foster, J. E., and Blankson, I. M., "Review of leading approaches for mitigating hypersonic vehicle communications blackout and a method of ceramic particulate injection via cathode spot arcs for blackout mitigation," NASA TM-2010-216220, February 2010.

[30] Starkey, R. P., "Hypersonic Vehicle Telemetry Blackout Analysis," *Journal of Spacecraft and Rockets*, Vol. 52, No. 2, 2015, pp. 426–438.

[31] Sawicki, P., Chaudhry, R. S., and Boyd, I. D., "Influence of Chemical Kinetics Models on Plasma Generation in Hypersonic Flight," *AIAA Scitech 2021 Forum*, AIAA Paper 2021-0057, 2021.

[32] Andrienko, D. A. and Boyd, I. D., "High fidelity modeling of thermal relaxation and dissociation of oxygen," *Physics of Fluids*, Vol. 27, No. 11, 2015, pp. 116101.

[33] Chaudhry, R. S., Grover, M. S., Bender, J. D., Schwartzentruber, T. E., and Candler, G. V., "Quasiclassical Trajectory Analysis of Oxygen Dissociation via O2, O, and N2," *2018 AIAA Aerospace Sciences Meeting*, AIAA Paper 2018-0237, 2018.

[34] Hanquist, K. M. and Boyd, I. D., "Modeling of Excited Oxygen in Post Normal Shock Waves," *2018 Joint Thermophysics and Heat Transfer Conference*, AIAA Paper 2018-3796, 2018.

[35] Stern, E. C., Poovathingal, S., Nompelis, I., Schwartzentruber, T. E., and Candler, G. V., "Nonequilibrium flow through porous thermal protection materials, Part I: Numerical methods," *Journal of Computational Physics*, Vol. 380, 2019.

[36] Holloway, M. E., Hanquist, K. M., and Boyd, I. D., "Assessment of Thermochemistry Modeling for Hypersonic Flow Over a Double Cone," *Journal of Thermophysics and Heat Transfer*, Vol. 34, No. 3, 2020, pp. 538–547.

[37] Kieweg, S. L., Ray, J., Weirs, V. G., Carnes, B., Dinzl, D., Freno, B., Howard, M., Phipps, E., Rider, W., and Smith, T., "Validation Assessment of Hypersonic Double-Cone Flow Simulations using Uncertainty Quantification, Sensitivity Analysis, and Validation Metrics," *AIAA SciTech 2019 Forum*, AIAA Paper 2019-2278, 2019.

[38] Ray, J., Kieweg, S. L., Dinzl, D., Carnes, B., Weirs, V., Freno, B., Howard, M., Smith, T., Nompelis, I., and Candler, G. V., "Estimation of inflow uncertainties in laminar hypersonic double-cone experiments," *AIAA SciTech 2019 Forum*, AIAA Paper 2019-2279, 2019.

[39] Boyd, I. D. and Schwartzentruber, T. E., *Nonequilibrium Gas Dynamics and Molecular Simulation*, Cambridge Aerospace Series, Cambridge University Press, 2017, p. 54–146.

[40] Martin, A., Scalabrin, L. C., and Boyd, I. D., "High performance modeling of atmospheric re-entry vehicles," *Journal of Physics: Conference Series*, Vol. 341, No. 1, 2012, pp. 012002.

[41] Farbar, E., Boyd, I. D., and Martin, A., "Numerical Prediction of Hypersonic Flowfields Including Effects of Electron Translational Nonequilibrium," *Journal of Thermophysics and Heat Transfer*, Vol. 27, No. 4, 2013, pp. 593–606.

[42] Scalabrin, L. C., "Numerical simulation of weakly ionized hypersonic flow over reentry capsules," *PhD thesis, University of Michigan*, 2007.

[43] Chaudhry, R. S., Boyd, I. D., Torres, E., Schwartzentruber, T. E., and Candler, G. V., "Implementation of a Chemical Kinetics Model for Hypersonic Flows in Air for High-Performance CFD," *AIAA Scitech 2020 Forum*, AIAA Paper 2020-2191, 2020.

[44] Steger, J. L. and Warming, R., "Flux vector splitting of the inviscid gasdynamic equations with application to finite-difference methods," *Journal of Computational Physics*, Vol. 40, No. 2, 1981, pp. 263–293.

[45] Karypis, G. and Kumar, V., "METIS: A Software Package for Partitioning Unstructured Graphs, Partitioning Meshes, and Computing Fill-Reducing Orderings of Sparse Matrices," University of Minnesota, MN, 1997.

[46] McBride, B. J., Zehe, M., and Gordon, S., *NASA Glenn Coefficients for Calculating Thermodynamic Properties of Individual Species*, NASA TP-2002-211556, NASA, John H. Glenn Research Center, Cleveland, Ohio, 2002.

[47] Wilke, C., "A viscosity equation for gas mixtures," *The Journal of Chemical Physics*, Vol. 18, No. 4, 1950, pp. 517–519.

[48] Blottner, F. G., Johnson, M., and Ellis, M., "Chemically Reacting Viscous Flow Program for Multi Component Gas Mixtures," SC-RR-70-754, Sandia Labs., Albuquerque, NM, 1971.

[49] Vincenti, W. and Kruger, C., *Introduction to Physical Gas Dynamics*, Krieger Publishing Company, 1982, pp. 21–22.

[50] Candler, G. V., Johnson, H. B., Nompelis, I., Gidzak, V. M., Subbareddy, P. K., and Barnhardt, M., "Development of the US3D Code for Advanced Compressible and Reacting Flow Simulations," *53rd AIAA Aerospace Sciences Meeting*, AIAA Paper 2015-1893, 2015.

[51] Wright, M. J., White, T., and Mangini, N., "Data Parallel Line Relaxation (DPLR) Code User Manual: Acadia-Version 4.01. 1," 2009.

[52] Mazaheri, A., Gnoffo, P. A., Johnston, C. O., and Kleb, W. L., "LAURA Users Manual: 5.5-64987," 2013.

[53] Millikan, R. C. and White, D. R., "Systematics of vibrational relaxation," *The Journal of Chemical Physics*, Vol. 39, No. 12, 1963, pp. 3209–3213.

[54] Chaudhry, R. S., Bender, J. D., Schwartzentruber, T. E., and Candler, G. V., "Quasiclassical Trajectory Analysis of Nitrogen for High-Temperature Chemical Kinetics," *Journal of Thermophysics and Heat Transfer*, Vol. 32, No. 4, 2018, pp. 833–845.

[55] Chaudhry, R. S. and Candler, G. V., "Statistical Analyses of Quasiclassical Trajectory Data for Air Dissociation," *AIAA Scitech 2019 Forum*, AIAA Paper 2019-0789, 2019.

[56] Chaudhry, R. S., Boyd, I. D., and Candler, G. V., "Vehicle-Scale Simulations of Hypersonic Flows using the MMT Chemical Kinetics Model," *AIAA Aviation 2020 Forum*, AIAA Paper 2020-3272, 2020.

[57] Marrone, P. V. and Treanor, C. E., "Chemical Relaxation with Preferential Dissociation from Excited Vibrational Levels," *The Physics of Fluids*, Vol. 6, No. 9, 1963, pp. 1215–1221.

[58] Kim, J. G. and Boyd, I. D., "State-Resolved Master Equation Analysis of Thermochemical Nonequilibrium of Nitrogen," *Chemical Physics*, Vol. 415, 2013, pp. 237–246.

[59] Panesi, M., Jaffe, R. L., Schwenke, D. W., and Magin, T. E., "Rovibrational Internal Energy Transfer and Dissociation of $N_2(^1\Sigma_g^+) - N(^4S_u)$ System in Hypersonic Flows," *The Journal of Chemical Physics*, Vol. 138, No. 4, 2013, pp. 044312.

[60] Schwartzentruber, T. E., Grover, M. S., and Valentini, P., "Direct Molecular Simulation of Nonequilibrium Dilute Gases," *Journal of Thermophysics and Heat Transfer*, Vol. 32, No. 4, 2017, pp. 892–903.

[61] Singh, N. and Schwartzentruber, T., "Non-Boltzmann vibrational energy distributions and coupling to dissociation rate," *Journal of Chemical Physics*, Vol. 152, No. 22, 2020.

[62] Singh, N. and Schwartzentruber, T., "Consistent kinetic–continuum dissociation model I: Kinetic formulation," *Journal of Chemical Physics*, Vol. 152, No. 22, 2020.

[63] Singh, N. and Schwartzentruber, T., "Consistent kinetic-continuum dissociation model II: Continuum formulation and verification," *Journal of Chemical Physics*, Vol. 152, No. 22, 2020.

[64] Adams, B. M., Bohnhoff, W. J., Dalbey, K. R., Ebeida, M. S., Eddy, J. P., Eldred, M. S., Hooper, R. W., Hough, P. D., Hu, K. T., Jakeman, J. D., Khalil, M., Maupin, K. A., Monschke, J. A., Ridgway, E. M., Rushdi, A. A., Seidl, D. T., Stephens, J. A., Swiler, L. P., and Winokur, J. G., "Dakota, A Multilevel Parallel Object-Oriented Framework for Design Optimization, Parameter Estimation, Uncertainty Quantification, and Sensitivity Analysis: Version 6.12 User's Manual," *Sandia National Laboratories, Tech. Rep. SAND2010-5001*, May 2020.

[65] Wiener, N., "The Homogeneous Chaos," *American Journal of Mathematics*, Vol. 60, No. 4, 1938, pp. 897–936.

[66] Crestaux, T., Le Maıˆtre, O., and Martinez, J.-M., "Polynomial Chaos Expansion for Sensitivity Analysis," *Reliability Engineering and System Safety*, Vol. 94, No. 7, 2009, pp. 1161–1172, Special Issue on Sensitivity Analysis.

[67] Gaitonde, D. V., Canupp, P. W., and Holden, M. S., "Heat transfer predictions in a laminar hypersonic viscous/inviscid interaction," *Journal of Thermophysics and Heat Transfer*, Vol. 16, No. 4, 2002, pp. 481–489.

[68] Roy, C. J., Gallis, M. A., Bartel, T. J., and Payne, J. L., "Navier-Stokes and direct simulation Monte Carlo predictions for laminar hypersonic separation," *AIAA Journal*, Vol. 41, No. 6, 2003, pp. 1055–1063.

[69] Nompelis, I., "Computational study of hypersonic double -cone experiments for code validation," *PhD thesis, University of Minnesota*, 2004.

[70] Nompelis, I. and Candler, G., "Investigation of hypersonic double-cone flow experiments at high enthalpy in the lens facility," *45th AIAA Aerospace Sciences Meeting and Exhibit*, AIAA Paper 2007-0203, 2007.

[71] Hao, J., Wang, J., and Lee, C., "Numerical Simulation of High-Enthalpy Double-Cone Flows," *AIAA Journal*, 2017, pp. 1–5.

[72] Holloway, M. E., Hanquist, K. M., and Boyd, I. D., "Effect of Thermochemistry Modeling on Hypersonic Flow Over a Double Cone," *AIAA Scitech 2019 Forum*, AIAA Paper 2019-2281, 2019.

[73] Holloway, M. E. and Boyd, I. D., "Assessment of Thermochemical Kinetics Modeling on Hypersonic Flow Over a Double Cone," *AIAA Scitech 2020 Forum*, AIAA Paper 2020-1228, 2020.

[74] Holden, M. S. and Wadhams, T., "P.,"Code Validation Study of Laminar Shock/Boundary Layer and Shock/Shock Interactions in Hypersonic Flow Part A: Experimental Measurements," AIAA 2001-1031," *39th AIAA Aerospace Sciences Meeting and Exhibit, Reno, NV, January*, 2001, pp. 8–12.

[75] MacLean, M., Holden, M., and Dufrene, A., "Comparison Between CFD and Measurements for Real-Gas Effects on Laminar Shock Wave Boundary Layer Interaction, 1," *Oral Presentation*, 2014.

[76] Holden, M. S., Wadhams, T. P., MacLean, M. G., and Dufrene, A. T., "Measurements of Real Gas Effects on Regions of Laminar Shock Wave/Boundary Layer Interaction in Hypervelocity Flows for "Blind' Code Validation Studies," *21st AIAA Computational Fluid Dynamics Conference*, AIAA Paper 2013-2837, 2013.

[77] Nompelis, I., Candler, G., and Holden, M., "Computational investigation of hypersonic viscous/inviscid interactions in high enthalpy flows," *36th AIAA Thermophysics Conference*, 2003, p. 3642.

[78] Nompelis, I. and Candler, G., "Numerical investigation of double-cone flow experiments with high-enthalpy effects," *48th AIAA Aerospace Sciences Meeting Including the New Horizons Forum and Aerospace Exposition*, 2010, p. 1283.

[79] Martin, A. and Boyd, I. D., "Non-Darcian Behavior of Pyrolysis Gas in a Thermal Protection System," *Journal of Thermophysics and Heat Transfer*, Vol. 24, No. 1, 2010, pp. 60–68.

[80] Martin, A. and Boyd, I., "Simulation of Pyrolysis Gas Within a Thermal Protection System," *40th AIAA Thermophysics Conference*, AIAA Paper 2008-3805, 2008.

[81] Wiebenga, J. and Boyd, I., "Computation of Multi-Dimensional Material Response Coupled to Hypersonic Flow," *43rd AIAA Thermophysics Conference*, AIAA Paper 2012-2873, 2012.

[82] Wiebenga, J. E., "High-Fidelity Material Response Modeling as Part of an Aerothermoelastic Framework for Hypersonic Flows," *PhD thesis, University of Michigan*, 2014.

[83] Cross, P., "Conjugate Analysis of Two-Dimensional Ablation and Pyrolysis in Rocket Nozzles," *PhD thesis, University of Michigan*, 2017.

[84] Nompelis, I. and Candler, G. V., "US3D Predictions of Double-Cone and Hollow Cylinder-Flare Flows at High-Enthalpy," *44th AIAA Fluid Dynamics Conference*, AIAA Paper 2014-3366, 2014.

[85] Boyd, I., "Aerothermochemistry Modeling: When Is High Fidelity Needed?" *AIAA Scitech 2019 Forum*, AIAA Lecture, 2019.

[86] Dufrene, A., Sharma, M., and Austin, J., "Design and Characterization of a Hypervelocity Expansion Tube Facility," *Journal of Propulsion and Power*, Vol. 23, No. 6, 2007, pp. 1185–1193.

[87] Yanes, N. J. and Austin, J. M., "Nitric Oxide Spectroscopic Measurements in a Hypervelocity Stagnation Flow," *AIAA Scitech 2019 Forum*, AIAA Paper 2019-0794, 2019, p. 0794.

[88] Park, C., "The Limits of Two-Temperature Kinetic Model in Air," *48th AIAA Aerospace Sciences Meeting Including the New Horizons Forum and Aerospace Exposition*, AIAA Paper 2010-911, 2010.